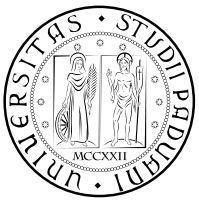

Università degli Studi di Padova

Sede Amministrativa: Università degli Studi di Padova

Dipartimento di Ingegneria Idraulica, Marittima, Ambientale e Geotecnica

SCUOLA DI DOTTORATO DI RICERCA IN
SCIENZE DELL'INGEGNERIA CIVILE E AMBIENTALE

CICLO XXII

TRANSPORT OF SOLUTES IN STREAMS WITH TRANSIENT STORAGE AND HYPORHEIC EXCHANGE

Direttore della Scuola: Ch.mo. Prof. Stefano Lanzoni

Supervisore: Ch.mo. Prof. Andrea Marion

Dottorando: Andrea Bottacin Busolin

31 Gennaio 2010

Abstract

Environmental quality and health safety assessment often requires modeling of solute transport in rivers. Conceptually, a stream can be divided into distinct compartments mutually interacting through bidirectional exchanges of mass and momentum. A distinction can generally be drawn between a main channel, where the velocities are relatively high, and different types of storage domains, where the average velocity is sensibly lower. The downstream propagation of dissolved substances in streams is influenced by exchanges between the main channel and surrounding retention zones, typically vegetated pockets, pools of recirculating or stagnant water, and permeable subsurface. Submerged vegetation and, at a small spatial scale, microbial biofilms also constitute additional retention domains which can significantly contribute to determining the fate of the transported substances.

A one-dimensional model for solute transport in rivers (STIR) with transient storage is presented within this thesis. The model is based on a stochastic approach which allows to express the concentration of a solute in the main channel of a stream as a function of the residence time distributions (RTDs) in the storage domains. As a general RTD model, STIR can be used either as a calibration model or as a predictive tool. When used as a calibration model, a form is assumed for the RTD in the storage zones, and the relevant parameters are determined by fitting the simulated breakthrough curves to concentration data from tracer tests. On the other hand, if enough information is available about the properties of

the system, specific modeling closures can be incorporated in STIR to represent individual exchange processes separately.

In this work applications of the STIR model to field cases are presented where the model is calibrated with tracer test data. Distinct forms of the RTD in the storage zones are assumed to assess the capability of the model to reproduce the observed tracer breakthrough curves. Results show that, when the RTD in the storage zones is represented as a weighted average of two exponential distributions, the model provides an excellent approximation of the experimental data for all the study reaches examined and a useful conceptual separation of the timescales of retention. However, since concentration distributions in streams result from a complex interaction between transport processes in the main channel and exchange processes with the storage domains, uncertainty can arise about the interpretation of the model parameters. The particular form assumed for the storage time distribution determines the parameters of both surface transport and transient storage. This limitation cannot be overcome with traditional field tracer tests, unless complementing the experimental data with an accurate hydrodynamic modeling of the flow in the main channel. In flume experiments where the hydraulic conditions can be strictly controlled, the effect of specific retention processes can be isolated, under proper assumptions, by comparison of the model parameters with those relative to a reference configuration of the system in which the retention processes under consideration are not present. This methodology is illustrated with an application of STIR to data from flume experiments with microbial biofilms.

Another important distinction often required in water quality assessments is between in-channel and subsurface transient storage. The near-stream region of the porous bed affected by the concentration of solutes in the stream is known as the hyporheic zone, and is recognized to be extremely important for the evolution of a riverine ecosystem. Exchange between the stream and the underlying

hyporheic zone is known to be primarily driven by advective processes which develop at several spatial scales because of separate mechanisms such as flow over bed forms, around obstacles and through bars and meanders. Specific modeling closures for the residence time distribution of bed form-induced hyporheic exchange are presented in this thesis for the case of homogeneous and stratified beds, extending previous works on the subject. These modeling closures can be incorporated in a general RTD transport model such as STIR to estimate in a predictive manner the effect of bed form-induced hyporheic exchange on the concentration of a solute in the surface water or, at least potentially, to estimate particular parameters of hyporheic exchange with an inverse approach.

Sommario

La valutazione della qualità delle acque e le operazioni di monitoraggio ambientale richiedono spesso la caratterizzazione dei processi di trasporto e ritenzione di soluti nei sistemi fluviali. La propagazione a valle delle sostanze disciolte in un corso d'acqua, come nutrienti e contaminanti, è influenzata da scambi di massa tra corrente principale, dove le velocità sono relativamente elevate, e circostanti zone d'immagazzinamento temporaneo, tipicamente zone vegetate, sacche di ritenzione laterali e substrato permeabile, dove le velocità sono sensibilmente inferiori. Anche la vegetazione sommersa e, su piccola scala spaziale, i biofilm microbici costituiscono domini di ritenzione addizionali che possono condizionare sensibilmente il destino delle sostanze trasportate.

Nel Capitolo 1 di questa tesi viene presentata una panoramica dei processi di trasporto attivi nei corsi d'acqua su diverse scale spaziali e temporali, evidenziando in particolare il loro contributo nell'equazione di bilancio di massa di un soluto. Il Capitolo 2 offre una rassegna dei principali modelli monodimensionali di trasporto ed immagazzinamento temporaneo proposti in letteratura. Nel Capitolo 3 viene presentato il modello di trasporto monodimensionale STIR (Solute Transport In Rivers). Tale modello si basa su un approccio stocastico che permette di esprimere la concentrazione di un soluto nel canale principale in funzione della distribuzione del tempo di residenza nei domini d'immagazzinamento. La formulazione a distribuzione generale del tempo di residenza rende STIR un modello flessibile e modulare che può essere usato sia come modello di calibrazione

sia come strumento predittivo. Quando utilizzato come modello di calibrazione, la stima dei parametri si basa su dati di concentrazione ottenuti mediante prove con tracciante in sito. Si procede dunque assumendo una certa forma funzionale per la distribuzione del tempo di residenza nelle zone d'immagazzinamento e determinando i relativi parametri in modo da minimizzare le differenze tra simulazioni e dati sperimentali. Quando siano disponibili sufficienti informazioni sulle proprietà di un corso d'acqua, specifiche chiusure modellistiche possono essere incorporate nel modello STIR per rappresentare separatamente particolari processi di ritenzione e valutare in modo predittivo la risposta del sistema all'immissione di un soluto.

Nel Capitolo 4 viene presenta un'applicazione del modello STIR a prove con tracciante in tre corsi d'acqua con caratteristiche molto diverse in termini di portata, substrato e vegetazione. Distinte forme della distribuzione del tempo di residenza nelle zone d'immagazzinamento sono assunte per valutare la capacità del modello di riprodurre le curve osservate. I risultati mostrano che, quando la distribuzione dei tempi d'immagazzinamento è espressa da una media pesata di due distribuzioni esponenziali, il modello fornisce un'ottima approssimazione dei dati sperimentali in tutti i tratti di studio esaminati ed un'utile separazione concettuale delle scale temporali caratteristiche dei processi di ritenzione. L'interpretazione fisica dei parametri può tuttavia presentare delle incertezze, in conseguenza del fatto che le distribuzioni di concentrazione nei corsi d'acqua risultano da una complessa interazione tra processi di trasporto nella corrente principale e processi di scambio con i domini di ritenzione. In particolare, se i parametri del trasporto superficiale non sono fissati a priori, essi dipendono dalla forma specifica assunta per la distribuzione dei tempi d'immagazzinamento. Questa limitazione non può essere superata attraverso tradizionali prove con tracciante, se non integrando i dati sperimentali con un'accurata modellazione idrodinamica del corso d'acqua. Nel caso di prove con tracciante eseguite in ca-

naletta, dove le condizioni idrauliche sono in genere strettamente controllate, l'effetto di particolari processi di ritenzione può essere isolato, sotto specifiche assunzioni, prendendo come riferimento una configurazione di base del sistema in cui tali processi non siano attivi. Questa metodologia viene illustrata nel Capitolo 5 con un'applicazione del modello STIR volta a caratterizzare l'effetto ritentivo di biofilm microbici mediante esperimenti in canaletta.

Negli studi di vulnerabilità di sistemi fluviali è utile distinguere tra processi d'immagazzinamento superficiale e sotto-superficiale. Risulta importante, in particolare, caratterizzare la ritenzione di soluti nella regione del letto, nota come zona iporeica, che è direttamente influenzata dalla concentrazione nella corrente superficiale. Essa costituisce infatti un importante ambiente di transizione e riveste un ruolo fondamentale per l'evoluzione di un ecosistema fluviale. Lo scambio tra la corrente e la sottostante zona iporeica è primariamente dovuto a processi convettivi che si sviluppano su diverse scale spaziali a causa dell'interazione fra corrente e irregolarità dell'alveo, quali forme di fondo, barre alternate e meandri. Nei Capitoli 6 e 7 sono derivate specifiche chiusure modellistiche per lo scambio iporeico indotto da forme di fondo in letti omogenei e stratificati che estendono precedenti studi in materia. Tali chiusure modellistiche possono essere incorporate in un modello di trasporto come STIR per stimare in modo predittivo l'effetto dello scambio iporeico indotto da forme di fondo sulla concentrazione di un soluto nell'acqua superficiale o, almeno potenzialmente, per stimare i parametri dell'immagazzinamento iporeico mediante un approccio inverso.

Contents

Abstract . . . . . **I**

Sommario . . . . . **V**

1 Physical transport processes in fluvial environments **1**

1.1 Advection 1

1.2 Molecular diffusion 3

1.3 Combined advection-diffusion processes 4

1.4 Turbulent diffusion 4

1.5 Dispersion 7

1.6 Transient storage 8

2 Literature review of stream transport models **13**

2.1 Introduction 13

2.2 The Transient Storage Model (TSM) 14

2.3 The diffusive model 16

2.4 The multi-rate mass transfer approach (MRMT) 18

2.5 The continuous time random walk approach (CTRW) 20

2.6 Fractional advection-dispersion equation (FADE) 21

3 The STIR model **25**

3.1 Introduction 25

3.2 The STIR model 26

3.2.1 Residence times in the surface stream and in the storage zones 26

3.2.2 Uptake probability for uniformly spaced storage zones . . . 29

3.2.3 Example 1. Residence time distribution in surface dead zones 30

3.2.4 Example 2. Residence time distribution of bed form-induced hyporheic retention 30

3.2.5 Solute concentration in the surface stream and in the storage domains 31

3.3 STIR and other approaches 35

3.4 Potential application 37

3.5 Conclusions 39

4 Applications of the STIR model: Three case studies **43**

4.1 Introduction 43

4.2 Site description 45

4.2.1 The Yarqon river, Israel 45

4.2.2 The Brenton torrent, Italy 49

4.2.3 The Desturo canal, Italy 49

4.3 Stream tracer experiments 51

4.4 Solute transport modeling 57

4.5 Results and discussion 60

4.6 Conclusions 68

5 Effect of microbial biofilms on the transient storage of solutes 71
5.1 Introduction 71
5.2 Experimental methods 72
5.3 Solute transport modeling 75
5.4 Model calibration 76
5.5 Results and discussion 79
5.6 Conclusions 87

6 Bed form-induced hyporheic exchange in homogeneous sediment beds 89
6.1 Introduction 89
6.2 Solute transport model in the porous medium 91
6.2.1 Velocity field 92
6.2.2 Advection-dispersion model 98
6.3 Residence time distributions 101
6.3.1 Pure advection 101
6.3.2 Effect of pore-scale dispersion 106
6.4 Discussion 110
6.5 Conclusions 114

7 Bed form-induced hyporheic exchange in stratified beds 117
7.1 Introduction 117
7.2 Hyporheic flow modeling for layered beds 119
7.2.1 Velocity field in the bed 119
7.2.2 Residence time distributions and mass exchange 123
7.3 Experiments 125
7.3.1 Experimental setup 125
7.3.2 Results 128
7.4 Comparison between model and experimental results 130
7.5 Conclusions 133

Notation **135**

Bibliography **143**

Chapter 1

Physical transport processes in fluvial environments

Transport of dissolved substances in streams is determined at a small scale of observation by advection and molecular diffusion. When phenomena are observed at a larger scale, thus considering quantities averaged in time and space, and when the flow domain is conceptually divided into distinct compartments, for example by separating surface from subsurface transport, additional processes become apparent known as dispersion and transient storage. This chapter presents an overview of how the physical transport processes active in fluvial environments are generally described at different spatial and temporal scales, highlighting in particular their contribution to the mass balance equation.

1.1 Advection

Advection is the process by which a conserved physical quantity is transported in a fluid in motion. In this work the transported quantity of interest is in particular the mass of a dissolved substance. The amount per unit volume is expressed by the concentration c [$\mathrm{M\,L^{-3}}$], while the motion of the fluid is entirely described by the velocity vector field $\mathbf{u} = (u, v, w)$ [$\mathrm{L\,T^{-1}}$] defined at each point as a function of time. If the substance behaves like a solute, that is, has the same density as the medium or does not feel significant effect of its buoyant weight, each element of it (molecule or particle) is displaced along the direction of the local velocity vector

following the same path as if it were an element of the medium. This assumption allows the advective transport to be modeled in a relatively simple way. The mass flux $\mathbf{\Phi}$ $[\mathrm{M L^{-2} T^{-1}}]$ can be written as

$$\mathbf{\Phi}(\mathbf{x}, \mathbf{t}) = c(\mathbf{x}, t)\mathbf{u}(\mathbf{x}, t), \tag{1.1}$$

where $\mathbf{x} = (x, y, z)$ is the coordinate vector in a Cartesian frame of reference and t is time.

The mass balance for a control volume leads to the following differential equation:

$$\frac{\partial c}{\partial t} = -\nabla \cdot \mathbf{\Phi}, \tag{1.2}$$

or, using the extended notation,

$$\frac{\partial c}{\partial t} = -\nabla \cdot (c\mathbf{v}) = -\left[\frac{\partial (cu)}{\partial x} + \frac{\partial (cv)}{\partial y} + \frac{\partial (cw)}{\partial z}\right]. \tag{1.3}$$

In fluvial hydraulics the fluid representing the medium in which substances are dissolved is water, which can well be regarded as incompressible, and the flow field is solenoidal ($\nabla \cdot \mathbf{v} \equiv \mathbf{0}$). Under this assumption, the continuity equation simplifies to

$$\frac{\partial c(\mathbf{x}, t)}{\partial t} + \mathbf{u} \cdot \nabla c(\mathbf{x}, t) = 0. \tag{1.4}$$

In steady conditions, the solution of equation (1.4) is simply a translation of the substance along the paths imposed by the flow field.

Pure advection does not exist alone in nature, as it is always associated at least to molecular diffusion. However, the significance of molecular diffusion in an advective process is negligible in most cases, due to the extremely low value of the diffusive flux. Advection is associated only to molecular diffusion when the flow field is slow, such as in laminar flows. One common application is the

flow of water carrying substances in a porous medium, such as an aquifer or the hyporheic zone, as long as the process is modeled at the scale of the pores of the medium.

An important property of advection, valid also when diffusion is significant, is that it determines the position of the center of mass of a solute cloud, thus making the advection equation often sufficient to estimate the average travel time of a solute between two subsequent positions in time.

The extension of the mass balance expressed by equation (1.4) to the transport of buoyant or heavy substances is straightforward. This may be the case of colloids or suspended solids which are affected by gravity as their density is either smaller or larger than the density of the medium. Their behavior can be modeled by adding a vertical velocity component with magnitude dependent on the particle size, shape and density.

1.2 Molecular diffusion

Molecular diffusion is the process by which matter is transported from one part of a system to another as a result of random molecular motions. A fundamental property of this process is that the flux of mass is always directed from higher to lower concentrations. A quantitative description of the diffusion process was first given by *Fick* (1855) who expressed the corresponding net flux of the transported substance as equal to the concentration gradient multiplied by a physical property called molecular diffusivity or diffusion coefficient, indicated by D_m $[\mathrm{L}^2\,\mathrm{T}^{-1}]$:

$$\mathbf{\Phi}(\mathbf{x}, t) = -D_m \nabla c(\mathbf{x}, t)\,, \tag{1.5}$$

where the symbol (∇) indicates the gradient differential operator.

When molecular diffusion is the only cause of mass transport, the mass bal-

ance equation is given by Fick's second law (or heat equation):

$$\frac{\partial c(\mathbf{x},t)}{\partial t} = D_m \nabla^2 c(\mathbf{x},t) = D_m \left[\frac{\partial^2 c(\mathbf{x},t)}{\partial x^2} + \frac{\partial^2 c(\mathbf{x},t)}{\partial y^2} + \frac{\partial^2 c(\mathbf{x},t)}{\partial z^2} \right]. \tag{1.6}$$

The value of the molecular diffusion coefficient varies according to the combination of solute and solvent. As far as water is concerned, molecular diffusion is easier for polar molecules and D_m is of the order of $10^{-9} \div 10^{-8}\,\mathrm{m^2\,s^{-1}}$. Conversely, apolar molecules diffuse in water at lesser rate due to hydrophobic effects. The molecular diffusion coefficient for these substances is of the order of $10^{-10}\,\mathrm{m^2\,s^{-1}}$.

1.3 Combined advection-diffusion processes

Whenever the fluid is in motion, advection and diffusion processes act simultaneously. The total flux is thus given by the sum of the advective and diffusive flux,

$$\mathbf{\Phi} = \mathbf{u}c - D_m \nabla c, \tag{1.7}$$

which leads to the following mass balance equation:

$$\frac{\partial c}{\partial t} = -\nabla \cdot (c\mathbf{u} - D_m \nabla c). \tag{1.8}$$

For an incompressible fluid, equation (1.8) becomes

$$\frac{\partial c}{\partial t} + u\frac{\partial c}{\partial x} + v\frac{\partial c}{\partial y} + w\frac{\partial c}{\partial z} = D_m \left[\frac{\partial^2 c}{\partial x^2} + \frac{\partial^2 c}{\partial y^2} + \frac{\partial^2 c}{\partial z^2} \right]. \tag{1.9}$$

1.4 Turbulent diffusion

Molecular diffusion produced by Brownian motion is no longer the dominant diffusion mechanism when the flow velocity becomes fast enough to overcome viscous forces that tend to keep fluid elements aligned along parallel paths. When

this condition is reached, the flowpaths become very irregular, and the fluid elements are entrained and transported by eddies which form either from the slowing effect of the bottom and side boundaries or from the disturbances introduced by geometrical irregularities. This type of flow is called turbulent, and is characterized by an enhanced momentum and mass transfer across the flow field. Diffusion of mass is no longer controlled by Brownian motion, but rather by the continuous displacement of fluid elements in all directions induced by turbulence. While molecular diffusion is isotropic, turbulent diffusion is typically different in each direction, as eddies are continuously stretched and deformed by the flow.

Turbulent flows are usually modeled splitting the physical quantities into time-averaged mean values and fluctuations around the mean. After manipulation of the advection-diffusion equation (1.9), a new mathematical transport term appears, which is the time-averaged product of the fluctuating values of velocity and concentration. If velocity and concentration fluctuations were statistically independent, then these terms would produce no net diffusive mass fluxes. It turns out instead that velocity and concentration irregularities are correlated and that the integral effect over time of turbulent fluxes is always much higher than the fluxes induced by Brownian motion. The time-averaged mass transport equation becomes

$$\frac{\partial \overline{c}}{\partial t} + \overline{u}\frac{\partial \overline{c}}{\partial x} + \overline{v}\frac{\partial \overline{c}}{\partial y} + \overline{w}\frac{\partial \overline{c}}{\partial z} = \frac{\partial}{\partial x}\left(D_{xx}^{T}\frac{\partial \overline{c}}{\partial x}\right) + \frac{\partial}{\partial y}\left(D_{yy}^{T}\frac{\partial \overline{c}}{\partial y}\right) + \frac{\partial}{\partial z}\left(D_{zz}^{T}\frac{\partial \overline{c}}{\partial z}\right), \tag{1.10}$$

where D_{xx}^{T}, D_{yy}^{T} and D_{zz}^{T} are eddy diffusion coefficients in the three spatial directions x, y and z, respectively, and the notation $\overline{(\ )}$ denotes temporal average. The molecular diffusion coefficient D_m is typically so much smaller than eddy diffusion coefficients that it can be neglected in the balance equation. A conceptual difference between (1.10) and (1.9) is that the value of the coefficients D_{xx}^{T}, D_{yy}^{T}

and D_{zz}^T is now determined by the flow regime, that is, they are flow properties, while D_m is independent of the flow and determined only by the combination of solute and solvent. Another difference resides in the fact that eddy diffusivity is scale dependent, while molecular diffusivity is scale independent. Eddy diffusivity typically scales with a 4/3 power of the length scale of the process. This implies that as diffusion makes the substance spread in the domain, diffusivity increases due to the effect of larger eddies that come into play. This dependence is important in large and deep water bodies such as the sea or lakes, where the diffusion process involves several different scales over time. In rivers, instead, the size of the eddies is controlled by water depth and width, and diffusivity is no longer affected by the scale of the process. An expression for the vertical dispersion coefficient D_{zz}^T in rivers can be derived from the logarithmic velocity profile:

$$D_{zz}^T = 0.067 u_* d_W \,, \tag{1.11}$$

where d_W is the water depth and u_* is the shear velocity. An approximate expression of the coefficient D_{yy}^T valid for uniform straight channels was empirically derived by *Fischer et al.* (1979) based on laboratory and field experiments:

$$D_{yy}^T = 0.15 u_* d_W \,. \tag{1.12}$$

The typical irregularity of the cross-section in natural streams, characterized by variations of both flow depth and width, enhances transverse mixing, and for natural streams, *Fischer et al.* (1979) suggested the relationship

$$D_{yy}^T = 0.6 u_* d_W \,. \tag{1.13}$$

For longitudinal mixing it can often be assumed that $D_{xx}^T = D_{yy}^T$.

These relationships can be used to estimate the distance L_{mix} from the injec-

tion point at which a solute can be considered to be well mixed over the cross-section. For a solute injected in the middle of the channel section, *Fischer et al.* (1979) suggested

$$L_{\text{mix}} = 0.1 \frac{U b^2}{D_{xx}^T}, \tag{1.14}$$

where U is the average flow velocity and b is the channel width. For a lateral injection the distance is 4 times greater.

1.5 Dispersion

Dispersion is defined as the combined effect of advection and diffusion acting in a flow field with velocity gradients. The effect of velocity gradients on the fate of a substance becomes apparent when spatial averaging of the physical quantities is carried out along with the temporal averaging described in § 1.4. In surface water bodies, it is often convenient to simplify the description of mass transfer by averaging velocity and concentration over the vertical direction (shallow water approach) or over a cross-section (unidirectional approach). Depth averaging is justified when dealing with large rivers, estuaries and lagoons, using the evidence that vertical mixing is usually much faster than lateral and longitudinal mixing, due to the limited extension of the domain in the vertical direction. The one-dimensional approach is justified when the transverse dimensions of the domain are small compared to the longitudinal dimension. This is the reason why the one-dimensional approach is commonly adopted for dispersion processes in rivers and channels. In the case of cross-sectional averaging of the physical quantities, the mass balance equation is reduced to the one-dimensional form:

$$\frac{\partial C(x,t)}{\partial t} + U(x,t)\frac{\partial C(x,t)}{\partial x} = \frac{1}{A(x,t)}\frac{\partial}{\partial x}\left(A(x,t)D_L(x,t)\frac{\partial C(x,t)}{\partial x}\right), \tag{1.15}$$

where C and U are the cross-sectional average concentration and flow velocity, respectively, A is the flow cross-sectional area [L^2], and D_L is the longitudinal

dispersion coefficient $[L^2 T^{-1}]$. Under the assumption of constant A and D_L, the solution of equation (1.15) for an instantaneous injection of a mass of tracer M_0 in $x = 0$ at time $t = 0$ is given by:

$$C(x,t) = \frac{M_0/A}{\sqrt{4\pi D_L t}} \exp\left[-\frac{(x-Ut)^2}{4D_L t}\right]. \tag{1.16}$$

The presence of a nonuniform velocity distribution over the cross-section induces solute molecules in different positions to travel different distances in a given interval of time. On the other hand turbulent transverse mixing induces the molecules to occupy different positions of the cross-section at subsequent instants of time, thereby reducing the differences of travel distance among them. Thus, the non-uniformity of the velocity distributions and turbulent transverse mixing play a competitive role in determining the variance of the concentration distributions. The longitudinal dispersion coefficient turns out to be proportional to the spatial variability of the flow field around its mean value and inversely proportional to the turbulent diffusivity. An approximated relationship for D_L valid for streams with large width-to-depth ratios was suggested by *Fischer* (1975) as

$$D_L = 0.011 \frac{U^2 b^2}{d_W u_*}, \tag{1.17}$$

which has been found to agree to experimental observations within a factor of 4 or so.

1.6 Transient storage

In natural streams, the downstream propagation of the transported substances is influenced by mass exchanges with different types of storage zones, typically vegetated pockets, dead zones and permeable subsurface, as illustrated in Figure 1.1. The superposition of retention phenomena acting at different timescales induces a non-Fickian behavior of the observed breakthrough curves that cannot

be reproduced using the classical advection-dispersion equation (1.15). This limitation has been proved since the early 50's by a number of studies using tracer tests (*Elder*, 1959; *Krenkel and Orlob*, 1962; *Thackston and Schnelle*, 1970; *Nordin and Sabol*, 1974; *Day*, 1975; *Nordin and Troutman*, 1980). The effect of retention phenomena on the concentration distributions can be summarized as follows:

- The skewness of the observed breakthrough curves is more pronounced than predicted by the advection-dispersion theory, and the curves are characterized by longer tails.
- The variance of the concentration distributions increases more than linearly in time.
- The concentration peak decreases more rapidly than the $-1/2$ power of time.
- The concentration peak moves at a lower speed than the average flow velocity.
- Part of the solute is not recovered at the measurement section, especially when solutes reacts with sediments, such as metals, or when the transported substances are affected by gravity.

In order to account for the temporary storage of solutes, the advection-dispersion equation (1.15) can be modified by including in the mass balance an additional flux due to mass exchange between the flow in the main channel and the surrounding storage zones. The equation then becomes:

$$\frac{\partial C}{\partial t} + U\frac{\partial C}{\partial x} = \frac{1}{A}\frac{\partial}{\partial x}\left(AD_L\frac{\partial C}{\partial x}\right) - \frac{P}{A}\Phi_S\,, \tag{1.18}$$

where Φ_S denotes the exchange flux at the stream-storage zone interface $[\mathrm{M\,L^{-2}\,T^{-1}}]$. The physical description and the modeling of the retention processes determin-

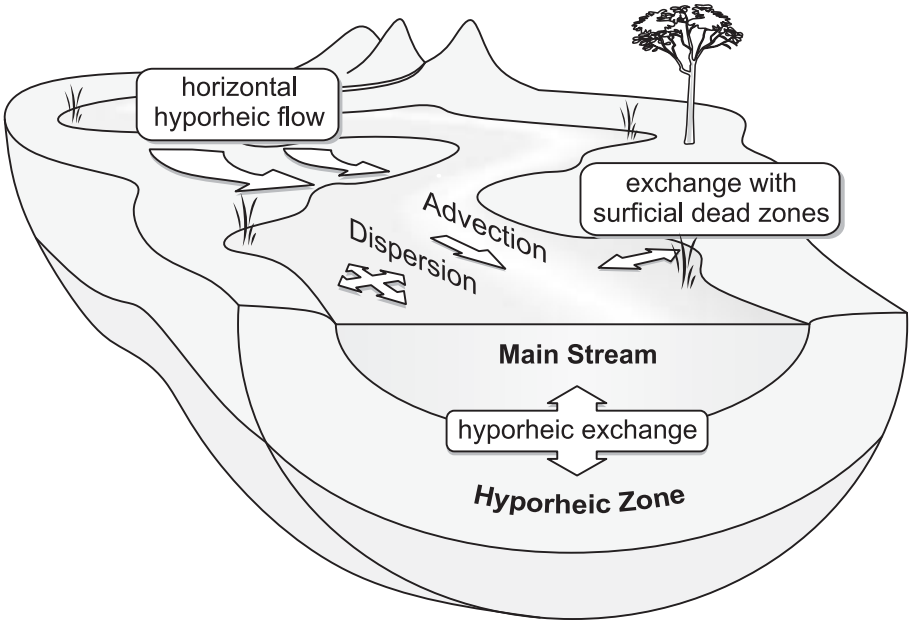

Figure 1.1. Illustration of the transport processes acting in a river. The downstream transport of solutes is governed by advection and hydrodynamic dispersion in the main stream, and by mass exchanges with different retention zones. These include vertical exchanges with the underlying sediments, where adsorption process may take place; lateral exchanges with surficial dead zones, typically vegetated pockets; and horizontal hyporheic flows induced by planimetric variation of the stream direction.

ing the additional storage term has been the subject of many studies in the recent years.

Storage processes can be classified in surface and subsurface processes. Natural streams are typically characterized by irregular cross-sections, with often vegetated lateral pockets acting like surface dead zones where the water can be stagnant or slowly moving. When the transported substances enter these dead zones, they can be retained for a long time before being released back to the main channel. While temporarily retained in these storage domains, reactive solutes can sorb on sediments, whereas heavy particles can settle. The combined effect

of deposition of heavy particles and adsorption of reactive solutes is particularly important: the formers in fact can become the substrate on which reactive solutes adsorb. Deposition and adsorption can cause a temporary or persistent mass loss, and influence significantly contamination processes in streams and rivers.

Subsurface storage processes result from exchange fluxes between the stream and the sediment bed over which water flows. Filtration through porous boundary of a river bed leads the dissolved substances within the porous medium where sorption onto the sediments, deposition of the finer suspended particulate matter and other biogeochemical reactions may significantly affect their fate. The near-stream region of the porous boundary affected by the concentration of solutes in the stream is called the hyporheic zone, and is recognized to be an important transition environment for the evolution of a riverine ecosystem.

Chapter 2

Literature review of stream transport models

2.1 Introduction

Hydrodynamic exchange with storage zones plays an important role in determining the fate of the transported substances in streams. The effect of transient storage is often clearly visible in the shape of breakthrough curves of stream tracer tests, which cannot be reproduced by the conventional ADE, especially when the timescales of retention are much larger than the travel time in the main channel. Long term retention processes are typically due to the temporary storage in the porous medium, in the so called hyporheic zones, while short term retention is commonly due to surface dead zones, such as side pockets of recirculating water or vegetated zones. The prediction of the exchange between a stream and the surrounding retention zones is an important component in the analysis of the contamination dynamics of fluvial environments. Retention processes in the hyporheic zones can be studied individually with mathematical or numerical models by simulating the transport dynamics of a solute in a sediment bed. This is usually done for idealized configurations by decoupling surface from subsurface flow. In the experimental approach relying on tracer tests, hyporheic retention is instead studied from the perspective of the surface transport, by evaluating its effect as a whole on the concentration of a solute in the surface water. This

approach is typically based on one-dimensional transport models consisting in properly modified advection-dispersion equations. A brief review of the main 1-D transport models proposed in the literature is given in the following sections.

2.2 The Transient Storage Model (TSM)

One of the most widely used transport models in field applications reported in the literature is the Transient Storage Model (TSM). The TSM was presented by *Bencala and Walters* (1983), although analogous formulations can be found in an earlier works (*Hays et al.*, 1966; *Nordin and Troutman*, 1980). This model has been widely applied to field experiments conducted both in small streams and large rivers (e.g. *Bencala*, 1984; *Castro and Hornberger*, 1991; *Vallet et al.*, 1996; *Mulholland et al.*, 1997a; *Harvey and Fuller*, 1998; *Runkel et al.*, 1998; *Choi et al.*, 1999; *Fernald et al.*, 2001).

In the TSM the net mass transfer from the main flow channel to the retention domains is assumed to be proportional to the difference of concentration between the surface water and a storage zone of constant cross-sectional area. The mathematical formulation of the TSM for non-reactive solutes is usually given as follows (*Nordin and Troutman*, 1980; *Bencala and Walters*, 1983; *Czernuszenko and Rowinski*, 1997; *Lees et al.*, 2000; *De Smedt and Wierenga*, 2005; *De Smedt*, 2006):

$$\frac{\partial C_W}{\partial t} + U\frac{\partial C_W}{\partial x} = D_L\frac{\partial^2 C}{\partial x^2} + \alpha(C_S - C_W), \tag{2.1a}$$

$$\frac{dC_S}{dt} = -\alpha\frac{A}{A_S}(C_S - C_W), \tag{2.1b}$$

where: U is the mean flow velocity [$\mathrm{L\,T^{-1}}$]; α is a transfer coefficient [$\mathrm{T^{-1}}$]; A/A_S is the ratio of stream to storage cross-sectional areas; C_W is the in-stream solute concentration [$\mathrm{M\,L^{-3}}$]; C_S is the concentration of solute in the storage zone [$\mathrm{M\,L^{-3}}$]; D_L is the longitudinal dispersion coefficient for the flow in the main channel [$\mathrm{L^2\,T^{-1}}$]; and t is time [T]. A numerical solution of equation (2.1) was

presented by *Runkel and Chapra* (1993), which formed the basis of their One-dimensional Transport with Inflow and Storage (OTIS), later extended by *Runkel* (1998) with a parameter estimation technique (OTIS-P).

Equation (2.1a) is a special case of (1.18) where the exchange flux is assumed to be equal to:

$$\Phi_S = \frac{A}{P}\alpha(C_W - C_S). \tag{2.2}$$

Often an additional flux, Φ_L, is included in the mass balance to account for possible mass gains due to lateral inflow. This is defined as

$$\Phi_L = q_L(C_W - C_S), \tag{2.3}$$

where q_L is the volumetric flux $[\mathrm{L\,T^{-1}}]$ and C_L is the concentration of solute in lateral inflow.

Equation (2.1b) can be solved to get C_S as a function of C_W:

$$C_S(x,t) = \alpha\frac{A}{A_S}\int_0^t C_W(x,t-\tau)e^{-\frac{\alpha A}{A_S}\tau}d\tau, \tag{2.4}$$

which shows that the TSM implies an exponential residence time distribution (RTD) in the storage zones with mean value $T = A_S/(\alpha A)$.

The particular form of the model given by equation (2.1) finds application to passive, conservative tracers, that is, non-reactive substances which do not decay over time. These effects can be accounted for by including in (2.1) a kinetic term as suggested by *Bencala and Walters* (1983). An extension of the model to account for reactivity of solutes was proposed by *Runkel et al.* (1996) who coupled the TSM with a submodel for equilibrium adsorption and other phenomena such as precipitation related to water pH values.

The parameters of the TSM are usually determined by fitting the model simulations to experimental breakthrough curves obtained by tracer tests. The intro-

duction of an additional flux in the mass balance allows a better representation of the breakthrough curves observed in natural streams. However, since the parameters can be determined only by calibration, they do not necessarily have physical meaning, because they are not directly related to the real dynamics of the physical processes generating transient storage. There is no theory that provides a relationship between the transfer rate α and the area A_S to measurable physical quantities of the system examined. This means that the results found in the application of the TSM to a particular system cannot be extended to another one with different characteristics.

The simplification of the physical processes involved in hyporheic exchange which is inherent in the TSM is a cause of uncertainty in the parameter estimation. Recent studies and field observations have demonstrated that when advective pumping into the bed is a significant exchange process the best fit TSM parameters are dependent on the timescale of the process and the upstream boundary condition (incoming concentration) (*Harvey et al.*, 1996; *Harvey and Wagner*, 2000; *Wörman et al.*, 2002; *Marion et al.*, 2003; *Zaramella et al.*, 2003; *Marion and Zaramella*, 2005a). This uncertainty of the TSM parameters often interferes with the observation of important results, such as the relationship between transient storage and the fluxes of reactive substances of interest (e.g., nutrients, contaminants) (*Hall Jr. et al.*, 2002; *Zaramella et al.*, 2006). From this consideration the need arises to extend transport models to account for specific retention processes that can be studied and modeled separately as a function of measurable physical quantities characterizing the system.

2.3 The diffusive model

A model for solute transport of conservative species where hyporheic exchange is represented by a diffusive term was suggested by *Jackman et al.* (1984). This model assumes solute penetration into the bed to be a vertical diffusion process

described by Fick's law. The equation governing the transport of a solute in the bed is therefore given by:

$$\frac{\partial C_S}{\partial t} = D_S \frac{\partial^2 C_S}{\partial y^2}, \tag{2.5}$$

where $C_S(t,x,y)$ and D_S are respectively the concentration and the dispersion coefficient in the porous medium. In the general equation (1.18), the flux at the stream-subsurface interface is assumed to be proportional to the local gradient of concentration in the bed:

$$\Phi_S(t,x) = -D_S \left.\frac{\partial C_S(t,x,y)}{\partial y}\right|_{y=0}, \tag{2.6}$$

where D_S is the diffusion coefficient in the porous medium. The boundary condition in $y = 0$ for equation (2.5) is given by $C_S = C_W$, whereas the initial condition is usually assumed to be $C_S(t = 0,x,y) = 0$. Assuming y positive downward, the solution of equation (2.5) for the given boundary and initial conditions is

$$C_S(t,x,y) = \frac{y}{2\sqrt{\pi D_S}} \int_0^t C_W(\tau,x) \exp\left[-\frac{y^2}{4D_S(t-\tau)}\right] \frac{d\tau}{(t-\tau)^{3/2}}, \tag{2.7}$$

and hence, from (2.6) we get

$$\Phi_S(t,x) = \frac{1}{2}\sqrt{\frac{D_S}{\pi}} \int_0^t \frac{C_W(\tau,x)}{(t-\tau)^{3/2}}\, d\tau. \tag{2.8}$$

The coupling of the advection-dispersion model for the surface flow and the vertical diffusion model for the subsurface yields:

$$\frac{\partial C_W}{\partial t} + U\frac{\partial C_W}{\partial x} = \frac{1}{A}\frac{\partial}{\partial x}\left(AD_L\frac{\partial C_W}{\partial x}\right) - \frac{P}{A}\sqrt{\frac{D_S}{4\pi}} \int_0^t \frac{C_W(\tau,x)}{(t-\tau)^{3/2}}\, d\tau. \tag{2.9}$$

It should be noted that the transfer mechanism assumed in the diffusive model is not reversible as in the TSM. In the TSM the fraction of solute entering the stor-

age domains is gradually released when the concentration in the surface water becomes lower than the concentration in the storage zone, whereas in the diffusive model the mass transfer is one-directional and the exchange with the bed generates a net mass loss of solute in the surface water.

2.4 The multi-rate mass transfer approach (MRMT)

In the MRMT formulation the flow domain is divided in mobile and immobile regions. In the mobile regions solute transport is modeled by the classical ADE, while immobile regions cause local interaction that retard tracer migration. In streams, the mobile domain is given by the main channel, while the storage zones represent the immobile regions. In the one-dimensional case, the migration of a solute along the mobile domain is described by the following mass balance equation (*Haggerty et al.*, 2000)

$$\frac{\partial C_W}{\partial t} + \Gamma_S(x,t) = \frac{\partial}{\partial x}\left(D_L \frac{\partial C_W}{\partial x} - U C_W\right), \tag{2.10}$$

where $\Gamma_S(x,t)$ $[\mathrm{ML}^{-3}\mathrm{T}^{-1}]$ is the source-sink term for the mass exchange with the immobile sites and it is commonly assumed to be independent of x. Equation (2.10) is essentially the same as (1.18) with $\Gamma_S(x,t) = -P/A\Phi_S(x,t)$.

The source-sink term $\Gamma_S(t)$ can be expressed as a derivative of the concentrations in the immobile domains (*van Genuchten and Wierenga*, 1976), but it is often more convenient to express it as a convolution integral, following *Carrera et al.* (1998). This is given by:

$$\begin{aligned}\Gamma_S(t) = \int_0^t \frac{\partial C_W(x,t-\tau)}{\partial \tau} f_M(\tau)\,d\tau &= \frac{\partial C_W(x,t)}{\partial t} * f_M(t) \\ &= C_W * \frac{\partial f_M(t)}{\partial t} + C_W(x,t) f_M(0) - C_W(x,0) f_M(t),\end{aligned} \tag{2.11}$$

where the asterisk denote convolution product, and $f_M(t)$ is a memory function [T^{-1}]. A general form of the memory function can be given as (*Haggerty et al.*, 2000; *Carrera et al.*, 1998)

$$f_M(t) = \int_0^\infty \alpha p_\alpha(\alpha) e^{-\alpha t}\, d\alpha\,, \tag{2.12}$$

where α is a rate coefficient [T^{-1}] and $p_\alpha(\alpha)$ is a probability density function of first-order coefficients [T].

Haggerty et al. (2000) presented a number of possible forms for the density $p_\alpha(\alpha)$. Among these, the truncated power law density has received particular attention in the last decade:

$$p_\alpha(\alpha) = \frac{\beta_{\text{tot}}(\kappa-2)}{\alpha_{\max}^{\kappa-2} - \alpha_{\min}^{\kappa-2}} \alpha^{k-3}, \quad \kappa > 0, \quad k \neq 2, \quad \alpha_{\min} \leq \alpha \leq \alpha_{\max}\,, \tag{2.13}$$

where $\alpha_{\max}$ [T^{-1}] is the maximum rate coefficient, $\alpha_{\min}$ [T^{-1}] is the minimum rate coefficient, and κ is the exponent, and β_{tot} is the capacity coefficient (*Haggerty and Gorelick*, 1995). The capacity coefficient is the zeroth moment of the density function of rate coefficients,

$$\beta_{\text{tot}} = \int_0^\infty p_\alpha(\alpha)\, d\alpha\,, \tag{2.14}$$

and turns out to be the ratio of mass in the immobile domain to mass in the mobile domain at equilibrium, or simply the ratio of the two volumes in absence of sorption (*Haggerty et al.*, 2000). The memory function $f_M(t)$ is given by

$$f_M(t) = \beta_{\text{tot}} \int_{\alpha_{\min}}^{\alpha_{\max}} \frac{(k-2)\alpha^{k-2} e^{-\alpha t}}{\alpha_{\max}^{k-2} - \alpha_{\min}^{k-2}}\, d\alpha\,. \tag{2.15}$$

This is a summation of exponential distributions with a power-law weighting function. The resulting memory function scales as $f_M \sim t^{1-k}$ between the times

$\alpha_{\max}^{-1}$ and $\alpha_{\min}^{-1}$. Equation (2.10) combined with the memory function given by (2.15) has been found to provide good approximation of experimental tracer breakthrough curves in a few cased studies (*Haggerty and Wondzell*, 2002; *Gooseff et al.*, 2003b, 2007).

2.5 The continuous time random walk approach (CTRW)

In the conceptual framework of the continuous time random walk (*Montroll and Weiss*, 1965; *Scher and Lax*, 1973), the motion of solute molecules (or "particles") is envisioned as a sequence of displacements (or "jumps") of variable length and duration considered as random variables. In this framework, the concentration of a solute at a given instant and position is derived statistically as the probability for a particle to occupy the specified position at the specified time. The classical advection-dispersion equation (ADE) can be derived as a special case of a continuous time random walk in which every displacement has the same length and occurs in random directions at regular time intervals (e.g. *Fischer et al.*, 1979). In the CTRW theory the length and duration of particle jumps are random variables with joint probability density function (PDF) $\Psi(x,t)$, and marginal distributions $\psi_L(x)$ and $\psi_T(t)$, respectively. This conceptualization of particle motion leads to the following generalized master equation (GME) :

$$\frac{\partial C(x,t)}{\partial t} = -\int_0^t f_M(t-\tau)\left[U\frac{\partial C(x,\tau)}{\partial x} - D_L\frac{\partial^2 C(x,\tau)}{\partial x^2}\right]d\tau\,, \tag{2.16}$$

where

$$U = \frac{1}{\bar{t}}\int_{-\infty}^{+\infty} x\psi_L(x)\,dx\,, \tag{2.17}$$

$$D_L = \frac{1}{2\bar{t}}\int_{-\infty}^{+\infty} x^2\psi_L(x)\,dx\,, \tag{2.18}$$

are the time-invariant velocity and longitudinal dispersion coefficient, respectively, over the averaging timescale $\bar{t}$. The function $f_M(t)$ in equation (2.16) is a

memory function defined in the Laplace domain as

$$\widetilde{f}_M(s) = s\bar{t}\frac{\widetilde{\psi}_T(s)}{1-\widetilde{\psi}_T(s)}, \tag{2.19}$$

where the symbol ($\widetilde{\ }$) denotes Laplace transform,

$$\widetilde{f}_M(s) = \int_0^\infty f_M(t)e^{-st}\,dt, \tag{2.20}$$

and s is the Laplace variable.

The structure of the GME (2.16) is analogous to the ADE, but with the addition of a convolution integral with the memory function $f_M(t)$. This memory function depends uniquely on the marginal distribution of the jump duration, $\psi_T(t)$, while the parameters U and D_L are given respectively by the first and second moment of the length PDF $\psi_L(x)$. The presence of a convolution integral implies that the equation is, in general, nonlocal in time. As a special case, the GME reduces to the conventional ADE when $\psi_T(t)$ is an exponential PDF, which implies that $f_M(t)$ is a Dirac delta function, $f_M(t) = \delta(t)$. By providing a suitable expression of $\psi_T(t)$, the GME can be used to describe the typical non-Fickian behavior of the observed tracer breakthrough curves. The CTRW approach has been widely applied to study anomalous dispersion in fractured and heterogeneous media (e.g. *Berkowitz and Scher*, 1995; *Scher et al.*, 2002), and has recently been applied to the transport of solutes in streams (*Boano et al.*, 2007).

2.6 Fractional advection-dispersion equation (FADE)

A generalization of the classical advection-dispersion equation can be given using mathematical tools of fractional calculus. The right and left derivative of order ϵ

can be defined respectively as (*Samko et al.*, 1993):

$$\partial^{\epsilon}_{+x} C(x,t) = \frac{1}{\Gamma(n-\epsilon)} \frac{d^n}{dx^n} \int_{-\infty}^{x} (x-\xi)^{n-\epsilon-1} C(\xi,t)\, d\xi\,, \tag{2.21a}$$

$$\partial^{\epsilon}_{-x} C(x,t) = \frac{(-1)^n}{\Gamma(n-\epsilon)} \frac{d^n}{dx^n} \int_{x}^{\infty} (\xi-x)^{n-\epsilon-1} C(\xi,t)\, d\xi\,, \tag{2.21b}$$

where n is the minimum integer greater than or equal to ϵ and

$$\Gamma(x) = \int_0^{\infty} \xi^{x-1} e^{-\xi} d\xi \tag{2.22}$$

is the gamma function. While the integer derivative provides information about the local function behavior, the fractional derivative provides information about the whole function *Blank* (1996). The fractional derivative operator can be said to be the weighted averaging operator of the entire function at a certain point, and the fractional order is linked to the spatial correlation length of the embedding system (*Kim and Kavvas*, 2006).

Using fractional order derivatives, Fick's law can be generalized to the form (*Chaves*, 1998; *Metzler and Klafter*, 2000; *Schumer et al.*, 2001)

$$\Phi = -D_{\epsilon} \left(\frac{1+\varsigma}{2} \partial^{\epsilon-1}_{+x} + \frac{1-\varsigma}{2} \partial^{\epsilon-1}_{-x} \right) C + UC\,, \quad 0 < \epsilon \leq 1\,, \tag{2.23}$$

where D_{ϵ} is a dispersion coefficient and $-1 \leq \varsigma \leq 1$ is a skewness parameter. For $\epsilon = 1$ and $\varsigma = 0$ (2.23) reduces to the classical Fick's law. Combining equation (2.23) with the continuity equation, the fractional advection-dispersion equation is obtained:

$$\frac{\partial C}{\partial t} + U \frac{\partial C}{\partial x} = D_{\epsilon} \left(\frac{1+\varsigma}{2} \partial^{\epsilon}_{+x} + \frac{1-\varsigma}{2} \partial^{\epsilon}_{-x} \right) C\,. \tag{2.24}$$

In writing (2.24) the flow cross sectional area A and the dispersion coefficient D_{ϵ} were assumed to be independent of x. The solution of equation (2.24) for

an impulsive injection of a mass of tracer M_0, that is $C(x,0) = M_0/A\delta(x)$, can be derived using the Fourier transform and is given by

$$C(x,t) = \frac{1}{4\pi^2}\frac{M_0}{A}\int_{-\infty}^{\infty} p(k,t)e^{ik(x-Ut)}dk\,, \tag{2.25}$$

where i is the immaginary unit, k is the wavenumber $[\mathrm{L}^{-1}]$ and $p(k,t)$ is a function is defined as

$$p(k,t) = \exp\left[|k^{\epsilon}|D_{\epsilon}\cos\left(\epsilon\frac{\pi}{2}\right)t\right] \times \exp\left[i|k^{\epsilon}|\varsigma D_{\epsilon}\sin\left(\epsilon\frac{\pi}{2}\right)t\right]. \tag{2.26}$$

This can be shown to be the characteristic function of a Levy distribution.

Depending on the parameters ϵ, ς and D_{ϵ}, the residence time distributions predicted by the fractional advection-dispersion equation can be sensibly skewed and heavy tailed resembling those typically observed in natural streams. Applications of the fractional ADE has been reported by *Deng et al.* (2004) and *Deng et al.* (2006) showing good agreement with experimental data. The main limitation of the fractional approach is that the real physics of the transport processes involved is hidden in a complex mathematical formalism making the parameters difficult to interpret.

Chapter 3

The STIR model[1]

3.1 Introduction

The models presented in the previous chapter provide a mathematical description of how the concentration of a solute transported in a stream is affected by retention processes. Among these, the MRMT and the CTRW approach enable general residence time distribution (RTD) modeling, which is a particularly flexible way to represent retention phenomena in streams. This chapter presents an alternative conceptual model (STIR) that provides a physically based description of the stream-storage zone interactions on river mixing. A first simpler version of the STIR model was presented by *Marion and Zaramella* (2005b) as a multiple process extension of the single process stochastic model proposed by *Hart* (1995). Here, the STIR model is presented in a comprehensive mathematical framework that extends the original formulation. It is shown that, under specific assumptions, STIR converges to other models, such as the TSM, the Multirate Mass Transfer (MRMT) and the CTRW approach. For practical applications STIR can be seen as an extension of Transient Storage Model (TSM) in which general forms of the

[1]The contents of this chapter have been published in: Marion, A., M. Zaramella, and A. Bottacin-Busolin (2008), Solute transport in rivers with multiple storage zones: The STIR model, *Water Resour. Res.*, 44, W10406.

storage time statistics can be implemented. The capability of the model is illustrated with a theoretical example. Further applications of the model to tracer test data from both natural streams and flume experiments will be presented in the next chapters.

3.2 The STIR model

The development of a model that mimics the longitudinal dispersion of a solute in a river, coupled with transient storage, requires the schematization of the system and an adequate degree of synthesis of the physics governing the processes. The stream is modeled as a one-dimensional system where x is the longitudinal distance, A is the cross-sectional area, U is the mean stream velocity and D_L is the longitudinal dispersion coefficient. It must be stressed that, in this conceptual framework, D_L accounts only for the effect of the surface flow field, and does not coincide with the "comprehensive" longitudinal dispersion coefficient often used to lump transient storage into the mass balance equation. Since the goal of this modeling approach is to separate the processes, the river is represented as a system composed by distinct physical domains interacting with each other through mass exchanges. The river is divided into the surficial stream in the main channel and different retention domains, such as surficial dead zones and the hyporheic layer. The downstream transport of solutes is assumed to be controlled by exchanges with N types of storage zones, each one characterized by a given residence time distribution.

3.2.1 Residence times in the surface stream and in the storage zones

The propagation of a solute along a river is treated as a stochastic process. The time needed for a particle to travel a distance x, indicated with $\mathcal{T}$, is a random variable with probability density function $r(t;x)$. The time $\mathcal{T}$ is the sum of a time $\mathcal{T}_W$ spent on the surface, with PDF $r_W(t;x)$, and a time $\mathcal{T}_S$ sum of the single residence times within the storage domains, $\mathcal{T}_S = \sum_{i=1}^{N} \mathcal{T}_{Si}$. A particle moving

from the main stream into a storage zone follows a certain path and may possibly return back to the main stream after some time. Particles may be uptaken once, twice or more, resulting in a global behavior that is the sum of individual paths partly in the main surface flow, partly in the retention domains. It is assumed that the longitudinal displacements within the storage zones are negligible compared to the displacement in the surface water. The number of times a particle is trapped in the i-th retention domain, $\mathcal{N}_i$, is a discrete random variable ($\mathcal{N}_i = 0, 1, 2\ldots$) with conditional distribution $p_i(n|\mathcal{T}_W = t_W)$. When a particle is trapped in a storage zone, it is released after a time with PDF $\varphi_i(t)$. Since the trapping events are assumed independent, the time $\mathcal{T}_{Si}$ has conditional density

$$r_{Si|n}(t) = \varphi_i(t) \underbrace{*\ldots*}_{n \text{ times}} \varphi_i(t) = [\varphi_i(t)]^{*n}, \tag{3.1}$$

given $\mathcal{N}_i = n$. Here the symbol $(*)$ denotes time convolution, so that $\varphi(t) * \varphi(t) = \int_0^t \varphi(\tau)\varphi(t-\tau)\,d\tau$, where τ is a dummy variable. When $n = 0$, equation equation (3.1) yields $r_{Si|0}(t) = \delta(t)$, where $\delta(t)$ is the Dirac delta function (s^{-1}). It follows that the conditional density of $\mathcal{T}_{Si}$ given $\mathcal{T}_W = t_W$ is

$$r_{Si}(t|t_W) = \sum_{n=0}^{\infty} p_i(n|t_W)\, r_{Si|n}(t). \tag{3.2}$$

When the transport process is dominated by advection, the uptake probability, p_i, can also be thought as a function of the travel distance, x, which is proportional to the mean time spent on the surface. The condition of dominant-advection is generally given as (*Rutherford*, 1994)

$$\frac{x}{U} \gg \frac{D_L}{U^2}, \tag{3.3}$$

which is satisfied in most practical applications in rivers. The spatial dependence could also be more appropriate when there is a low density of retention zones.

The probability of a particle to be uptaken at a given instant is assumed to be unconditioned by its previous storage history, then $\mathcal{T}_{Si}$, $i = 1,\ldots,N$, are mutually independent, and the conditional density of $\mathcal{T}_S$ given $\mathcal{T}_W = t_W$ is

$$r_S(t|t_W) = r_{S_1}(t|t_W) * \ldots * r_{S_N}(t|t_W). \tag{3.4}$$

A particle moving along the stream follows an irregular path due to turbulence. Following well established results from the literature (*Taylor*, 1954; *Elder*, 1959; *Fischer*, 1968), the motion of a particle limited only to surface flow in the main channel can be described as equivalent to a Brownian motion with drift, and the relevant residence time distribution can be inferred from the solution of the advection-dispersion equation (ADE). If it is now assumed that the entrapment within the storage zones does not modify the particle pathways, then the residence time within the surface stream remains unaltered. Thus, when the computational domain is $x > 0$, with boundary condition at infinity $C(x \to \infty, t) = 0$, the function $r_W(t;x)$ is given by:

$$r_W(t;x) = \frac{x}{2\sqrt{\pi D_L t^3}} \exp\left[-\frac{(x-Ut)^2}{4D_L t}\right]. \tag{3.5}$$

Equation equation (3.5) is derived from the solution of the ADE for an input mass pulse, $UC - D_L \partial_x C = M_0/A\delta(t)$ at $x = 0$, where M_0 is the injected mass.

It is now possible to express the overall residence time distribution within a stream reach of length x as

$$r(t;x) = \int_0^t r_W(t-\tau;x)\, r_S(\tau|t-\tau)\, d\tau\,. \tag{3.6}$$

Alternatively, when the total storage time is assumed to be dependent on the

travel distance, thus using $r_S(t;x)$ instead of $r_S(t|t_W)$, the overall RTD is given by:

$$r(t;x) = r_W(t;x) * r_S(t;x). \tag{3.7}$$

3.2.2 Uptake probability for uniformly spaced storage zones

Under the assumption of uniform distribution of storage zones along the river, the uptake probability can be expressed as follows. The probability for a particle in the surficial stream to be stored in the i-th domain in a time interval δt is assumed to be proportional to the length of the interval. It is expressed as $\alpha_i \delta t$, where α_i [T^{-1}] is the probability per unit time, which is taken to be constant both in time and space (although the temporal constance is not strictly required). The quantities α_i represent the rates of transfer or, in other words, the flow rate into the storage zones per unit surficial volume. When hyporheic exchange with the stream bed is considered, the relevant rate α_B can be expressed as

$$\alpha_B = \frac{q_B}{d_W}, \tag{3.8}$$

where q_B is the average flow rate into the sediments per unit bed area [$\mathrm{L\,T}^{-1}$], and d_W is the flow depth [L].

Since the probability for a particle to be caught in the i-th storage zone at a given instant is independent from its previous history, the probability for a particle to be caught n times in a time interval t_W is given by the Poisson distribution with parameter $\alpha_i t_W$:

$$p_i(n|t_W) = \frac{(\alpha_i t_W)^n}{n!} e^{-\alpha_i t_W}. \tag{3.9}$$

Alternatively, the uptake probability can be thought as a function of the distance from the injection point, $x_0 = 0$, thus

$$p_i(n;x) = \frac{(\alpha_i x/U)^n}{n!} e^{-\alpha_i x/U}. \tag{3.10}$$

It is finally noted that, when equation equation (3.9) is used for the uptake probability, the Laplace Transform (LT) of the overall residence time distribution expressed by equation equation (3.6) can be arranged, after some mathematical manipulations, in the following form (*Margolin et al.*, 2003):

$$\widetilde{r}(s;x) = \int_0^\infty r(t;x)\, e^{-st}\, dt = \widetilde{r}_W \left(s + \sum_{i=1}^{N} \alpha_i (1 - \widetilde{\varphi}_i(s)); x \right), \tag{3.11}$$

where the symbol $\widetilde{(\cdot)}$ denotes Laplace Transform of the function it is applied to. Equation equation (3.11) shows that in Laplace domain the resulting residence time PDF is the same found in the absence of any retention process, but with a frequency shift that depends on the storage time PDFs.

3.2.3 Example 1. Residence time distribution in surface dead zones

The exchange with surface dead zones of finite volume is well represented by an exponential RTD. The expression of the single-uptake storage time PDF is then the following

$$\varphi_D(t) = \frac{1}{T_D}\, e^{-t/T_D}, \tag{3.12}$$

where T_D is a time scale, equal to the mean residence time. In practice the effect of the surface dead zone retention usually acts in a relatively short time scale compared to hyporheic retention, and can often be measured by tracer tests.

3.2.4 Example 2. Residence time distribution of bed form-induced hyporheic retention

Hyporheic flows are hardly measurable by direct methods, such as tracer tests, unless very long and very expensive techniques are designed (*Johansson et al.*, 2001; *Wörman et al.*, 2002; *Gooseff et al.*, 2003a; *Jonsson et al.*, 2003, 2004). The Advective Pumping Model (APM) (*Elliott and Brooks*, 1997a) provides an expression for the cumulative residence time function within the sediments for bed

form-induced exchange. Elliott's solution was given in term of an implicit function of time, whereas the application of equations equation (3.6), equation (3.7) and equation (3.11) requires an explicit form of the PDF of the residence time within the sediments $\varphi_B(t)$. An analytical expression of $\varphi_B(t)$ that approximates the exact solution for the case of the bed form-induced exchange is (*Marion and Zaramella*, 2005b):

$$\varphi_B(t) = \frac{\pi/T_B}{\frac{\beta T_B}{t} + \left(\frac{t}{T_B} + 2\right)^2}, \tag{3.13}$$

where the parameter β satisfies the following equation:

$$\int_0^\infty \varphi_B(t)\,dt = \int_0^\infty \frac{\pi/T_B}{\beta T_B/t + (t/T_B + 2)^2}\,dt = 1\,. \tag{3.14}$$

Equation equation (3.14) is a necessary condition to make $\varphi_B(t)$ a PDF and is satisfied by $\beta = 10.66$. Parameter T_B represents a residence timescale in the subsurface. The proposed residence time PDF is a single parameter heavy-tailed distribution that, for $t \to \infty$, decays as a power law, $\varphi_B(t) \sim \pi T_B t^{-2}$. Comparison between the exact and the approximate expression of $\varphi_B(t)$ is reported in Figure 3.1.

3.2.5 Solute concentration in the surface stream and in the storage domains

In this section, a relationship between the in-stream solute concentration and the residence time distribution is derived.

Consider a stream reach of length x in which a mass M_0 is instantaneously injected at the upstream section, $x_0 = 0$, at time $t_0 = 0$. At any instant $t > 0$, a part of the total mass is distributed in the main surficial stream, while a part is temporarily retained within the storage domains. The relevant masses are indicated by M_W and M_S, respectively. The total concentration is then defined as:

$$C(x,t) = \lim_{\delta x \to 0} \frac{\delta M_W(x,t) + \delta M_S(x,t)}{A\delta x} = C_W(x,t) + \lim_{\delta x \to 0} \frac{\delta M_S(x,t)}{A\delta x}, \tag{3.15}$$

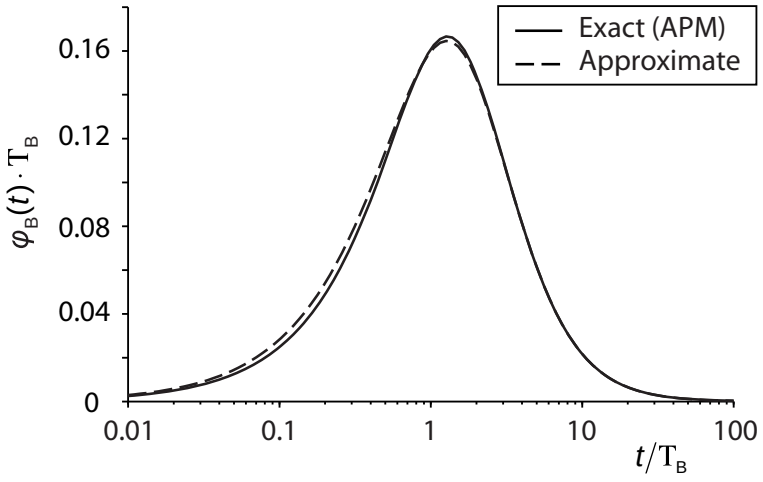

Figure 3.1. Comparison between the exact and the approximate PDF of the residence time within the sediment. The gap between the two curves is visible only at early times and is negligible for practical applications.

where $\delta M_W(x,t)$ and $\delta M_S(x,t)$ are the masses contained within the spatial interval $[x, x+\delta x]$ at time t in the superficial stream and in the storage zones, respectively.

The quantity $r(t;x)dt$ represents the fraction of mass flowing through the downstream section in the time interval $[t, t+dt]$, and the flux is given by the convolution of $r(t;x)$ with the input flux $\phi_0(t)$. For a mass pulse concentrated in time this is given by $\phi_0(t) = M_0/A\delta(t)$. The variation per unit time of the total concentration is equal to the opposite of the divergence of the local flux, $\phi_0(t) * r(t;x)$, hence

$$\frac{\partial C_\delta(x,t)}{\partial t} = -\frac{\partial}{\partial x}\int_0^t \phi_0(\tau) r(t-\tau;x)\, d\tau = -\frac{M_0}{A}\frac{\partial r(t;x)}{\partial x}, \tag{3.16}$$

where the subscript δ is used to denote the solute concentration generated by a mass pulse. The difference between the input and the output flux at the stream-

storage zone interface is linked to the variation of $C - C_W$ according to:

$$\frac{\partial(C - C_W)}{\partial t} = \sum_{i=1}^{N} \left(\alpha_i C_W(x,t) - \int_0^t \alpha_i C_W(x,\tau) \varphi_i(t-\tau)\, d\tau \right). \tag{3.17}$$

If the total concentration is initially equal to the concentration in the surface stream, $C(x, t = 0) = C_W(x, t = 0)$, equation *equation* (3.17) can be written in the Laplace domain as

$$s\widetilde{C}(x,s) = \left[s + \sum_{i=1}^{N} \alpha_i (1 - \widetilde{\varphi}_i(s)) \right] \widetilde{C}_W(x,s), \tag{3.18}$$

and defining the new variable

$$\nu(s) = s + \sum_{i=1}^{N} \alpha_i (1 - \widetilde{\varphi}_i(s)), \tag{3.19}$$

we obtain

$$\widetilde{C}(x,s) = \frac{\nu(s)}{s} \widetilde{C}_W(x,s). \tag{3.20}$$

By combining equation (3.20) with the LT of equation (3.16), we get:

$$\widetilde{C}_{W\delta}(x,s) = -\frac{M_0/A}{\nu(s)} \frac{\partial \widetilde{r}(s;x)}{\partial x}, \tag{3.21}$$

which relates the superficial concentration and the overall residence time distribution. Now, using expression equation (3.11), equation (3.21) becomes

$$\widetilde{C}_{W\delta}(x,s) = \widetilde{C}_{AD\delta}(x, \nu(s)), \tag{3.22}$$

where $C_{AD\delta}(x,t)$ is the solution of the advection-dispersion equation (ADE) with the boundary condition given by the same input mass pulse.

If the residence time in the storage zones is assumed to be dependent on the

distance from the injection point, and equation equation (3.7) is used instead of equation (3.6), an alternative expression can be found for the concentration C_W. The balance expressed by equation (3.17) now becomes

$$\frac{\partial(C - C_W)}{\partial t} = -\phi_0(t) * r_W(t;x) * \frac{\partial r_S(t;x)}{\partial x}. \tag{3.23}$$

Combining equation (3.23) with equation (3.16), with $r(t;x) = r_W(t;x) * r_S(t;x)$, and integrating over time, we get, for a mass pulse,

$$C_{W\delta}(x,t) = C_{AD\delta}(x,t) * r_S(t;x). \tag{3.24}$$

Equations equation (3.22) and equation (3.24) provide a relationship between the system elementary responses in case of pure advection-dispersion and the case with temporary storage. Although these relations have been derived considering a mass pulse concentrated in time, $M_0/A\delta(t)$, they are also valid for a mass initially concentrated in space and for a concentration pulse. In any case, the elementary response, $C_{W\delta}$, can always be derived from corresponding solutions of the ADE. Once the elementary response is known, the solution to the general case of an initially distributed mass and a given time dependent boundary condition is readily found by spatial and temporal convolution, respectively.

It is finally noted that, far from the injection point, when condition equation (3.3) holds, the residence time function in the main channel is well approximated by

$$r_W(t;x) \simeq \frac{Q}{M_0} C_{AD\delta}(x,t), \tag{3.25}$$

and therefore, using equation (3.24),

$$C_{W\delta}(x,t) \simeq \frac{M_0}{Q} r(t;x), \tag{3.26}$$

which provides a direct relation between the overall residence time distribution and the concentration in the surface stream. The validity of equation (3.26) was one of the assumptions of the original version of the STIR model (*Marion and Zaramella*, 2005b).

3.3 STIR and other approaches

It is now shown that, under certain assumptions, the STIR model converges to other established models. If the transport process in the superficial water is assumed to be Fickian, with additional fluxes due to mass exchanges with the storage zones, and if the downstream transport of the temporarily stored mass is neglected, then the mass balance for the in-stream solute concentration can be written as:

$$\frac{\partial C_W(x,t)}{\partial t} + U\frac{\partial C_W(x,t)}{\partial x} = D_L\frac{\partial^2 C_W(x,t)}{\partial x^2} + \\ - \sum_{i=1}^{N}\left(\alpha_i C_W(x,t) - \int_0^t \alpha_i C_W(x,\tau)\varphi_i(t-\tau)d\tau\right). \tag{3.27}$$

Equation equation (3.27) is formally similar to the advection-dispersion-mass transfer equation (2.10) used by *Haggerty et al.* (2000), extended to account explicitly for different retention processes through the relevant residence time PDFs. When a single type of storage zone is considered, and the single-uptake residence time function $\varphi(t)$ is given by equation (3.12) with $T_D = A_S/(\alpha A)$, equation equation (3.27) becomes equivalent to the TSM equations, equation (2.1a) and equation (2.1b).

Using Laplace Transforms, equation (3.27) becomes

$$\left[s + \sum_{i=1}^{N}\alpha_i\left(1-\widetilde{\varphi}_i(s)\right)\right]\widetilde{C}_W(x,s) + U\frac{\partial \widetilde{C}_W(x,s)}{\partial x} - D_L\frac{\partial^2 \widetilde{C}_W(x,s)}{\partial x^2} = C_{W0}(x), \tag{3.28}$$

where $C_{W0}(x) = C_W(x, t=0)$ is the initial in-stream concentration distribution. It

is now observed that, if $C_{AD}(x,t)$ is a solution of the classical advection-dispersion equation (ADE) with initial condition $C_{AD}(x,t=0) = C_{W0}(x)$, then $\widetilde{C}_{AD}(x,\nu(s))$, with $\nu(s)$ given by equation (3.19), is a solution of equation (3.28). Hence, when the uptake process is considered a temporal Poisson process, and the transport in the main channel is assumed to be Fickian, the stochastic approach of the STIR model leads to the exact solution of equation equation (3.27).

The Continuous Time Random Walk approach as proposed by *Boano et al.* (2007) for solute transport in rivers is now considered. As explained in § 2.5, this approach relies on the following Generalized Master Equation (GME):

$$\frac{\partial C(x,t)}{\partial t} = \int_0^t f_M(\tau)\left[-U\frac{\partial C(x,t-\tau)}{\partial x} + D_L\frac{\partial^2 C(x,t-\tau)}{\partial x^2}\right]d\tau\,, \tag{3.29}$$

where $f_M(t)$ is a memory function. The GME is written in the Laplace domain as

$$s\widetilde{C}(x,s) - C_0(x) = \widetilde{f}_M(s)\left[-U\frac{\partial \widetilde{C}(x,s)}{\partial x} + D_L\frac{\partial^2 \widetilde{C}(x,s)}{\partial x^2}\right], \tag{3.30}$$

with $\widetilde{f}_M(s)$ given by

$$\widetilde{f}_M(s) = s\bar{t}\frac{\widetilde{\psi}_T(s)}{1-\widetilde{\psi}_T(s)}, \tag{3.31}$$

where $\psi_T(t)$ is the PDF of the jump durations (or transition rate probability), and $\bar{t} = x/U$ is the average travel time. When $\psi_T(t)$ is given by an exponential PDF, $\psi_T(t) = \exp(-t/\bar{t})/\bar{t}$, the memory function $f_M(t)$ is a Dirac delta function, and equation equation (3.29) reduces to the ADE (*Margolin and Berkowitz*, 2000). If solute uptake into the storage zones is assumed to be a Poisson process that only immobilizes the particles without changing the pathways, the Laplace Transform of $\psi_T(t)$ can be expressed as $\widetilde{\psi}_T(s) = \widetilde{\psi}_{T0}(s + \sum_i \alpha_i(1-\widetilde{\varphi}_i(s))) = \widetilde{\psi}_{T0}(\nu(s))$, where $\psi_{T0}(t)$ is the PDF of the jump durations in the absence of any retention process (an exponential PDF) (*Margolin et al.*, 2003; *Cortis et al.*, 2006; *Boano et al.*, 2007). For this choice of $\psi_T(t)$ it is readily seen that, if $C_{AD}(x,t)$ is a solution of the ADE

with initial condition $C_{AD}(x, t = 0) = C_0(x)$, then

$$\widetilde{C}(x,s) = \frac{\nu(s)}{s}\widetilde{C}_{AD}(x,\nu(s)) \tag{3.32}$$

is a solution of equation equation (3.30). This relation coincides with equation (3.21) for the total concentration. The main difference between the CTRW approach and the STIR model, as for the MRMT formulation, is that the CTRW is more comprehensive, being based on less restrictive assumptions, at least in its general form. The CTRW provides an overall description of solute transport without the need to split the physical domains. This makes it advantageous when a separation between surface transport and storage is not needed. As a counterpart, the CTRW is less explicit when a distinct parameterization of individual processes is required, for example when individual modeling closures are under investigations.

3.4 Potential application

An example is now used to illustrate the application of STIR to assess the effects of different transport processes in a river. An application to an ideal case is presented where surface retention, hyporheic retention and reversible adsorption are sequentially added.

The simulation is performed for a uniform river with depth $d_W = 0.75\,\mathrm{m}$ and width $b = 20\,\mathrm{m}$. The flow rate is $Q = 5\,\mathrm{m^3 s^{-1}}$ and the longitudinal dispersion coefficient is assumed to be $D_L = 5\,\mathrm{m^2 s^{-1}}$. The hyporheic retention is treated using the pumping model (APM) where the exchange parameters are linked to the bed form wavelength λ and the sediments permeability K by the relations:

$$\mathrm{T}_B = \frac{\lambda^2\theta}{4\pi^2 K h_m}, \tag{3.33}$$

$$q_B = \frac{2Kh_m}{\lambda}, \tag{3.34}$$

where θ is the sediment porosity and h_m is the half-amplitude of the sinusoidal dynamic head on the surface given by *Felhman* (1985):

$$h_m = 0.28\frac{U^2}{2g}\begin{cases}\left(\dfrac{H/d_W}{0.34}\right)^{3/8}, & H/d_W \leq 0.34\\ \left(\dfrac{H/d_W}{0.34}\right)^{3/2}, & H/d_W > 0.34\end{cases}, \tag{3.35}$$

where H is the bed form height. It is assumed that the sediment permeability is $K = 5\times10^{-3}\,\mathrm{m\,s^{-1}}$, the porosity is $\theta = 0.3$ and the bed forms have uniform height $H = 0.05\,\mathrm{m}$ and wavelength $\lambda = 10H$. The application of the advective pumping theory gives a rate of transfer $\alpha_\mathrm{B} = q_\mathrm{B}/d_W = 2.3\times10^{-5}\,\mathrm{s^{-1}}$ and a time scale for the residence time within the sediments $\mathrm{T_B} = 441\,\mathrm{s}$. When reversible, equilibrium adsorption of solutes to sediment surfaces is present, the net effect on the hyporheic retention can be modeled by simply multiplying this time scale by a retardation factor $R_\mathrm{ad} > 1$ (*Zaramella et al.*, 2006).

The exchange parameters for the transient storage in the dead zones are here simply defined as follows: the rate of transfer α_D is taken to be two orders of magnitude larger than α_B, while the mean residence time in the dead zones $\mathrm{T_D}$ is taken to be an order of magnitude shorter than $\mathrm{T_B}$. In practical applications these parameters can often be determined by model calibration on the basis of tracer tests.

An injection of a tracer at a constant rate for two hours is simulated, and the resulting concentration is evaluated 2 km downstream from the source. Figure 3.2 shows, in linear space (a) and in log-log space (b), the normalized concentration distributions obtained by gradually incorporating different transport processes: curve (i) is the distribution relevant to in-stream advection-dispersion; curve (ii) represents the distribution obtained by adding the exchange with dead zones; curve (iii) is obtained by adding the bed form-induced hyporheic ex-

change; finally, curve (iv) represents the combined effect of surficial transport, surface and hyporheic retention, and reversible sorption to sediments with a retardation factor $R_{ad} = 2.5$. It is clear that the transient storage in the subsurface generates a delay in the downstream propagation of solutes and a longer tail in the breakthrough curves. Figure 3.3 shows, for the case (iii), a comparison between the breakthrough curves obtained using equation equation (3.22), which assumes a temporal Poisson process, and the concentration obtained with equation equation (3.24), assuming a spatial Poisson process. The two equations provide very similar results due to the dominance of advection over surface dispersion in this example.

3.5 Conclusions

Solute transport in rivers is influenced by complex interactions between the overlying stream and the sediment bed. Direct measurements by tracer tests usually allow the evaluation of the short-term exchange processes only. Exchanges with surface dead zones and with the hyporheic zone generate an overall effect characterized by the superposition of processes acting at different time scales. A model has been presented here that simulates the effect of temporary retention on longitudinal solute transport in rivers. A relation between the in-stream solute concentration and the residence time distributions in different storage domains has been derived by representing the main stream-storage zone exchange as a stochastic process. This formulation allows for each process to be represented separately by a physically based RTD and transfer rate. When the hyporheic exchange is primarily driven by pressure variations on the bed surface induced by irregularities such as bed forms, the advective pumping theory (*Elliott and Brooks*, 1997a, see Chapter 6) can be used to model the temporary detainment of solutes into the bed. Adsorption processes onto the sediment surface can be easily included by applying a retardation factor to the timescale of hyporheic retention.

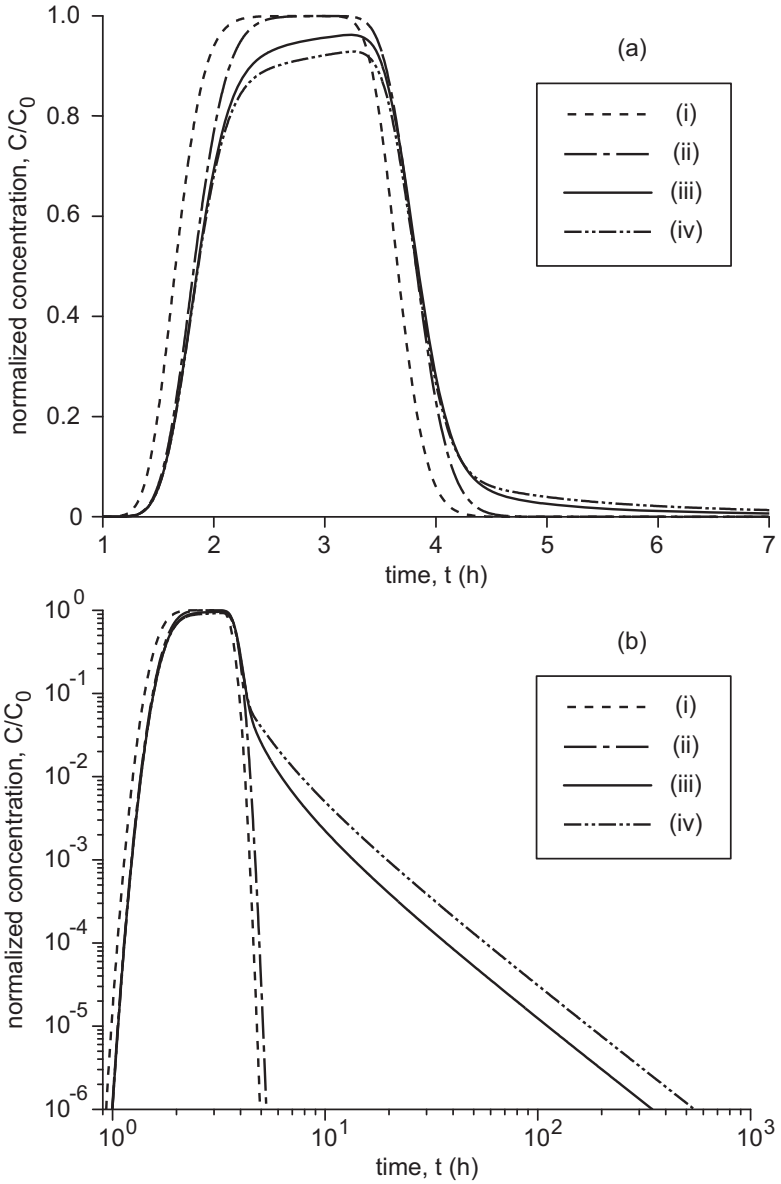

Figure 3.2. Normalized breakthrough curves of an ideal example 2 km downstream of the injection point. Curve (i) represents the advection and dispersion processes in the main surficial stream; curve (ii) was obtained by adding the fast exchanges with the surface dead zones; curve (iii) represents the combined effect of the surficial transport and the deep exchange with sediments; curve (iv) accounts for all the previous processes and for adsorption reactions to the sediment surfaces with a retardation factor $R_{ad} = 2.5$.

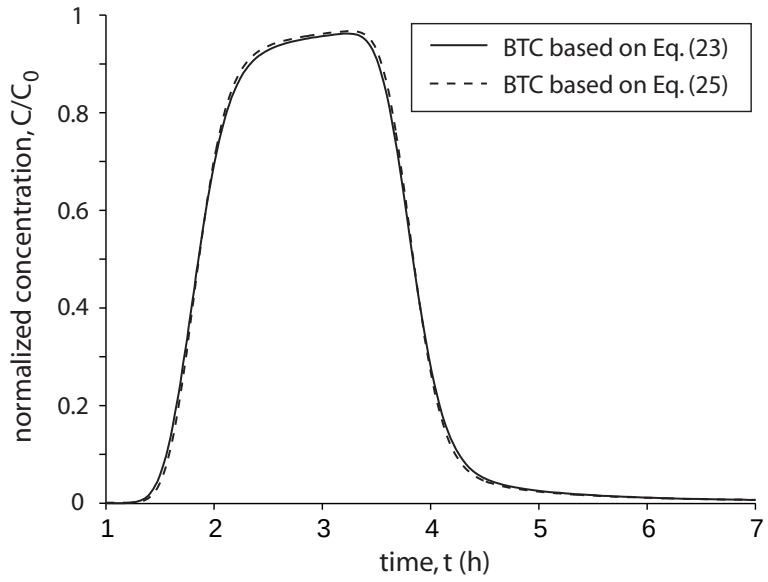

Figure 3.3. Comparison between the concentration distribution predicted by equation equation (3.22), which assumes a temporal Poisson process, and equation (3.24), assuming a spatial Poisson process. The two equations give very similar results because the condition of dominant advection equation (3.3) is well satisfied in this case.

On the other side, fast exchanges with the dead zones can be represented by an exponential RTD. In both cases solute uptake into the storage zones can be taken to be a Poisson process. Other retention phenomena, such as the horizontal hyporheic flows induced by meanders, can similarly be modeled if an appropriate RTD is provided. STIR has also the potential to include the effects of other parameters such as heterogeneity (see Chapter 7 for the case of a stratified bed). Nevertheless, it must be stressed that the model complexity, and the number of parameters, may always be adapted to the practical problem on the basis of the available information and on the objectives of the analysis. A single exponential distribution, or a power-law RTD (as suggested by *Haggerty and Wondzell* (2002)), can be used when there is no need to distinguish between the different storage processes. Conversely, problems requiring an estimate of the hyporheic contamination could be more adequately solved by using a distinct parametrization for

shallow and deep retention. Because the storage within the surficial dead zones and the storage within the sediments are generally characterized by very different time scales, parameter estimation is expected to yield values that are more representative of the physics of the processes. This is partly confirmed by the work of *Choi et al.* (2000) on multiple storage zone extension of the TSM .

Finally it is shown that, under specific assumptions, STIR, MRMT and CTRW yield the same solutions. This leads to a deeper understanding of their respective theoretical formulations and applicability.

Chapter 4

Applications of the STIR model: Three case studies

4.1 Introduction

In many practical applications it is important to characterize transient storage in streams in order to understand the impact of distributed or localize input of contaminants or to understand nutrient cycling in stream ecosystems (*Mulholland et al.*, 1997b; *Thomas et al.*, 2003; *Gooseff et al.*, 2004). Retention processes increase the contact time between dissolved substances and the sediments or microbial communities, such as periphyton or biofilms, thus determining the response of a fluvial system to sources of contamination. Transient storage results from the exchange between the relatively fast moving water in the main channel and storage domains of different type. An important distinction is between the exchange with surface dead zones, such as vegetated side pools or zones of recirculating water (*Thackston and Schnelle*, 1970; *Valentine and Wood*, 1977), and the exchange with the subsurface, with the so called hyporheic zone (*Bencala and Walters*, 1983; *Savant et al.*, 1987). Reach-integrated transport dynamics in streams is usually characterized via tracer experiments: a dissolved tracer is injected in the stream water and the tracer concentration is measured at a section downstream. Breakthrough curves (BTCs) are then simulated with a transport model which is calibrated by fitting the simulations to the experimental data.

This procedure allows to determine velocity, dispersion and retention parameters.

Since in-channel and hyporheic storage processes act simultaneously, tracer tests cannot provide a distinction between these two types of storage mechanisms. *Choi et al.* (2000) experimented with a two storage zone model with exponential RTDs and showed that, unless the timescales of the two storage processes are sensibly different, a multiple storage zone model is unable to discern between the two retention components. Nevertheless, it should be noted that in the work of *Choi et al.* (2000) the breakthrough curves were analyzed in linear scale, thus neglecting important information related to the tail behavior of the BTCs. *Haggerty and Wondzell* (2002) showed that tracer breakthrough curves of a 2nd mountain stream showed a power-law tailing over a wide range of times. Subsequent works by *Gooseff et al.* (2005) and *Gooseff et al.* (2007) provided further experimental evidence of power-law behavior, although part of the data presented in these studies could not be described by a power-law RTD model.

This chapter presents an application of STIR to three case studies: an Israelian river, Yarqon, and two Italian streams, the Brenton torrent and the Desturo canal. The STIR model is calibrated for different study reaches with tracer test data. Two distinct modeling closures are used to represent transient storage. One assumes that the statistics of the residence time in the retention domains is represented by a weighted average of two exponential distributions, as in the model proposed by *Choi et al.* (2000), whereas the other one assumes that transient storage is represented by a power-law RTD, as proposed by *Haggerty et al.* (2000). Results for the two different RTD models are compared and related to the properties of the streams under consideration.

4.2 Site description

4.2.1 The Yarqon river, Israel

The basin of the Yarqon River spreads out along a wide area of the Israeli territory, from the West Bank down to the plain of Tel Aviv. The total extension of the basin is approximately 1805 km^2. The most important affluent of the Yarqon River is the Ayalon River, which drains all the southern area, including Jerusalem region, and flows into the Yarqon River 2 km upstream of its estuary. The population of the entire river basin counts approximately 750,000 inhabitants. Agricultural and industrial activities are present in this area, as well as trading and urban development, leading to one of the highest population density in Israel. The climate is Mediterranean, having long, warm and dry summers, and cold and rainy winters, with high annual rainfall, whose values change with the altitude. January is the colder month, with temperatures from 5 to 15°C, the warmest one is August, with temperatures ranging from 18 to 38°C. Measurements of the Hydrological Service of Israel at the Tel Aviv station (records since 1961) show that the annual rainfall height on the river basin is approximately 550 mm. The mean water discharge at the river sources is about 0.16 $m^3 s^{-1}$. The highest rainfall generally begins in November and ends in March. As a consequence the highest runoff occurs between December and March. During the other period of the year, water flow rates are much lower or even equal to zero, depending on the amount of water drawn at the sources. Most of the water flowing into the river comes from the industrial effluents of several waste-water treatment plants (WWTPs). The growth of the population, associated to the industrial and agricultural development since 1948, made water quality of the Yarqon River increasingly polluted. Contamination is mainly due to the drawing of the river sources and the drainage of the industrial effluents into the main river. As a consequence, many species were extinguished, the lack of predators led to a rapid

increase of mosquitoes, finally increasing the risk for health and hygiene of the population. Recently the regular water discharge of the river has grown, and the water quality and the ecosystem characteristics have been improved. In 1988 the Authority of the Yarqon River basin was founded, with the aim to improve water quality and hydro-geological safety. Local Authorities and several Governmental Agencies joined together in order to plan new waste-water treatment plants and the removal of sediments from the river-bed, in the attempt to bring it back to its original slope and facilitate its natural flow. New water resources were channeled into the river and the embankments were equipped with communication trenches and cycle tracks. Sources of pollution in the entire river basin were reduced during the years from 1994 to 2000. Improvements in waste-water treatment and in water re-use for river rehabilitation are still required. The planimetric map of the river is shown in Figure 4.1. It flows entirely along the coastal strip: the total length is 28 km, the sources altitude is about 50 m above sea level, and its mean bed-slope is 1.8‰. These characteristics of the river profile involve the formation of many meanders, which are typical of mild bed-slopes. The Rosh-Ha Ayin springs were the main water source of the Yarqon River until 1950 (annual runoff was $220,000,000\,\mathrm{m}^3$). Subsequently the water discharge was nearly completely diverted to cover part of the national water demand, i.e. irrigation of the dry southern region and drinking water supply, and nowadays only a small percentage (1%) still flows along the water course. Two natural reservoirs are settled in this area: the Yarkon National Park and the Afeq National Park, which boast wealth of flora and fauna in natural pools. The river flows along a not very populated area for the first 7 km-long reach, and it is uncontaminated until the confluence with the Qanah River, which receives contributes by many industrial effluents before flowing into the Yarqon River. Indeed, the Hades River, which is an affluent of the Qanah River, transports the urban secondary effluents from the Kfar Sava-Hod Hashron WWTP (about $1000\,\mathrm{m}^3\mathrm{hr}^{-1}$ water discharge,

150,000 Equivalent Inhabitants capacity). This plant produces insufficient water softening, in particular for what concerns nutrient removal. During the dry season, its effluent is the main water supply of the Yarqon River and its main pollution source. The central course of the river, a 17 km-long reach, flows around the high populated area of Tel Aviv. Pollution comes from the secondary effluents of Kfar Sava-Hod Hasharon WWTP and from the secondary/tertiary effluents of Ramat Hasharon WWTP (about 69 $m^3 s^{-1}$ water discharge) located approximately 7 km downstream of Kfar Sava-Hod Hasharon WWTP. This treatment plant has a smaller capacity (5000 Equivalent Inhabitants), but a better effectiveness, and it respects the drainage limits given by the River Basin Plan, as a result of an upgrade carried out in 1999. Its discharge reaches the Yarqon River through the Hadarim River. It is noticed that, during the dry season, the effluents of these plants are the main outflows for the Yarqon River, as a consequence of the huge water drawing at the sources and along the river course. Other affluents are small rivers having discontinuous water discharges, as the Shillo River, whose pollution is not meaningful during the rainy season, as the polluted surfaces of the river basin are washed away. A measure for reducing pollution in this area is to allow water reaeration by using small dams or bed sills. The last 4 km-long river reach is navigable, and it is affected by tides and brackish waters. The area around the river mouth shows many erosions for the presence of infrastructures nearby the coastal line. In February 2004 the Committee of Planning and Construction of Tel Aviv approved the demolition of several works and the realization is currently in progress of barriers made with 80 m-long artificial reefs.

A map of the Yarqon river showing the location of the measurement stations is presented in Figure 4.1. Two pictures of the Yarqon river illustrating typical study reaches are shown in Figure 4.2.

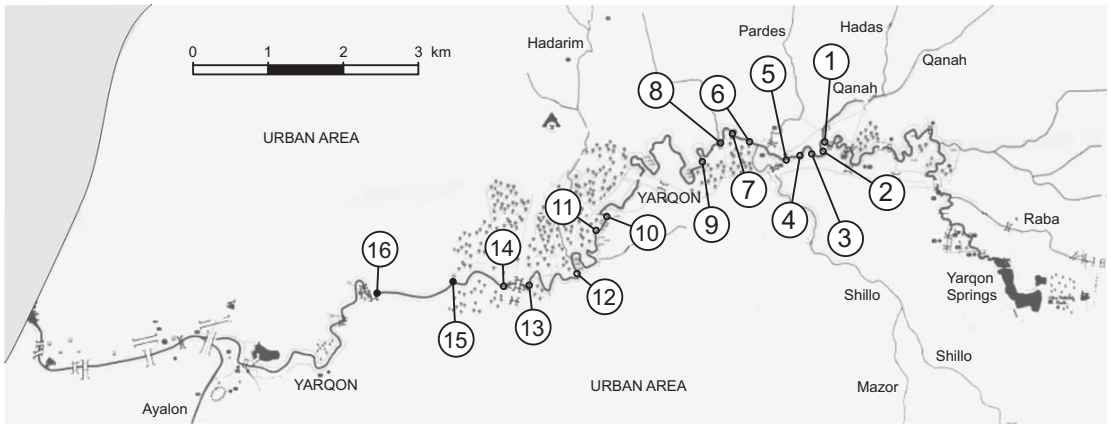

Figure 4.1. Map of the Yarqon river and location of the measurement stations.

Figure 4.2. Pictures of the Yarqon river illustrating typical study reaches.

4.2.2 The Brenton torrent, Italy

The Brenton torrent is an Italian torrential stream located in the area of Treviso in Northern Italy. The tributary catchment has an area of approximately 60 km^2; the elevation from the average sea level varies from 45 to 496 m; the length of the channel is about 13.5 km with an average slope of 4.2‰.

The Brenton catchment basin was formed for the most part by the deposition of sediments transported by the Piave river since the last glaciations. The transported sediments are primarily coarse debris of grit and limestone. The bed is made of a thick, high permeable layer of gravel and is characterized by the presence of iron hydroxide due to the dissolving and hydrolyzing effect that meteoric waters, containing carbonic acid, exert on the gravel.

The overall length of the study reach is about 5.8 km and is characterized by an average slope equal to 4.2‰. The channel is primarily straight but has a few 90° bends and a few large radius bends. The channel cross-section is regular with no flood plains and without sensible variations of the flow cross sectional area, except for a few localized contractions. The channel bed is almost entirely natural, with only a few quite short reaches in which the banks are reinforced with concrete or stone. The banks are thickly vegetated. A map of the Brenton torrent showing the position of the measurement stations of the experimental tests is given in Figure 4.3. Pictures of typical study reaches are given in Figure 4.4.

4.2.3 The Desturo canal, Italy

The Desturo canal is a small 5.6 km-long drainage canal which is part of the drainage basin of the Venice Lagoon in Northern Italy. The canal is located just outside of a urban settlement and is used for irrigation proposes. The Desturo canal is affected by pollution due to distributed inputs of fertilizers used in the agricultural activity. However, the main sources of pollution are due to input of

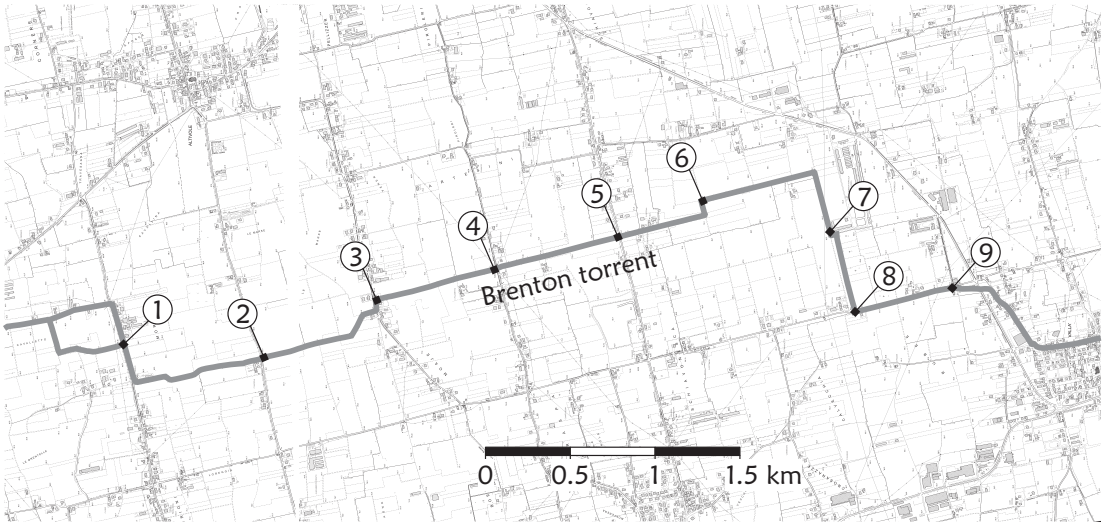

Figure 4.3. Map of the Brenton torrent and position of the measurement stations.

Figure 4.4. Pictures of the Brenton torrent illustrating typical study reaches.

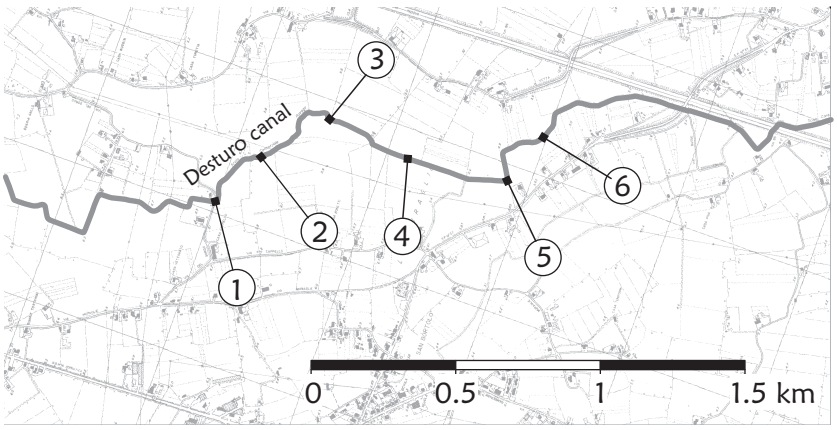

Figure 4.5. Map of the Desturo canal and position of the measurement stations.

waters from a waste-water treatment plant of the nearby Monselice village and to inputs of non-treated water during rain periods from urban drainage systems.

The total length of the study reach is equal to 3300 m and has almost uniform characteristics with few channel bends. The channel cross section is trapezoidal with flood plains and natural banks. The vegetation on the banks is quite thin, with virtually no masts and bushes. The sediment bed is made of a sandy-silty material and at the time of the tests the channel bottom was characterized by the presence of algae, submerged vegetation, and pieces of marsh reeds. A map showing the planimetry of the canal and the location of the measurement stations is given in Figure 4.5. Pictures of a study reach are shown in Figure 4.6.

4.3 Stream tracer experiments

Tracer tests were carried out in the Yarqon river in April 2005, in the Breton torrent in June-July 2007, and in the Desturo canal in October 2007. The experiments consisted in both instantaneous (slug) and continuous (step) injections of rhodamine WT (RWT) fluorescent dye. For step injections, a peristaltic pump was used to ensure a constant continuous rate of input throughout the injection period. In each test RWT concentrations were measured at two downstream sections with a sampling period of 10 s using portable field fluorometers (Turner

Figure 4.6. Pictures of the Desturo canal illustrating a typical study reach.

Design SCUFA). In addition to tracer concentrations, the fluorometers measured water turbidity, which was then used in the detrend procedure of the tracer BTCs to remove artifact generated by variations of water turbidity. Part of the curves are excluded from the analysis presented here due to poor quality of the data, either because the concentration signal was too noisy or because the tail values of the concentration curves could not be obtained for sufficiently long times to permit an unambiguous determination of the model parameters. A summary of the experimental conditions in terms of injected mass M_0 and length of the injection period Δt_{inj} (with $\Delta t_{\text{inj}} = 0$ for slug tests) is given in Table 4.1a for the Yarqon river, Table 4.2a for the Brenton torrent and Table 4.3a for the Desturo canal.

The location of the injection and the measurement sections was chosen so that the study reaches could be considered as approximately uniform. The length of the reaches, L, varies from around 660 to 1900 m for the Yarqon river (Table 4.1b), from 620 to 2160 m for the Brenton torrent (Table 4.2b), and from 260 to 340 m for the Desturo canal (Table 4.3b). In all cases, the distance from injection allowed the tracer to be well mixed over the cross-section at the measurement stations.

Flow discharges during the tracer tests were obtained from data provided by local consortia equipped with their own meters. The flow cross-sectional area was inferred from technical cartography of the channel sections and partly from direct measurements along the study reaches. Values of the flow discharge Q, average flow velocity U, and mean advective travel time $t_{ad} = L/U$ are reported in 4.1b, 4.2b and 4.3b for the Yarqon river, the Brenton torrent and the Desturo canal, respectively. The ranges of flow discharges considered in the tracer experiments are $0.21 \div 0.41\,m^3\,s^{-1}$ for the Yarqon river, $0.68 \div 1.5\,m^3\,s^{-1}$ for the Brenton torrent, and $0.042 \div 0.053\,m^3\,s^{-1}$ for the Desturo canal. Mean advective travel times in the study reaches ranges from about 1 to 3 hours for the Yarqon river, from 10 to 50 min for the Brenton torrent, and from 20 to 40 min for the Desturo canal.

Test	1	2	3
(a) Experimental procedure			
M_0 (g)	21	21	$63 + 53^{b}$
Δt_{inj} (s)	0^{a}	0^{a}	$3700{+}0^{b}$
(b) Study reaches			
Reach	1–5	5–6	8–9	14–16
L (m)	1084	816	657	1887
Q ($m^3 s^{-1}$)	0.21	0.21	0.43	0.41
A (m^2)	1.06	2.18	2.71	2.15
t_{ad} (s)	5391	8345	4141	9895
(c) Parameters of model with two exponential RTDs			
D_L ($m^2 s^{-1}$)	0.24	0.25	0.49	2.80
α_1 ($\times 10^{-4} s^{-1}$)	7.4	9.4	7.3	7.3
α_2 ($\times 10^{-4} s^{-1}$)	0.25	0.78	0	0.54
T_1 (s)	163	109	436	340
T_2 (s)	2382	1720	—	3781
RMSE[c] ($\times 10^{-2}$)	1.36	4.36	10.29	5.85
(d) Parameters of power-law RTD model			
D_L ($m^2 s^{-1}$)	0.42	0.20	1.88	3.80
α ($\times 10^{-2} s^{-1}$)	0.29	0.20	1.02	0.42
κ[c]	2.05	1.74	2.67	1.86
RMSE[c] ($\times 10^{-2}$)	3.26	5.41	8.03	7.10

[a] $\Delta t_{inj} = 0$ indicates an instantaneous (slug) injection.

[b] In Test 3 a mass of tracer of 63 g was injected continuously for a period of 3700 s after which a slug injection of 53 g was performed at $t = 3700$ s.

[c] The parameters RMSE and κ are unitless.

Table 4.1. Summary of test and model parameters for the Yarqon river.

Test	1	2	3
(a) Experimental procedure			
M_0 (g)	50.3	50.3	30.0
Δt_{inj} (s)	780	780	600
(b) Study reaches			
Reach	5–6	6–7	6–8	6–9
L (m)	620	1080	1560	2160
Q ($\text{m}^3\,\text{s}^{-1}$)	1.5	1.5	1.5	0.68
A (m^2)	1.45	1.34	1.57	0.96
t_{ad} (s)	599	962	1632	3036
(c) Parameters of model with two exponential RTDs			
D_L ($\text{m}^2\,\text{s}^{-1}$)	1.98	2.01	1.85	1.95
α_1 ($\times 10^{-4}\,\text{s}^{-1}$)	2.8	15.5	5.0	4.9
α_2 ($\times 10^{-4}\,\text{s}^{-1}$)	0.26	0.11	0.18	0.06
T_1 (s)	51	52	66	104
T_2 (s)	733	912	1081	1735
RMSE[a] ($\times 10^{-2}$)	4.94	2.53	3.26	2.90
(d) Parameters of power-law RTD model			
D_L ($\text{m}^2\,\text{s}^{-1}$)	2.58	4.75	3.79	3.50
α ($\times 10^{-2}\,\text{s}^{-1}$)	0.010	0.342	0.072	0.167
κ[a]	1.17	2.63	1.93	2.36
RMSE[a] ($\times 10^{-2}$)	5.07	3.19	4.49	3.86

[a] The parameters κ and RMSE are unitless.

Table 4.2. Summary of test and model parameters for the Brenton torrent.

Test	1	2	3
(a) Experimental procedure			
M_0 (g)	3.24	3.24	3.24
Δt_{inj} (s)	1500	1320	1260
(b) Study reaches			
Reach	1–2	2–3	3–4	5–6
L (m)	262	305	336	278
Q ($\text{m}^3\,\text{s}^{-1}$)	0.045	0.045	0.053	0.042
t_{ad} (s)	1114	1440	2329	2040
(c) Parameters of model with two exponential RTDs			
A (m^2)	0.19	0.21	0.36	0.31
D_L ($\text{m}^2\,\text{s}^{-1}$)	0.10	0.14	0.09	0.10
α_1 ($\times 10^{-4}\,\text{s}^{-1}$)	13.5	10.1	11.0	11.0
α_2 ($\times 10^{-4}\,\text{s}^{-1}$)	2.73	1.50	0.70	4.27
T_1 (s)	99	171	140	60
T_2 (s)	367	365	397	280
RMSE[a] ($\times 10^{-2}$)	2.02	5.40	1.96	4.29
(d) Parameters of power-law RTD model			
D_L ($\text{m}^2\,\text{s}^{-1}$)	0.84	1.08	0.37	0.38
α ($\times 10^{-2}\,\text{s}^{-1}$)	0.56	0.72	0.57	0.55
κ[a]	2.22	2.43	2.46	2.40
RMSE[a] ($\times 10^{-2}$)	5.48	5.93	3.73	5.54

[a] The parameters κ and RMSE are unitless.

Table 4.3. Summary of test and model parameters for the Desturo canal.

4.4 Solute transport modeling

RWT tracer transport along the study reaches was simulated using the STIR model for general residence time distribution modeling. As shown in Chapter 3, under the assumption of Fickian transport in the surface water in the main channel, the STIR model is equivalent to the following advection-dispersion-mass-transfer equation:

$$\frac{\partial C_W(x,t)}{\partial t} + U\frac{\partial C_W(x,t)}{\partial x} = D_L\frac{\partial^2 C_W(x,t)}{\partial x^2} - \alpha\left(C_W(x,t) - \int_0^t C_W(x,t-\tau)\varphi(\tau)\,d\tau\right), \tag{4.1}$$

where $C_W(x,t)$ is the solute concentration in the surface water [$\mathrm{M\,L^{-3}}$], U is the average flow velocity [$\mathrm{L\,T^{-1}}$], given by the ratio of the flow rate and the average flow cross-sectional area $U = Q/A$, D_L is the longitudinal dispersion coefficient [$\mathrm{L^2\,T^{-1}}$], α is the rate of transfer [$\mathrm{T^{-1}}$], and $\varphi(t)$ is the probability density function (PDF) of the residence times in the storage zones [$\mathrm{T^{-1}}$]. The assumption of uniformity along the study reach implies that U, D_L, α and the PDF $\varphi(t)$ are constant in time and space.

In Chapter 3 it was shown that the overall residence time distribution (RTD) in a stream segment of length L can be expressed in the Laplace domain as:

$$\widetilde{r}(t;x) = \widetilde{r}_W\left(s + \alpha(1-\widetilde{\varphi}(s)); L\right), \tag{4.2}$$

where $\widetilde{r}_W$ is the Laplace transform of the residence time distribution in the main channel. In the time domain equation (4.2) implies the following series expansion:

$$r(t;x) = \sum_{m=0}^{\infty}\int_0^t r_W(\tau;L)\frac{(\alpha\tau)^m}{m!}e^{\alpha\tau}\left(\varphi(t-\tau)\right)^{*m}d\tau, \tag{4.3}$$

where $(\varphi(t))^{*m}$ denotes the m-fold convolution of the function $\varphi(t)$ with itself. Estimating the residence time distribution in the storage zones from a tracer

breakthrough curve is similar to performing a blind deconvolution where also the residence time function in the main channel has to be determined. The problem is solved here by assuming a certain form of the RTD in the storage zones and in the main channel and by taking the parameter values that best-fit the experimental data in a least-square sense. The assumption of Fickian transport in the main channel implies that the corresponding RTD is in the form associated to the classical ADE:

$$r_W(t;x) = \frac{x}{2\sqrt{\pi D_L t^3}} \exp\left[-\frac{(x-Ut)^2}{4D_L t}\right]. \tag{4.4}$$

For the stastistics of the storage time, two different distributions were tested: one assuming retention to be represented by a weighted average of two exponential distributions and one assuming a power-law RTD as proposed by *Haggerty et al.* (2000).

In the two-exponential distribution model, the residence time PDF in the storage zones is given as follows:

$$\varphi(t) = \frac{1}{\alpha}\left[\alpha_1\varphi_1(t) + \alpha_2\varphi_2(t)\right], \tag{4.5}$$

where

$$\alpha = \alpha_1 + \alpha_2, \tag{4.6}$$

and

$$\varphi_1(t) = \frac{1}{T_1} e^{-t/T_1}, \tag{4.7a}$$

$$\varphi_2(t) = \frac{1}{T_2} e^{-t/T_2}. \tag{4.7b}$$

Here, α_1 and $\varphi_1(t)$ are the transfer rate and residence time PDF associated to short timescale retention, respectively, and α_2 and $\varphi_2(t)$ are the transfer rate and

residence time PDF associated to longer timescale retention. The decomposition given by equations (4.5)–(4.6) can be interpreted as a two-storage zone representation of transient storage where shorter timescales are expected to be associated to surface dead zone storage, whereas longer timescales are associated to hyporheic exchange.

The truncated power-law model proposed by *Haggerty and Wondzell* (2002) and presented in § 2.4 can be shown to be equivalent to the following assumption of the PDF $\varphi(t)$ in equation (4.1):

$$\varphi(t) = \frac{1-\kappa}{T_{\max}^{1-\kappa} - T_{\min}^{1-\kappa}} \int_{T_{\min}}^{T_{\max}} T^{-1-\kappa} e^{-t/T}\, dT\,, \tag{4.8}$$

where $-\kappa$ is the exponent of the power-law, corresponding to the slope of the breakthrough curve at late times. The function $\varphi(t)$ is linked to the memory function $f_M(t)$ used by *Haggerty et al.* (2000, § 2.4) by the following relation:

$$\varphi(t) = -\frac{1}{f_M(0)} \frac{df_M(t)}{dt}. \tag{4.9}$$

Equation (4.8) defines a power-law function in the interval $T_{\min}$ and $T_{\max}$ where the $\varphi(t) \sim t^{\kappa}$. Following *Gooseff et al.* (2007), the limit timescales $T_{\min}$ and $T_{\max}$ are determined by bracketing the timescales of the solute breakthrough curve from the tracer experiment; $T_{\min}$ is always chosen to be 10 s and $T_{\max}$ is always chosen to be the last time of data acquisition in the field, since the injection. It is thus accepted that the late-time window of detection of the stream tracer experiments is the timescale of the latest arrival of detectable tracer concentrations in the stream.

The longitudinal dispersion coefficient D_L, and the parameters of retention, namely α_1, α_2, T_1 and T_2 for the two-exponential RTD model, and the parameters α and κ in the power-law model, are determined by fitting the simulated

breakthrough curves to the experimental data. Model calibration is performed in mixed-scale using a linear scale to fit the bulk of the curve and log-scale to fit the tail. In the optimization procedure the following root mean square is minimized:

$$\mathrm{RMSE} = \left[\frac{1}{N}\left(\frac{\sum_{i\in I_U}\left(C_{\mathrm{sim},i} - C_{\mathrm{obs},i}\right)^2}{\left(\max_{i\in I} C_{\mathrm{obs},i} - \min_{i\in I} C_{\mathrm{obs}}\right)^2} + \frac{\sum_{I\in I_L}\left(\log C_{\mathrm{sim},i} - \log C_{\mathrm{obs},i}\right)^2}{\left(\max_{i\in I} \log C_{\mathrm{obs},i} - \min_{i\in I} \log C_{\mathrm{obs},i}\right)^2}\right)\right]^{1/2} \tag{4.10}$$

where C_{obs} and C_{sim} are the observed and simulated concentration values, respectively, I_U and I_L are the sets of the observed values higher and lower than a given threshold concentration, respectively, $I = I_U \cup I_L$ is the total set, and N is the number of elements in I. The threshold value was set equal to 20% of the peak concentration. Particular care was taken in calculating $\min(\log C_{\mathrm{obs},i})$ by neglecting the concentration values closer to zero, generally by excluding from the computation 5% of the total set corresponding to the lowest values. The optimization was performed using the differential evolution method for global optimization by *Storn and Price* (1997, see also *Price et al.*, 2005).

4.5 Results and discussion

Transient storage processes in natural streams generate a delay in the downstream transport of a tracer inducing longer tails in the observed BTCs and increasing the skewness of the concentration distributions. Here, the STIR solute transport model has been used in combination with tracer test data to characterize transient storage in three case studies.

The results of the calibration of the STIR model with the two-exponential closure for the storage time distribution are presented in Table 4.1c, 4.2c and 4.3c for the Yarqon river, the Brenton torrent and the Desturo canal, respectively. A graphical comparison between the experimental data and the simulated break-

through curves is given in Figure 4.7 for the Yarqon river, Figure 4.8 for the Brenton torrent, and in Figure 4.9 for the Desturo canal. The curves are plotted in both linear and semi-log scale to emphasize their tail behavior, on which the retention parameters are primarily dependent.

In the study reaches of the Yarqon river the average timescale T_1 of fast transient storage varies from 163 to 436 s, with an average value of 262 ± 152 s (Table 4.1c). The mean residence time T_2 associated to long timescale retention varies from 1720 to 3781 s and appears to be higher for increasing average advective residence times t_{ad}. In Reach 8–9 of Test 2, the optimization procedure converges to $\alpha_2 \approx 0$, whereas the timescale T_1 converges to a value higher the other reaches ($T_1 = 436$ s), indicating that a single exponential distribution is sufficient in this case to adequately represent the BTC. In the study reaches of the Brenton torrent T_1 ranges from 51 s to 104 s, with an average value of 68 ± 25 s, and it is clearly higher for increasing t_{ad} (Table 4.2c). The same increasing trend is visible for the timescale T_2 which varies from 733 to 1735 s as the mean advective travel time t_{ad} increases from 600 to 3000 s. In the Desturo canal the timescale T_1 ranges from 60 s to 171 s, with average 117 ± 48 s, whereas T_2 ranges from 280 to 397 s, with average 352 ± 50 s. In this case, an increasing trend of T_1 and T_2 with t_{ad} is not evident.

The transfer rates are found to be higher in the Desturo canal, with α_1 in the range $(1.0 \div 1.35) \times 10^{-3}\,\mathrm{s}^{-1}$ and $\alpha_2 = (0.70 \div 4.27) \times 10^{-4}\,\mathrm{s}^{-1}$, compared to the Brenton torrent where $\alpha_1 = (0.28 \div 1.55) \times 10^{-3}\,\mathrm{s}^{-1}$ and $\alpha_2 = (0.06 \div 0.26) \times 10^{-4}\,\mathrm{s}^{-1}$, and the Yarqon river, where $\alpha_1 = (0.73 \div 0.94) \times 10^{-3}\,\mathrm{s}^{-1}$ and $\alpha_2 = (0 \div 0.78) \times 10^{-4}\,\mathrm{s}^{-1}$. It can be noticed that the transfer rate associated to the longer timescale retention component are at least an order of magnitude lower than the transfer rate associated to the shorter one. This is consistent with the fact that fast transient storage in surface dead zones is typically characterized by high exchange fluxes, whereas the transient storage in the hyporheic zones is associated to relatively

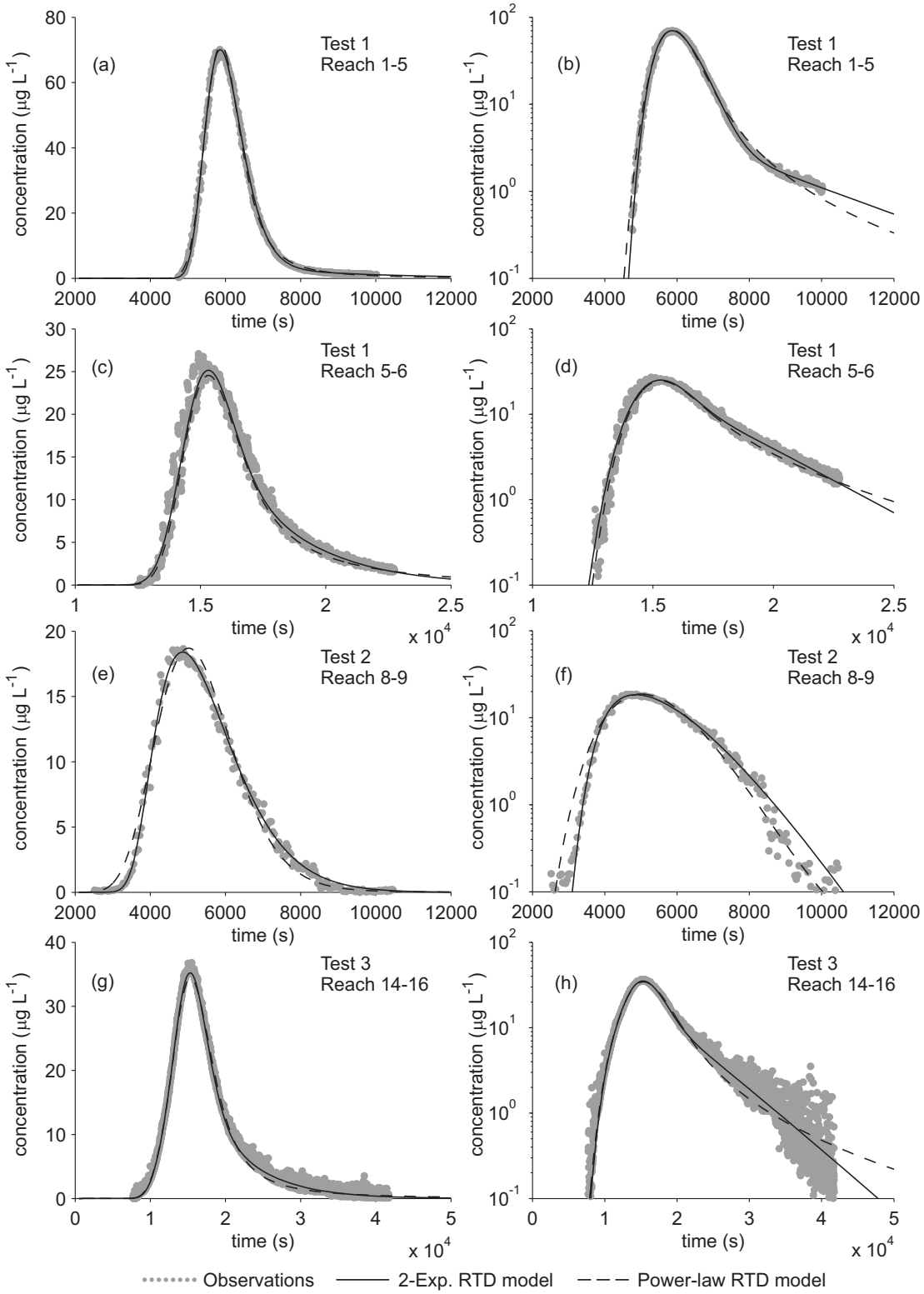

Figure 4.7. Observed and simulated breakthrough curves for the Yarqon river (left) in linear scale and (right) semi-log scale.

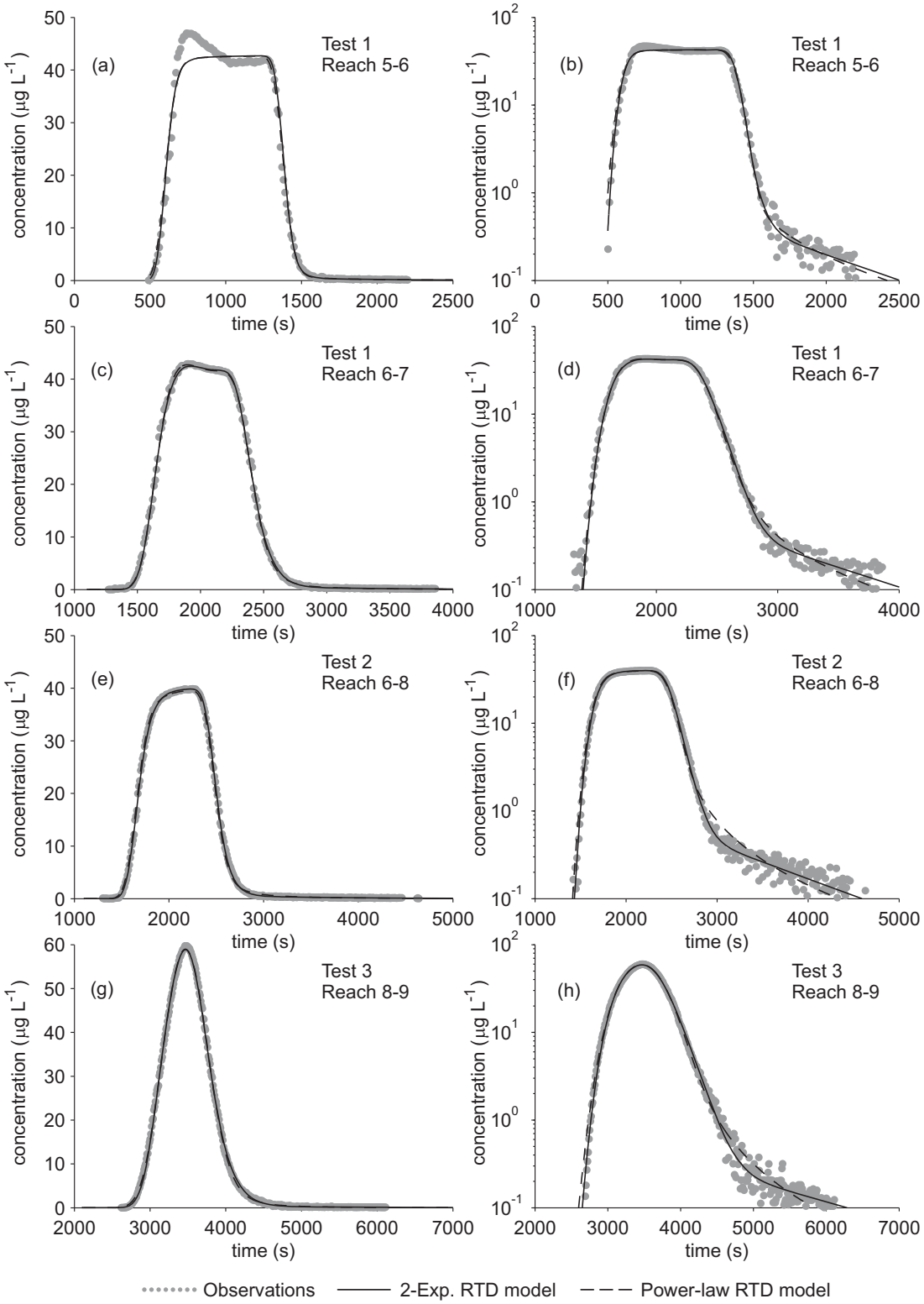

Figure 4.8. Observed and simulated breakthrough curves for the Brenton torrent (left) in linear scale and (right) semi-log scale.

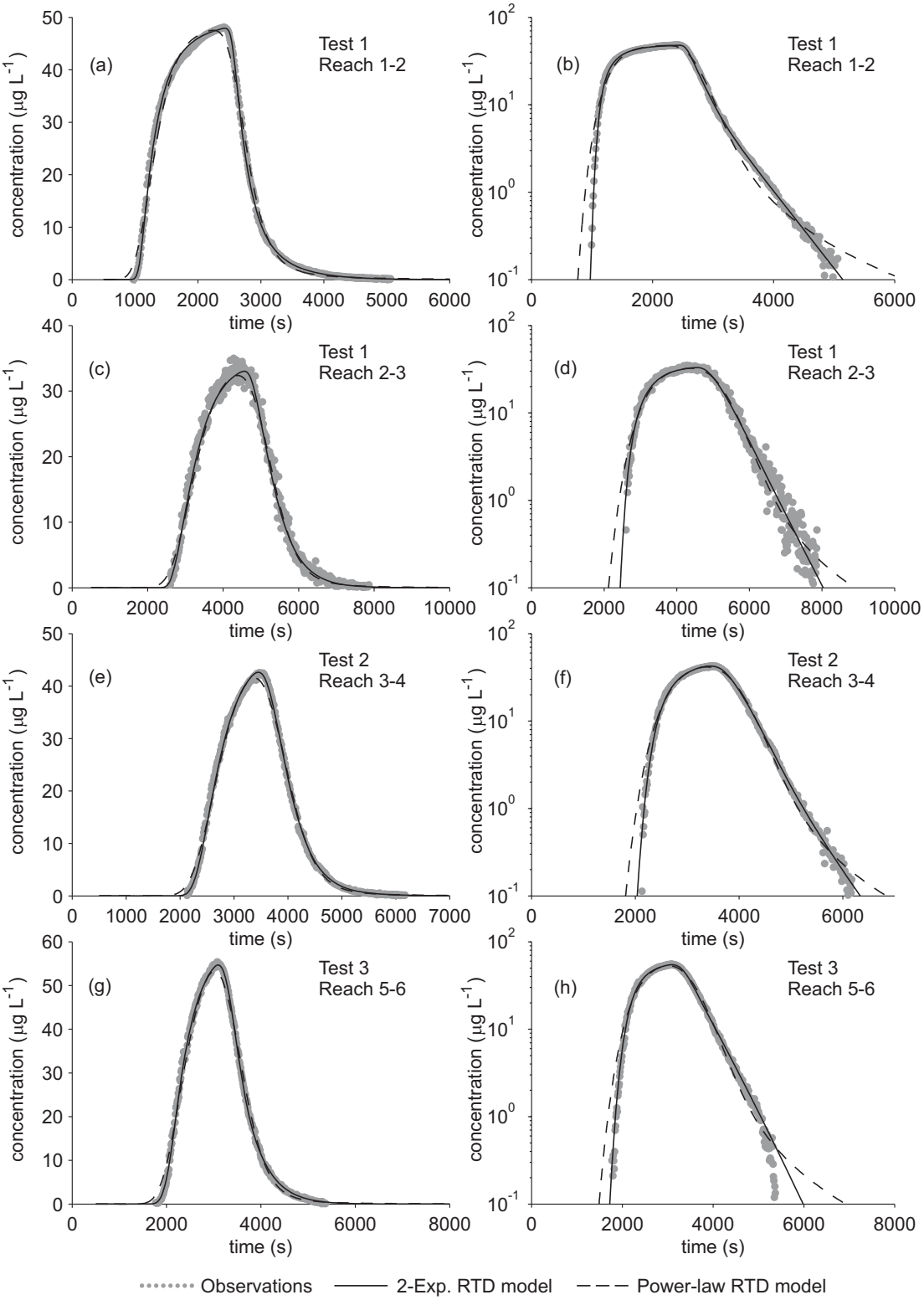

Figure 4.9. Observed and simulated breakthrough curves for the Desturo canal (left) in linear scale and (right) semi-log scale.

small transfer rates and long residence times. The values of α_1 and α_2 do not exhibit particular trends as a function of the average advective travel time, t_{ad}.

Despite the apparent dependence of the parameters T_1 and T_2 on the timescale of observation, it is possible to compare the retention parameters of the Desturo canal with the parameters of the Brenton torrent since the range of values of t_{ad} for the reaches of the former overlaps with the range of t_{ad} for the reaches of the latter. The higher values of the timescale T_2 characterizing the Brenton torrent can be seen as a consequence of the higher permeability of the bed, which implies significant hyporheic fluxes in the subsurface. In the Desturo canal, the low permeability of the bed implies that the subsurface fluxes are extremely small, and the observed retention effects are likely to be primarily due to surface dead zones and, in particular, to the thick submerged vegetation characterizing the channel bed. Nevertheless, it is not possible to compare unambiguously the properties of short timescale retention in the streams analyzed. In the Brenton torrent the longitudinal dispersion coefficients are an order of magnitude greater than those found in the Desturo canal, which allows a wider range of retention phenomena to be lumped in the parameter D_L. A proper comparison would require the value of D_L to be determined independently of the retention parameters.

An important parameter of the two-exponential RTD model is given by the ratio of the two timescales of retention T_2/T_1. When this ratio is close to 1, the breakthrough curves can be well represented by a single exponential distribution, and hence the conventional TSM model with a single storage zone is expected to provide acceptable approximations of the experimental data. This is the case of the Desturo canal for which the mean ratio is T_2/T_1 is 3.3 ± 1.1. In a semi-log graph, the corresponding breakthrough curves tend to follow a linear pattern after the concentration peak. High ratios are instead found in the Yarqon river and the Brenton torrent, for which the average ratio T_2/T_1 is 11.3 ± 5.3 and 16.3 ± 7.1, respectively. When plotted in semi-log scale, the relevant breakthrough curves

shows a long tail behavior. In particular, in the case of the Brenton torrent, the decreasing part of the curve is characterized by a clear change of slope (Figure 4.8): the part of the curve between the concentration peak and the bend is associated to quicker exchange processes and determines primarily the value of T_1 and α_1; the subsequent part the curve is associated to long term retention and is related to the parameters T_2 and α_2. The rising part of the curve is mainly associated to advection and dispersion processes in the main channel and the steepness of the curve depends primarily on the value on the longitudinal dispersion coefficient.

The results of the parameter calibration for the power-law model are presented in Table 4.1d, 4.2d and 4.3d for the Yarqon river, the Brenton torrent and the Desturo canal, respectively. In the Yarqon river the exponent κ ranges from 1.64 to 2.67, and there is no dependence of either κ or α on t_{ad}. In the the Brenton torrent the exponent κ varies from 1.17 to 2.63, with higher transfer rates associated to higher κ. In the Desturo canal, the calibration procedure converged to values of κ close to 2.4, but the model is clearly unable to represent the late time behavior of the breakthrough curves as it can be seen by visual inspection of Figure 4.9. The values of the longitudinal dispersion coefficients obtained with the power-law RTD model are higher (from 4 to 8 times greater in the Desturo canal) than those obtained with the two-exponential RTD model. In the case of the Desturo canal, the values of D_L determined with the power-law model do not seem to be adequate to represent the transport dynamics in the main channel, since the rising part of the simulated breakthrough curves do not well approximate the experimental data. The result further suggests that D_L should be determined separately, for example with an adequate hydrodynamic modeling of the flow in the main channel.

A comparison of the RMSE values for the two models presented shows that, on the average, the model assuming two exponential RTDs to represent transient storage provides better fits of the observed concentration data than the truncated

power-law model. This is not only a consequence of the higher flexibility allowed by a higher number of calibration parameters: in fact, when plotted in a semi-log scale, many of the experimental breakthrough curves show linear patterns in the decreasing part following the concentration peak, indicating an exponential behavior of the tails. This is particularly evident in the case of the Desturo canal (Figure 4.9). It should be noted, however, that when the results of the two models are compared in linear scale, the difference appears rather small.

The methods used in this study does not allow to clearly distinguish between in-channel and subsurface, hyporheic transient storage. Nevertheless, it is likely that long BTC tails observed in some of the reaches result from hyporheic exchange. The modeling closure assuming transient storage to be represented by two exponential RTDs allows a simple conceptual separation of fast and slow exchange: the former is expected to be associated to surface dead zones and the latter to hyporheic zones. This modeling closure has the property that the two residence time distributions adopted for fast and slow exchange have the same functional form, thereby permitting a direct comparison of the timescale parameter, that is the mean residence time for an exponential PDF. However, the experimental results presented here seem to suggest that the timescales of retention T_1 and T_2 of the two-exponential RTD model are dependent on the spatial and temporal scale of observation, thus making the parameters difficult to compare between stream reaches of different travel time. The scale dependent behavior of the mean residence time is implicit in the power-law RTD model, for which a mean residence time cannot be defined (*Haggerty and Wondzell*, 2002). Nevertheless, the power-law model as proposed by *Haggerty et al.* (2000) did not provide good approximation of the late time behavior of the observed breakthrough curves in a number cases.

It is also relevant to note that the storage parameters are expected to be dependent on the flow discharge, which determines both the fluxes and the mean

residence times in the storage zones. The main limitation of the tracer test approach is that it is not possible to generalize the results to conditions different than those directly observed in the experiments. In Chapter 3 it was shown that transfer rates can be defined as the ratio of the flux at the stream-storage zone interface and a length scale, typically the water depth or the hydraulic radius, both increasing with the flow discharge. The average cross-sectional area A_S of the storage zones is also expected to increase with flow discharge, and the resulting mean residence time depends on the ratio between the storage volume and the flux into the storage zones. Furthermore, the mixing in the surface water is known to be dependent on the flow velocity, with higher mixing associated to higher velocities, which in turn affects the shape of the concentration distributions. Different retention processes can also be activated by different flow regimes, making it difficult to make reliable predictions about the behavior of the storage parameters with different flow discharges.

4.6 Conclusions

Tracer breakthrough curves result from a complex multiple convolution of the RTD in the main channel and the RTDs in the storage zones. Separating in-channel transport from transient storage using tracer breakthrough curves is an ill-posed mathematical problem. Here, tracer test data were analyzed with the STIR model using the classical inverse approach: a certain functional form was assumed for the RTD in the storage zones and in the main channel, and the relevant parameters were determined by fitting the model predictions to tracer test data. Two different modeling closures were tested: one assuming the residence time statistics in the storage zones to be represented by a weighted average of two exponential distributions, and one assuming a truncated power-law distribution in the form proposed by *Haggerty et al.* (2000) (§ 2.4). In both cases the RTD in the main channel was assumed to be in the form associated to the con-

ventional advection-dispersion equation. Results show that the two-exponential RTD model is able to represent with excellent approximation the observed breakthrough curves in all the study reaches of the three the streams analyzed. The mean residence times T_1 and T_2 in the storage zones, which are parameters of the exponential distributions, were found to be dependent on the timescale of observation. In particular, T_1 and T_2 show an increasing trend for increasing mean advective travel times, t_{ad}, suggesting that the storage parameters of two different streams should be compared only for similar values of t_{ad}. Further investigations are certainly needed to understand the relationship between the timescale of observation and the calculated storage parameters.

The power-law RTD model provided good fit of the observed concentration data in some of the study reaches, but in many cases it was found inadequate to represent the tail behavior of the tracer BTCs. The observed dependence of the longitudinal dispersion coefficient, D_L, on the particular RTD assumed in the storage zones suggests that tracer test data should be integrated with hydrodynamic modeling of the surface flow in the main channel. This would allow the parameters D_L and the average flow cross-sectional area A to be determined separately from transient storage. A deconvolution approach could then be used to infer the contribution of retention processes to solute transport.

Chapter 5

Effect of microbial biofilms on the transient storage of solutes[1]

5.1 Introduction

Microbial life in streams is often dominated by biofilms (matrix-enclosed communities including bacteria, archaea, algae, fungi and protozoa) coating the sediments (*Sigee and Sigee*, 2005). Understanding the controls of biofilms on solute transport is essential given the contributions of streams to biogeochemical fluxes (*Battin et al.*, 2008; *Mulholland et al.*, 2008). Biofilms differentiate into complex physical structures such as filamentous streamers floating in the water and thereby adapt to the hydrodynamic conditions (*Battin et al.*, 2003). Biofilm differentiation also results from interactions between mass transport and conversion processes (*Wimpenny and Colasanti*, 1997), and from shear-induced erosion and compacting (*Battin et al.*, 2003). Ultimately, this differentiation can create retention domains at the streambed-streamwater interface, which can act as solute storage zones in support of biological activity as shown in a range of studies. For

[1]The contents of this chapter have been published in: Bottacin-Busolin, A., G. Singer, M. Zaramella, T. J. Battin, and A. Marion (2009), Effects of Streambed Morphology and Biofilm Growth on the Transient Storage of Solutes, *Environ. Sci. Technol.*, 43 (19), 7337-7342.

instance, *Kim et al.* (1990) and *Kim et al.* (1992) simulated nitrate retention by periphytic (i.e., phototrophic) biofilms based on hydrologic advection-dispersion transport, transient storage (*Bencala and Walters*, 1983) and Michaelis-Menten uptake kinetics. *Mulholland et al.* (1994) used an advection-dispersion model to show how dispersion coefficients and transient storage zones increase with periphytic biomass. *DeAngelis et al.* (1995) showed the effect of periphytic biofilms on stream hydraulics using a single storage zone model, which was then extended to include hyporheic exchange as a separate retention domain to consider the effect of periphyton on subsurface nitrogen cycling (*Dent and Henry*, 1999). *Gooseff et al.* (2004) attributed rapid nitrate removal to the transient storage zone created by periphytic mats rather than to the hyporheic zone. Recently, *Orr et al.* (2009) reported hyporheic processes to dominate nutrient retention when periphytic biomass is low, whereas nutrient retention became allocated to the benthic zone as biomass developed and clogged the sediments.

In this chapter, results are presented from tracer experiments carried out in streamside flumes with low submergence-streambeds. The experiments were designed to evaluate how solute transient storage is mutually affected by bed morphology and related biofilm. Illuminating this link is important to help restore headwater streams. The analysis presented here is based on the theoretical framework of the STIR model (Chapter 3), which allows for general residence time modeling of processes acting at different temporal and spatial scales. The particular method used to determine the parameters of the model allowed to separate effects of biofilms and bed-induced hydrodynamics.

5.2 Experimental methods

Streambeds were constructed in five streamside flumes (length: 40 m, width: 0.4 m; Lunz am See, Austria). The bottom of each flume was shaped from impermeable bedforms with wavelength $\lambda = 1$ m, horizontal distance between the crest

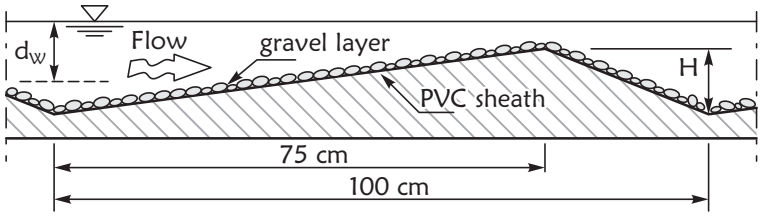

Figure 5.1. Longitudinal sketch of a bedform.

and the upstream trough $\lambda_c = 0.75\,\mathrm{m}$, and height $H = 2, 4, 6, 8, 10\,\mathrm{cm}$, respectively (Figure 5.1). Bedforms were covered with a single layer of indigenous, clean and graded (median grain diameter: 9.2 mm) sediment which served as substratum for biofilm growth (Figure 5.2). This set-up with limited size of hyporheic storage zones simulated stream reaches with bedrock and constrained hyporheic zones. All flumes were continuously fed from the same header tank with raw stream water (Oberer Seebach) in a once-through mode to assure identical water chemistry and microbial inoculum. Periodically measured concentrations of $NO_3 - N$, $NH_4 - N$ and dissolved organic carbon (DOC) averaged $0.57 \pm 0.24\,\mathrm{mg\,L^{-1}}$ (mean $\pm$ standard deviation, $n = 22$ number of samples), $4.4 \pm 4.25\,\mu\mathrm{g\,L^{-1}}$ ($n = 24$), and $1.49 \pm 0.52\,\mathrm{mg\,L^{-1}}$ ($n = 39$), respectively. Concentrations of $PO_4 - P$ were mostly below the detection limit ($< 3\,\mu\mathrm{g\,L^{-1}}$). Water temperature averaged $9.1 \pm 1.3°C$. The flow rate was adjusted to $2.25 \pm 0.10\,\mathrm{L\,s^{-1}}$ by fixing the water level in the header tank and checked daily throughout the experiment. Uniform flow conditions were obtained by adjusting a tilting weir at the downstream flume end. The resulting flow can be described as shallow rough-bed flow as it is typical in natural headwater streams at base flow. Slopes of the flumes were adjusted to yield identical flume-scale flow velocities but with increasing spatial heterogeneity of flow velocity, roughness and water depth.

Sterile unglazed ceramic coupons were used ($1 \times 2\,\mathrm{cm}$), as surrogate for natural substratum in biofilm studies (*Battin et al.*, 2003; *Besemer et al.*, 2007), to determine the areal content of chlorophyll-*a* (*Besemer et al.*, 2007). Coupons were

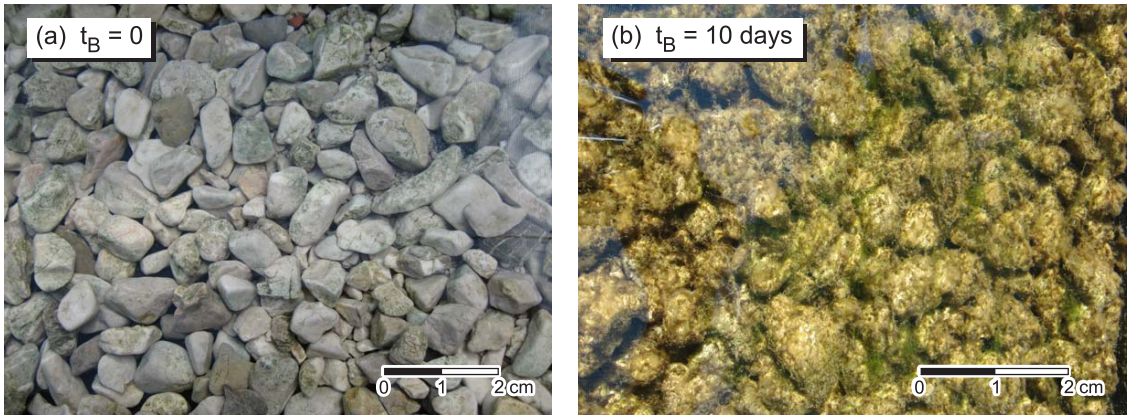

Figure 5.2. (a) Bed with clean gravel and (b) after 10 days of biofilm growth.

sampled from triplicate bedforms at the crest, in the trough, upstream and downstream of the crest at 4 occasions during biofilm growth. Chlorophyll-*a* served as surrogate for algal biomass in the highly phototrophic biofilms (*Besemer et al.*, 2007). As major building blocks, algae, rather than bacteria, typically confer the main physical structure to these biofilms. Data were z-standardized to remove temporal variability from the primary data induced by biofilm growth, simplify statistical analysis and to increase statistical power for tests of correlation with bedform height.

Tracer tests were performed with the fluorescent dye Rhodamine-WT (RWT) continuously ($\Delta t_{\text{inj}} = 30\,\text{min}$) injected upstream using a peristaltic pump with constant flow rate (total injected mass $M_0 = 400\,\text{mg}$); baffles ensured rapid cross-sectional mixing. Submersible field fluorometers (Turner Designs SCUFA and GGUN-FL20) were used to measure RWT concentration at the flume effluent. RWT may partly adsorb to mineral and organic surfaces, but its sensitivity is greatly superior to halide tracers (e.g., NaCl). In fact, $98 \pm 1\%$ of the RTW in the effluent was recovered and no relationship was found between recovery and bedform height or biofilm development. Therefore, adsorption effects appear negligible. Furthermore, RWT adsorption, seemingly irreversible (*Smart and Laidlaw*,

1977) and zero-order (*Dierberg and DeBusk*, 2005), should not affect the shape of the breakthrough curves.

5.3 Solute transport modeling

The STIR model is used here to describe the transport dynamics of Rhodamine-WT in the experimental flumes. It is assumed that the transport of RWT in the surface water is due to advection and Fickian dispersion processes so that the conventional advection-dispersion equation applies. The exchange dynamics with the storage zones is assumed to be a temporal Poisson process. As shown in Chapter 3, under these assumptions the STIR model reduces to the following equation:

$$\frac{\partial C_W(x,t)}{\partial t} + U\frac{\partial C_W(x,t)}{\partial x} = D_L\frac{\partial^2 C_W(x,t)}{\partial x^2} - \alpha\left(C_W(x,t) - \int_0^t C_W(x,t-\tau)\varphi(\tau)\,d\tau\right), \tag{5.1}$$

where $C_W(x,t)$ is the solute concentration in the surface water [ML^{-3}], U is the average flow velocity [LT^{-1}], given by the ratio of the flow rate and the average flow cross-sectional area $U = Q/A$, D_L is the longitudinal dispersion coefficient [$\mathrm{L}^2\mathrm{T}^{-1}$], α is the rate of transfer [T^{-1}], and $\varphi(t)$ is the probability density function (PDF) of the residence times in the storage zones [T^{-1}]. It is assumed that the stream reach is uniform, implying that U, D_L, α and the PDF $\varphi(t)$ are constant in time and space.

According to equation (5.1), the retained mass in a given stream reach of length L can be computed by integrating in space and time the solute fluxed at the stream-storage zone interface:

$$M_S(t) = A\int_0^L\int_0^t\left(\alpha C_W(x,t') - \int_0^{t'}\alpha C_W(x,\tau)\varphi(t'-\tau)\,d\tau\right)dt'dx. \tag{5.2}$$

In the Laplace domain this expression becomes:

$$\widetilde{M}_S(s) = A\frac{\alpha}{s}(1-\widetilde{\varphi}(s))\int_0^L \widetilde{C}_W(x,s)\,dx. \tag{5.3}$$

The total retained mass can be used as a storage parameter describing as whole the effects of retention processes on solute transport in the experimental systems described here.

5.4 Model calibration

The effect of biofilm on solute retention has been quantified as follows. The model is fitted to the experimental breakthrough curves relevant to the beds without biofilm. This allows determining the parameters of the surface transport, D_L and A, and the retention parameters due to solute exchange with the bottom layer of gravel, $\alpha(t_B = 0)$ and $\varphi(t; t_B = 0)$, where t_B is the age of biofilms [T]. Since comparison between the experimental breakthrough curves at subsequent phases of biofilm growth suggests increased retention, the exchange rate and the storage time function are expressed as follows:

$$\alpha(t_B) = \alpha(t_B = 0) + \delta\alpha(t_B), \tag{5.4a}$$

$$\varphi(t; t_B) = \frac{1}{\alpha(t_B)}\left[\alpha(0)\varphi(t;0) + \delta\alpha(t_B)\delta\varphi(t; t_B)\right], \tag{5.4b}$$

where $\delta\alpha(t_B)$ and $\delta\varphi(t; t_B)$ represent the increment with respect to the initial configuration (at $t_B = 0$). These additional terms are determined by fixing the parameters of the superficial transport, D_L and A, and the previously found retention parameters $\alpha(0)$ and $\varphi(t;0)$. The resulting exchange rate and retention function reflect the various effects of biofilms on solute transport. These may include the storage in biofilm pores, micro-eddies around biofilm streamers, changes in the near-bed flow field and in the related interfacial hydrodynamic exchange. In this sense the overall statistics of the residence times in the storage zones should not

be considered as the result of the sum of the residence times in distinct physical domains.

Determining the parameters of the surface transport and the basic retention for the bed without biofilm the storage time function was assumed to be representable as a normalized sum of two exponential PDFs:

$$\varphi(t) = \frac{1}{\alpha} \sum_{i=1}^{2} \frac{\alpha_i}{T_i} e^{-t/T_i}, \tag{5.5}$$

where

$$\alpha = \sum_{i=1}^{2} \alpha_i . \tag{5.6}$$

This assumption corresponds to the following conceptualization of the problem. Transport processes acting on time scales of the longitudinal advection due to the mean flow velocity are represented by the advection and dispersion terms and are considered as part of the superficial transport. Processes acting on longer time scales are considered retention processes and are split into fast and long term retention. The use of two exponential PDFs provides good fit of the experimental breakthrough curves, both in linear and log-scale. Conversely, if only on exponential PDF is used, as in the TSM, it is not possible to obtain acceptable representation of the tails of the breakthrough curves (Figure 5.3). On the other hand, if more than two exponential PDFs are used to represent the storage time function, and a lower bound for the corresponding mean residence time is not imposed, a portion of what is identified as superficial transport may become part of the retention processes. Previous studies used an extended version of the TSM to identify two distinct storage zones with exponential residence time distributions (*Gooseff et al.*, 2004; *Harvey et al.*, 2005).

A decomposition similar to equations (5.5) and (5.6) is adopted for $\delta\varphi(t; t_B)$, but now an arbitrary large number of exponential PDFs can be used as basis func-

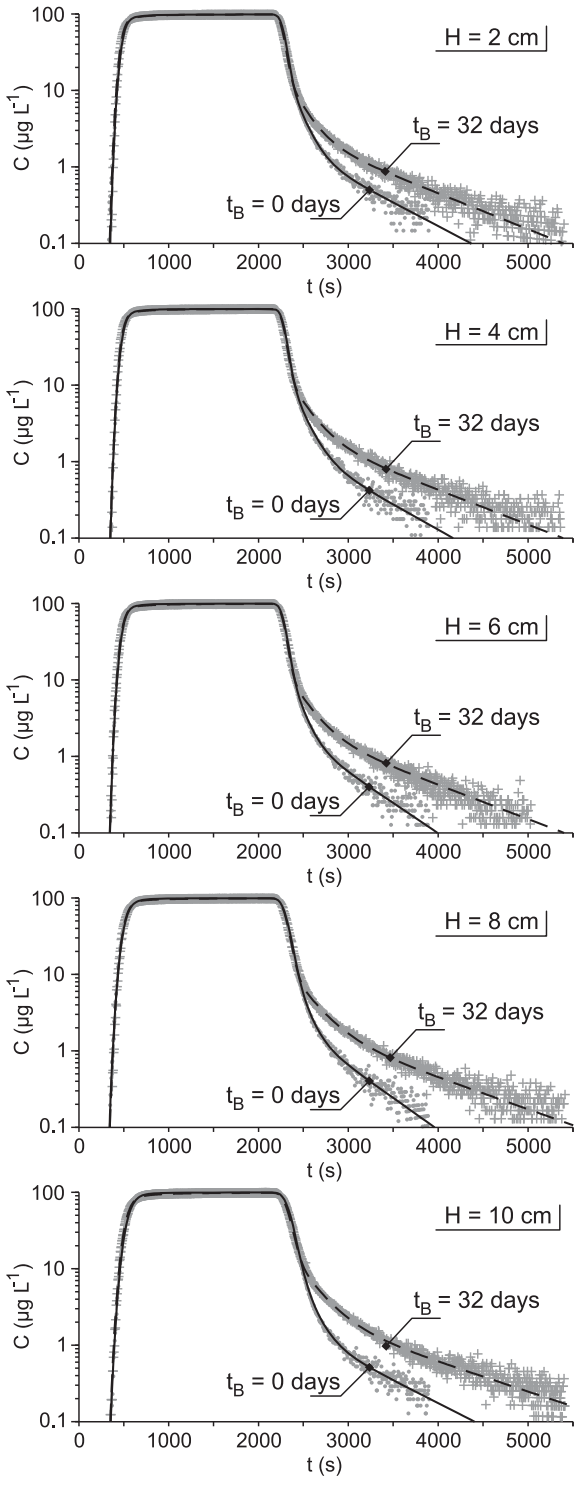

Figure 5.3. Experimental observations (dots) and simulated best-fit breakthrough curves (lines) for biofilm ages $t_B = 0$ and $t_B = 32$ days and bedform height ranging from $H = 2$ cm to $H = 10$ cm.

tions. Since the parameters of the superficial transport and of the basic retention are constant, the solution converges to a unique function $\delta\varphi(t;t_B)$ and exchange rate $\delta\alpha(t_B)$ within the time range of the experimental observations.

Model calibration is performed in mixed-scale using a linear scale to fit the bulk of the curve and log-scale for the tail using the same methodology described in § 4.4.

5.5 Results and discussion

Experimental work combined with the STIR model allowed to investigate the effect of biofilm-induced transient storage as a function of both bed morphology and biofilm age. The breakthrough curve fitting procedure for the initial configuration of the bed with clean gravel ($t_B = 0$) shows that both exchange rates, α_1 and α_2, and the mean residence times in the storage zones, T_1 and T_2 are characterized by variations between the flumes up to 20% of their respective mean value; however, no particular trend was observed (Table 5.1, Figure 5.3). A detailed analysis of the behavior of these parameters shows that when transfer rates are lower, the average residence times tend to increase. This behavior is tentatively attributed to flow irregularities. Only adequately long residence times are represented by the storage term in the model, while retention processes acting on small time scales are represented as part of the surface flow field and affect the longitudinal dispersion coefficient. The long-term retention is expected to be associated with the bottom layer of gravel, which had similar characteristics for all the flumes. However, the physically constrained gravel layer prevents deeper exchange into the bed as expected from bedform-induced pumping (*Elliott and Brooks*, 1997a,b). However, the storage effect due to flow detachment and to the formation of a local eddy with low velocities downstream of the bedform, constitutes a retention process acting on the same time scale as the superficial advection and dispersion processes. Since the flow is characterized by low submergence, the increase

H (cm)	2	4	6	8	10
A (m^2)	0.027	0.027	0.027	0.028	0.030
U ($m\,s^{-1}$)	0.083	0.083	0.083	0.080	0.075
D_L ($m^2\,s^{-1}$)	0.019	0.019	0.020	0.028	0.030
α_1 ($\times 10^{-5}\,s^{-1}$)	37.4	33.3	37.3	35.8	34.0
T_1 (s)	112	121	100	107	118
α_2 ($\times 10^{-5}\,s^{-1}$)	4.19	3.63	4.61	4.55	3.80
T_2 (s)	667	650	603	615	660

Table 5.1. Estimated parameters of the STIR model for beds without biofilm ($t_B = 0$).

in bedform height affects the whole surface flow field by increasing its heterogeneity (i.e., the velocity variance), which can be represented by an enhanced dispersion coefficient. The coefficient D_L is almost 60% higher with bedforms of $H = 10\,cm$ than of $H = 2\,cm$ (Table 5.1), and there is a clear increasing trend for the itermediate flumes. The flow cross-sectional area, A, as well as the average velocity, $U = Q/A$, where $Q = 2.25\,L\,s^{-1}$, are almost constant for all the flumes, with a slight increasing trend with bedform height. This increase is limited to 10% of the mean value, which is equal to $A = 0.028\,m^2$ and corresponds to an average depth $d_W = 7\,cm$.

Once the parameters for the superficial flow field and the basic retention for the beds without biofilms are determined, the additional retention parameters $\delta\alpha$ and $\delta\varphi(t)$ are estimated for the biofilm ages $t_B = 8, 18, 26, 32\,days$ while holding the formers fixed. The simulated concentration curves (Figure 5.3) were obtained by decomposing the additional retention function, $\delta\varphi(t)$, into 3 exponential PDFs according to equation (5.5) and (5.6). No further improvement of the data fitting

was observed with an increased number of basis functions. Biofilm effects on solute retention were isolated from comparison of results from different biofilm growth stages, and by calculating the stored mass associated to the exchange parameters derived from model calibration. Figure 5.4 shows the temporal behavior off the biofilm-induced increment of retained mass δM_S [M] relative to the initial configuration without biofilm ($t_B = 0$) for $H = 2$ and 10 cm. δM_S has an increasing trend until the tracer addition stops, and it would theoretically continue asymptotically in the case of a constant continuous injection. The subsequent decrease is due to the advective transport outside the physical domain following gradual release from the retention volumes. Transient storage clearly increases monotonically with biofilm growth over the whole time span of a tracer test, as the curve of stored mass corresponding to a given time t_B (i.e. biofilm age) is always located above the curves from the previous time points. The trend of peak values of the stored mass indicates that solute retention increases with biofilm age with a decreasing rate. In fact, it is also expected to asymptotically reach a limit value when stationary phase of biofilm growth (and constant biofilm thickness) is reached as a balance between factors such as the transfer of nutrients, conversion rates and detachment forces (steady state equilibrium).

Comparison of the initial temporal trend of the retained mass between the different flumes (Figure 5.4) suggests an effect of bed morphology on biofilm storage (i.e., increasing mass transfer from $H = 2$ cm to $H = 10$ cm). The peak values of the biofilm-induced increment of retained mass, $\delta M_{\mathrm{S,max}}$, are significantly and positively related to bedform height for all biofilms older than 8 days (Figure 5.5), and the slope of this relationship, depends on biofilm age (coefficient of determination $R^2_{\mathrm{det}} = 0.90$, probability[2] $P_0 < 0.05$, $n = 5$) and on average chlorophyll-*a* ($R^2_{\mathrm{det}} = 0.97$, $P_0 < 0.05$, $n = 4$). Similarly, slightly weaker relationships can be

[2]Probability of rejecting, when true, the null hypothesis that the angular coefficient of linear regression is zero.

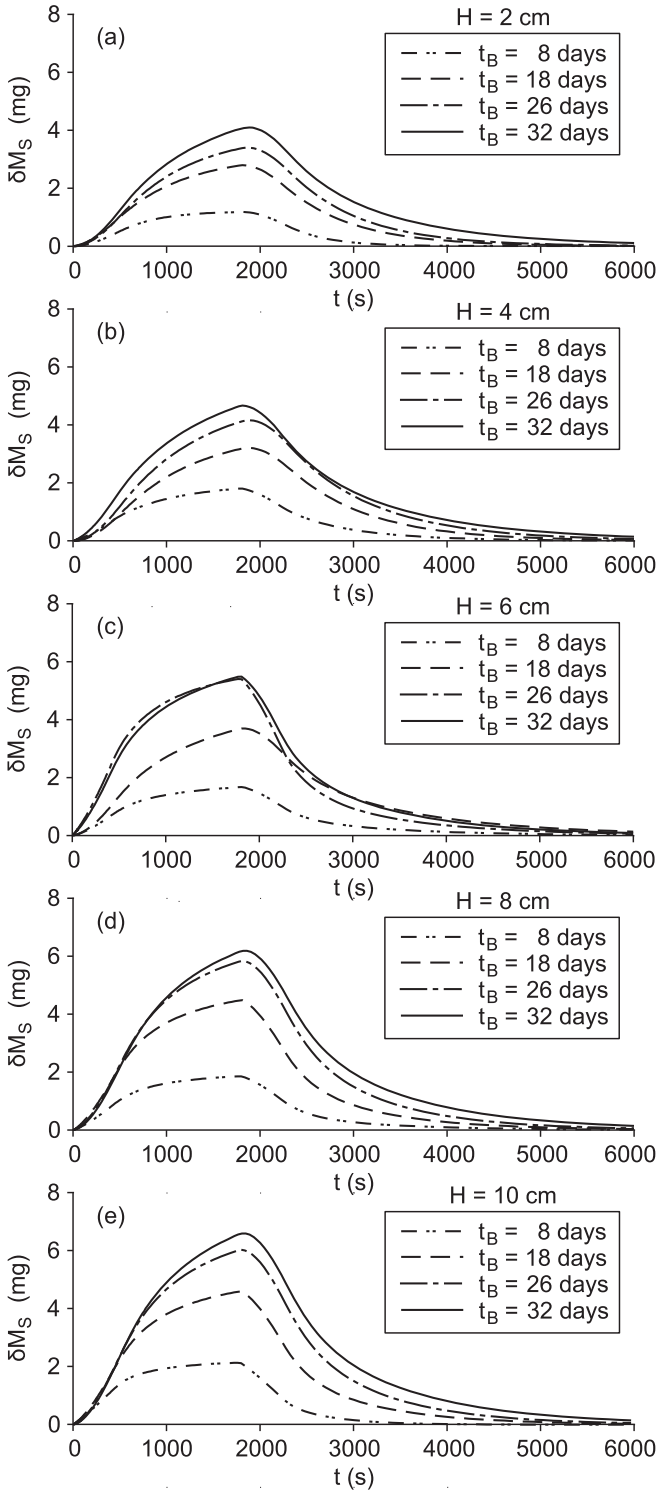

Figure 5.4. Plots of the increment of retained mass, $\delta M_S(t;t_B,H) = M_S(t;t_B,H) - M_S(t;t_B = 0,H)$, versus time, t, for different biofilm ages, t_B.

found for $M_{S,max}$, the peak values of the total retained mass which include the basic retention for $t_B = 0$ (Figure 5.5). This clearly shows an effect of bedform height on the ability of biofilms to create additional retention zones, and further suggests that this effect becomes stronger with biofilm age and biomass. This could be due to enhanced biofilm growth in flumes with higher bedforms which would lead to increasingly diverging biomass among the flumes over time and could explain the trends of $\delta M_{S,max}$ and $M_{S,max}$. Indeed, when the observed standardized values of chlorophyll-*a*, z_{Chla}, are plotted against bedform height (Figure 5.6), an increasing trend is suggested ($R^2_{det} = 0.71$, $P_0 < 0.07$), indicating that bed topography may influence the dynamics of biofilm growth leading to a higher overall biomass in environments with higher heterogeneity. An explanation for this behavior lies in the increased velocity variance associated with a higher variability of bed elevation and generating more turbulent flow field, which in turn ameliorate nutrient transfer. On the other hand, if detachment is limiting biofilm differentiation, the observed behavior may be due to the downstream shift of the flow reattachment point for higher bedforms implying an extended zone of low shear stress. This effect may exceed the increase of shear stress downstream of the reattachment point up to the crest and induce an overall reduction of the biofilm detachment rate.

Biofilm biomass (clorophyll-*a*) explained a large fraction of the variance of biofilm-induced transient storage $\delta M_{S,max}$ (Figure 5.7), even though a secondary effect of bedform height on $\delta M_{S,max}$ is still visible. A multiple linear regression model $\delta M_{S,max}$ as the dependent variable and chlorophyll-*a* and bedform height as independents identified significant influences of both predictors ($P_0 < 0.001$ for chlorophyll-*a*, $P_0 < 0.05$ for bedform height, F-value $F_{2,12} = 52.2$, overall $P_0 < 0.001$, adjusted $R^2_{det} = 0.88$). Thus, higher bedforms allow biofilms with the same chlorophyll-*a* content to increase their retention capacity.

Residuals from a linear model explaining the biofilm-induced increment of

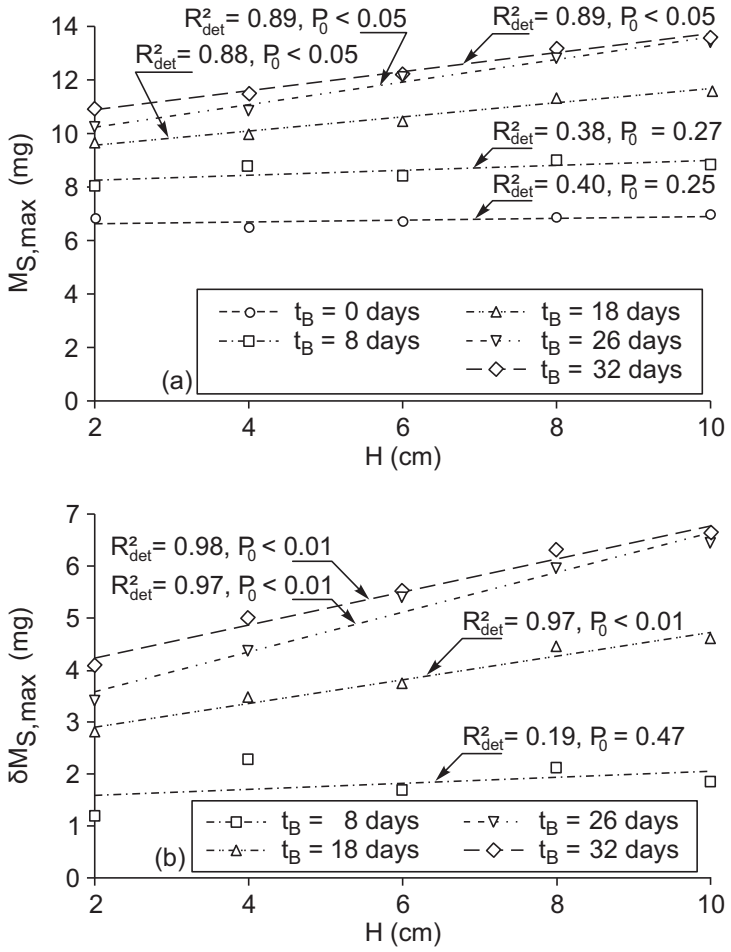

Figure 5.5. (a) Plots of the maximum values of the retained mass, $M_{\mathrm{S,max}}(t;t_B,H)$, and (b) of the increment of retained mass $\delta M_{\mathrm{S,max}}(t;t_B,H)$ versus bedform height, H, for different biofilm ages, t_B. The quantity $M_{\mathrm{S,max}}$ includes the effect of the basic retention in the absence of biofilm, which is subtracted to get $\delta M_{\mathrm{S,max}}$.

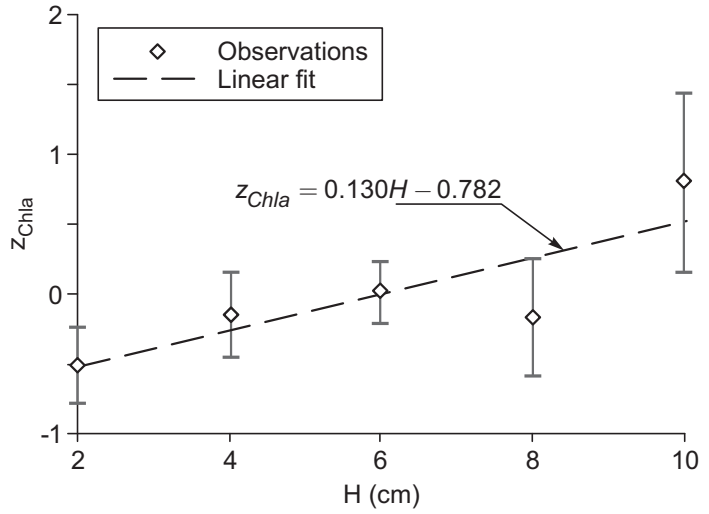

Figure 5.6. Average chlorophyll-*a* versus bedform height. Since chlorophyll-*a* increases markedly during biofilm growth, data from 4 sampling dates was *z*-standardized within each date to remove temporal variation before the averaging and comparison of flumes. Error bars represent 95% confidence interval.

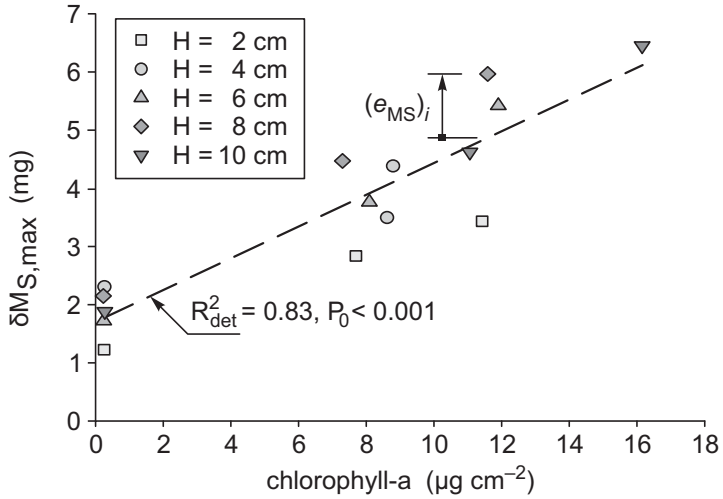

Figure 5.7. Plots of the maximum values of the additional retained mass due to biofilm, $\delta M_{S,max}$ versus chlorophyll-*a*. The positive slope of the linear regression indicates a positive correlation between transient storage and biomass.

retained mass ($\delta M_{S,max}$) as a function of chlorophyll-*a* (indicated by e_{MS}, Figure 5.7) can be regarded as a descriptor of an effect of biofilm mediated by the bedform. In fact, when plotted against bedform height (Figure 5.8), a curvilinear relationship becomes evident, suggesting saturation with increasing bedform height. Apart from increased penetration efficiency due to bedform-associated turbulence, this behavior may be attributable to complex interactions between biofilm architecture and near-bed flow field. Indeed biofilms developed different architectures in relation to the different bed morphology and hydrodynamic conditions. Biofilms developed directed architectures with filamentous streamers at exposed microhabitats (bedform crests), while biofilm growing in quiescent zones between bedforms largely consisted of non-directed coalescing microcolonies. These patterns were pronounced in flumes with higher bedforms and induced turbulence (*Besemer et al.*, 2007). Thus, biofilms are expected to increase transient storage not only via biomass effect, but also by the formation of an explicit spatial architecture, developed as an adaptation to local hydrodynamic conditions. Indeed, biofilm architecture can be regarded as a remarkable adaption to optimize solute (i.e., nutrient and energy substrate) replenishment in a given hydrodynamic environment (*Battin et al.*, 2003) and therefore it can also explain the overall increase of biomass with bedform height. Thus, higher retention would result from biofilm structural differentiation, which in turn favors biofilm growth and further increases the retention volume.

Overall, the transient storage induced by biofilm is sizable compared to the storage in the porous bed, as $M_{S,max}$ reaches values varying from 150% to around 200% of the initial retention $M_S(t_B = 0)$, for $H = 2$ and 10 cm, respectively (Figure 5.5). This is valid at least in this particular case in which the depth of the sediment layer is limited as in constrained hyporheic zones (*Orr et al.*, 2009). While benthic biofilms can clog the underlying sediments and thereby reduce solute penetration, streamers may increase turbulent mass transfer, which is a

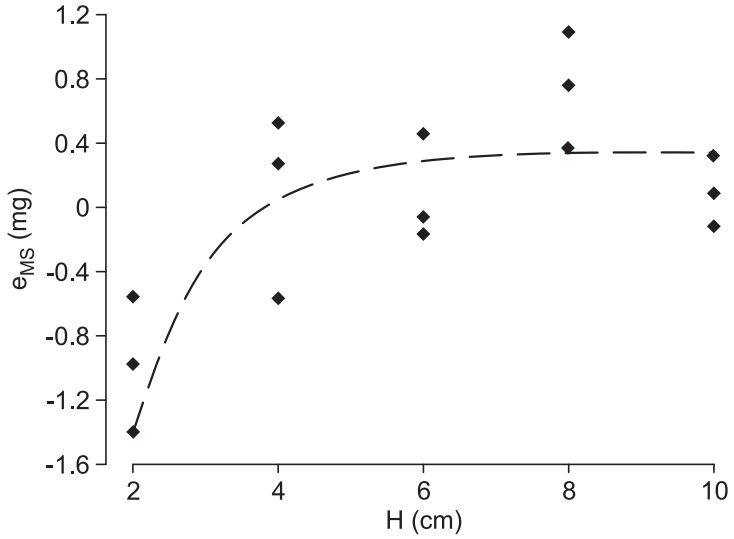

Figure 5.8. Residuals from a linear model explaining $\delta M_{\mathrm{S,max}}$ as a function of chlorophyll-*a*, indicated by e_{MS}, can be regarded as descriptors of an effect of biofilm mediated by the bedform, that may be attributable to biofilm architecture. Residuals show a saturating trend with bedform height, as suggested by a data fit to an exponential rise to a maximum (broken line).

complex fluid-structure interaction problem that remains largely unexplored.

5.6 Conclusions

Bed morphology plays a fundamental role in determining the hydrodynamic conditions affecting biofilm growth. Experimental evidence is given here by quantifying the transient storage of tracers in biofilms through the analysis of breakthrough curves following plateau injections. The effect of the biofilm was isolated from the comparison of results obtained at different stages of growth. This was achieved by applying a deconvolution method based on the STIR model presented in Chapter 3. Results show a clear effect on solute transient storage due to biofilms, which appears to be different in beds with different morphology. Biofilm-induced mass transfer was affected by both biomass and physical struc-

ture. Flumes with higher bedforms were found to be characterized by higher biofilm biomass, which is associated to a larger retention volume. Increasing bedform height induces biofilms to locally develop hydrodynamically adapted architectures (e.g., streamers) that can increase the mass transfer into the cavities of the porous structure of biofilms. The results show the potential of interdisciplinary work combining large-scale experimental set-ups and modeling to unravel basic mechanisms underlying environmental processes related to microbial biofilms and solute transport dynamics. Technical developments in the area of flow measurements at the spatial scale of biofilms also open a possible frontier for future studies. The description of the flow field at such scales will possibly allow to explain the physical transport processes that are lumped into the calibration coefficients of an integral transport model such as STIR.

Chapter 6

Bed form-induced hyporheic exchange in homogeneous sediment beds[1]

6.1 Introduction

In the previous chapters a general residence time distribution solute transport model was presented and applied to a few case studies. In these applications, particular forms were assumed for the residence time distributions in the storage zones and the relevant parameters were determined by fitting the simulated breakthrough curves to experimental concentration data from tracer tests. If enough information is available about the properties of the system under consideration, general residence time transport models can also be used as predictive tools, at least in principle. Specific modeling closures can indeed be incorporated to represent retention processes defined on smaller spatial scales than those examined in tracer tests. This is for example the idea behind the Advective Storage Path (ASP) model presented by *Wörman et al.* (2002).

[1] The contents of this chapter are subject of a paper under review: Bottacin-Busolin, A., and A. Marion (??), On the combined role of advective pumping and mechanical dispersion in bed form-induced hyporheic exchange, submitted to *Water Resour. Res.*

On very short temporal scales the exchange with the bed is dictated by turbulent diffusion across a thin surficial layer of the bed, usually referred to as the Brinkman layer. The interfacial diffusion of momentum was originally investigated by *Brinkman* (1949) and the resulting interaction between the seepage flow and the free surface turbulent flow above it has subsequently been investigated by a number of authors (*Nagaoka and Ohgaki*, 1990; *Shimizu et al.*, 1990; *Zhou and Mendoza*, 1993). On longer timescales and larger spatial scales, hyporheic flows are induced primarily by the interaction of the stream flow with topographical irregularities of the enclosing boundaries, or by planimetric variations of the flow direction. Topography-driven hyporheic exchange has been particularly studied over the years because of its importance in determining the long term response of a fluvial system to both natural and anthropic inputs of nutrients and contaminants. Many works have investigated the effects of topographical features such as slope irregularities (*Harvey and Bencala*, 1993), meanders and channel bends (*Boano et al.*, 2006a; *Marion and Zaramella*, 2006; *Cardenas*, 2003; *Cardenas et al.*, 2004) and alternating bars (*Tonina and Buffington*, 2007). Bed form-induced hyporheic exchange in particular has been extensively investigated because bed forms, such as ripples and dunes, are frequently found in rivers and their effect can usually be detected within the typical timescales of tracer tests.

Elliott and Brooks (1997a) proposed a conceptual model which came to be known as the Advective Pumping Model (APM). In the APM surface and subsurface flow are decoupled and the effect of the former on the latter is represented via a sinusoidal pressure variation imposed on a flat surface representing the top boundary of the bed. Later studies examined how bed form-induced hyporheic exchange is affected by bed form geometry (*Marion et al.*, 2002; *Cardenas and Wilson*, 2007), arbitrary surface topography (*Wörman et al.*, 2006, 2007), heterogeneities of the porous medium (*Salehin et al.*, 2004; *Marion et al.*, 2008b; *Sawyer and Cardenas*, 2009), physicochemical properties of the transported substances

(*Packman and Brooks*, 2001; *Packman et al.*, 2000b,a), unsteady flows (*Boano et al.*, 2006b), and groundwater discharge (*Cardenas and Wilson*, 2006; *Boano et al.*, 2008).

In the present chapter, a few important aspects of bed form-induced hyporheic exchange are examined adopting some of the simplifying assumptions made by *Elliott and Brooks* (1997a). With this approach the effect of the stream gradient and the propagation of bed forms on the long term behavior of the RTDs is analyzed considering the combined role of advection and pore-scale dispersion in the porous medium. Simulations show that, at late times, the statistical distributions of the residence time in the bed can show both exponential and power law behavior, with different exponents associated to advective pumping and pore scale dispersion. The results provide important clues about the choice of suitable forms of the RTDs to be used in calibration models such as STIR to identify the signature of hyporheic retention on solute breakthrough curves.

6.2 Solute transport model in the porous medium

The analysis of the transport of a passive solute in a stream bed is here limited to two spatial dimensions. A Cartesian frame of reference is adopted where x is the longitudinal coordinate, oriented along the flow direction, and y is the vertical coordinate, positive upwards. Following *Elliott and Brooks* (1997a), the physical quantity driving the hyporheic flow in the porous medium is represented by a sinusoidal head distribution imposed on the surface of a semi-infinite flat bed. The wavelength of the head distribution coincides with the bed form length, indicated by λ, and the amplitude, H, can be linked to the bed form height and the characteristics of the surface flow. The porous medium is considered to be isotropic and homogeneous, with uniform hydraulic conductivity, K, and porosity, θ.

6.2.1 Velocity field

The interaction between streamwater flow and bed forms induces sinusoidal pressure variations over the bed surface. The pressure is lowest over the crest and separation region downstream of it and rises rapidly to its highest value in the vicinity of the reattachment region near the base of the upslope. These head variations induce flowpaths going into the bed where the pressure is higher, and out of the bed where it is lower. The wavelength of the head fluctuations is equal to the bed form wavelength, λ, and the amplitude depends on the bed form geometry and flow properties. In case of a stationary bed, the pumping effect induced by the sinusoidal pressure variation on the bed surface is the main hyporheic exchange process driven by bed forms responsible of the penetration penetration of solutes into the bed.

According to Darcy's law, the average pore water (seepage) velocity is given by

$$\mathbf{u} = (u, v) = -K\nabla h, \tag{6.1}$$

where u and v are the horizontal and vertical components of the Darcy velocity, respectively, and $h(x, y)$ is the hydraulic head in the porous medium. The flow of an incompressible fluid in a homogeneous isotropic bed where Darcy's law holds is governed by the Laplace equation

$$\nabla^2 h = \frac{\partial^2 h}{\partial x^2} + \frac{\partial^2 h}{\partial y^2} = 0\,. \tag{6.2}$$

Equation (6.2) is solved for a semi-infinite porous medium with the following boundary conditions. On the bed surface, the sinusoidal head variation induced by bed forms is superimposed to the linear decrease due to the energy gradient of the overlying stream flow, whereas the sinusoidal head variation vanishes at

an infinite depth in the porous medium. In mathematical notation,

$$h = h_m \sin(kx) - Sx, \qquad y = 0, \tag{6.3a}$$

$$h = Sx, \qquad y \to -\infty, \tag{6.3b}$$

where $k = 2\pi/\lambda$ is the wave number, h_m is the semi-amplitude of the sinusoidal head over the bed surface, and S is the stream gradient. The semi-amplitude h_m is related to the characteristics of the overlying stream, such as average velocity and flow depth, and to the bed form geometry (i.e. height and shape). Following *Elliott and Brooks* (1997a), the boundary condition (6.3a) is applied on $y = 0$ rather than on the actual bed surface. This simplification well represents hyporheic exchange except at very short timescales because the unevenness of the bed profile induces only minor changes in the length and shape of the flowpaths within the porous medium.

Periodic boundary conditions are imposed on the lateral boundaries, that is

$$h(x = 0, y) = h(x = \lambda, y) + \lambda S, \qquad y < 0, \tag{6.4a}$$

$$\frac{\partial h}{\partial x}(x = 0, y) = \frac{\partial h}{\partial x}(x = \lambda, y), \qquad y < 0. \tag{6.4b}$$

The solution for the hydraulic head is then

$$h(x, y) = h_m \sin(kx) e^{ky} - Sx, \tag{6.5}$$

Using Darcy's equation (6.1), the velocity field in the bed is finally recovered:

$$u(x, y) = -u_m \cos(kx) e^{ky} + u_s, \tag{6.6a}$$

$$v(x, y) = -u_m \sin(kx) e^{ky}, \tag{6.6b}$$

where $u_m = kKh_m$ is the semi-amplitude of the pumping induced velocity on the

bed surface, $y = 0$, and $u_s = KS$ is the velocity induced by the stream gradient.

The velocity field can be written in nondimensional form using the following normalization for space and time:

$$x^* = kx, \quad y^* = ky \quad t^* = \frac{t}{T}, \tag{6.7}$$

where

$$T = \frac{\theta}{k^2 K h_m}, \tag{6.8}$$

is a time scale of hyporheic exchange, and where θ is the porosity of the bed material. The normalized velocity field can then be given as

$$u^* = \frac{u}{u_m} = -\cos(x^*)e^{y^*} + u_s^*, \tag{6.9a}$$

$$v^* = \frac{v}{u_m} = -\sin(x^*)e^{y^*}, \tag{6.9b}$$

where $u_s^* = S/(kh_m)$ is the seepage velocity induced by the stream gradient normalized by the characteristic seepage velocity due to pumping. *Elliott and Brooks* (1997b) performed flume experiments with sand beds covered by bed forms and found values of u_s^* in the range from 0.04 to 0.11. They also suggested that this range of values can be considered as typical of field cases where the bed is covered with dunes and form drag dominates the total drag.

The average volumetric flux into the bed surface is given by:

$$q^* = -\frac{1}{\lambda}\frac{k}{u_m}\int_0^{\lambda/2} v(x, y = 0)\, dx = -\frac{1}{2\pi}\int_0^{\pi} v^*(x^*, y^* = 0)\, dx^* = \frac{1}{\pi}. \tag{6.10}$$

The case of moving bed forms can be handled in a similar way by assuming a frame of reference moving at the speed of bed form propagation, U_b. In this frame of reference the bed forms appear stationary while the fluid, including pore water, has an additional component of velocity in the streamwise direction equal

to $-U_b$. Far from the bed surface, deep in the porous medium where the pumping effect is negligible, the pore water appears moving with velocity $u_s/\theta - U_b$. When $u_s/\theta - U_b = 0$, i.e. if the bed form celerity matches the gradient induced underflow, the velocity field is symmetrical. Typical flowpaths for $u_s/\theta - U_b = 0$ are shown in Figure 6.1. When $u_s/\theta - U_b \neq 0$, the symmetry disappears and the solutions can be classified in four cases illustrated in Figure 6.2: (a) $-u_m < u_s - \theta U_b < 0$, (b) $0 < u_s - \theta U_b < u_m$, (c) $u_s - \theta U_b < -u_m$ and (d) $u_s - \theta U_b > u_m$. However, it is important to notice that the interface flux, as well as the vertical component of velocity, are independent of $u_s/\theta - U_b$, and transport quantities such as penetration depth and residence times are dependent on the magnitude of $u_s/\theta - U_b$ but are independent of its sign. The analysis can therefore be simplified by considering only the absolute value of the relative underflow velocity, defined in dimensionless form as

$$U^*_{\mathrm{uf}} = \left| \frac{u_s - \theta U_b}{u_m} \right| = \left| u^*_s - U^*_b \right| . \tag{6.11}$$

As shown in Figure 6.1, for $U^*_{\mathrm{uf}} = 0$ two distinct symmetrical advective cells are visible with flowpaths penetrating indefinitely in the porous medium. For $U^*_{\mathrm{uf}} < 0$ (Figure 6.2a-b) the flowpaths outline two nonsymmetrical cells: a smaller one where the direction of the horizontal velocity component is the same as the underflow, and a larger one where it is mainly opposite. The flowpath separating the two advective cells converges in a stagnation point at a finite depth. Situation where $U^*_{\mathrm{uf}} < 1$ are typical of still or slow moving bed forms.

For rapidly moving bed forms U^*_{uf} can be higher than 1. In this case (illustrated in Figure 6.2c-d) there is only one advective cell, the streamwise component of the seepage velocity has the same direction of the underflow and there is no stagnation point. The flowpath penetrating most deeply in the bed, which outlines the lower boundary of the advective hyporheic zone, reattaches to the bed surface in a point of tangency.

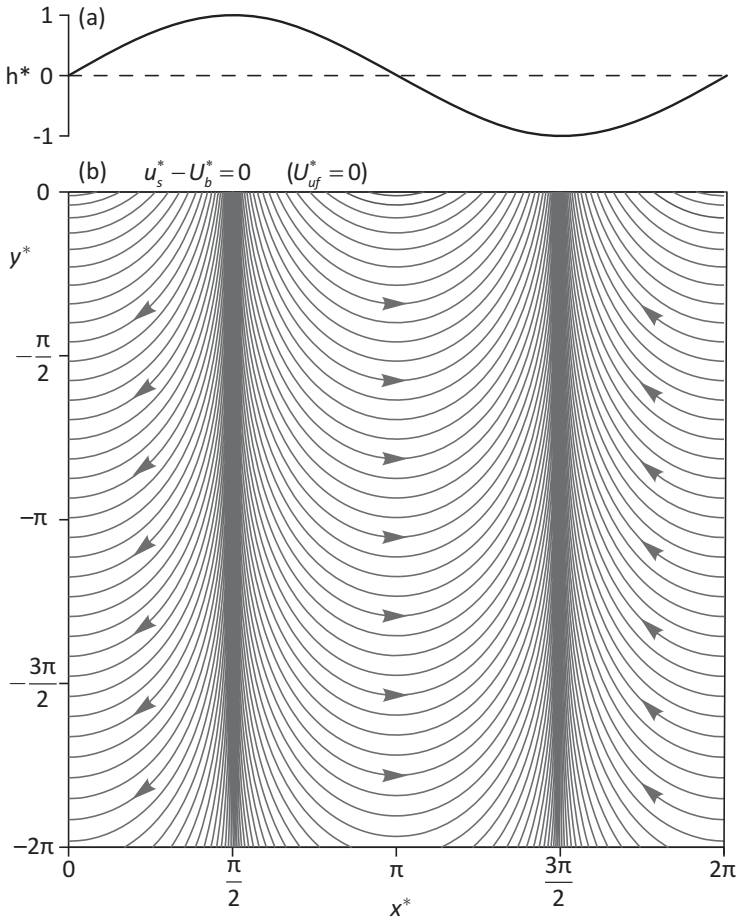

Figure 6.1. (a) Bed form-induced sinusoidal head distribution and (b) streamlines for $U^*_{\mathrm{uf}} = 0$. The frame of reference moves at the speed of bed form propagation U_b.

The minimum hyporheic zone depth, for purely advective flows, is the depth of the stagnation point (Figure 6.2a-b) for $U^*_{\mathrm{uf}} < 1$ and zero for $U^*_{\mathrm{uf}} > 1$ (Figure 6.2c-d). The maximum hyporheic depth is given by the deepest point crossed by a streamline going into and out of the bed. This is located at $x^* = \pi$ when the direction of the relative underflow velocity is positive, and $x^* = 0, 2\pi$ when it is negative. The average penetration depth is calculated as the total area of the hyporheic zone divided by λ. Figure 6.3 shows a plot of the minimum, maximum and average penetration depth of the hyporheic zone as a function of the relative underflow velocity U^*_{uf} in both (a) semi-log scale (U^*_{uf} in log-scale) and (b) log-log

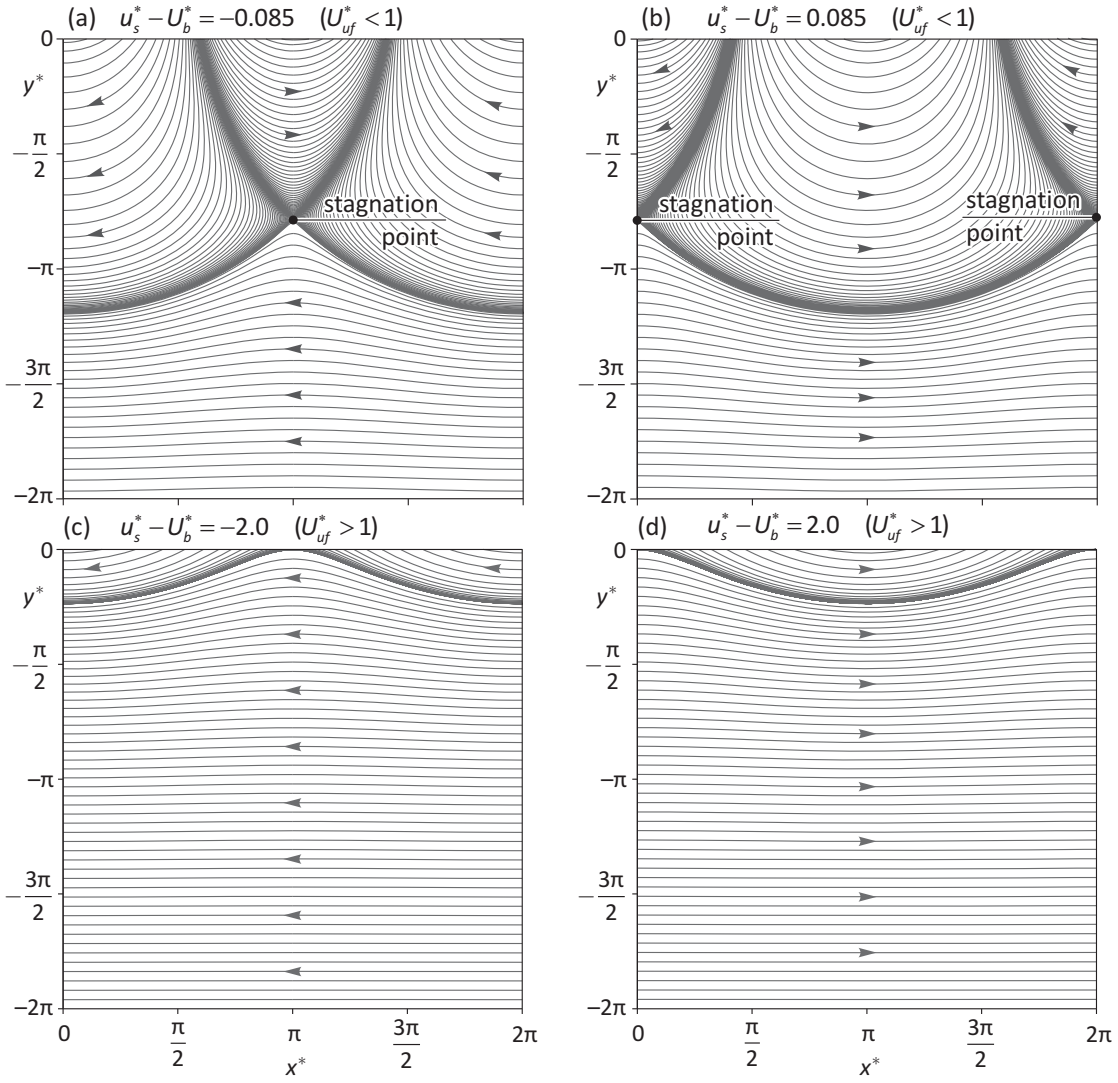

Figure 6.2. Streamlines of bed form-induced hyporheic exchange for (a) $u_s^* - U_b^* = -0.085$, (b) $u_s^* - U_b = 0.085$, (c) $u_s^* - U_b^* = -2.0$ and (c) $u_s^* - U_b^* = 2.0$. The frame of reference moves at the speed of bed form propagation. For $U_{uf}^* < 1$ two advective cells are visible: a larger cell where the average flow direction is the same as the underflow and a smaller one where it is opposite. The latter shrinks as U_{uf}^* increases and disappears for $U_{uf}^* > 1$.

scale. The penetration depth decreases linearly with $\log(U^*_{\mathrm{uf}})$ for $U^*_{\mathrm{uf}} < 1$ and is inversely proportional to U^*_{uf} for $U^*_{\mathrm{uf}} > 1$. An expression that well approximates the average depth d^* of the hyporheic zone as a function of U^*_{uf} is the following

$$d^* = \begin{cases} \dfrac{e}{\pi} - \log(U^*_{\mathrm{uf}}), & U^*_{\mathrm{uf}} < 1\,, \\ \dfrac{e}{\pi}(U^*_{\mathrm{uf}})^{-1}, & U^*_{\mathrm{uf}} \geq 1\,, \end{cases} \tag{6.12}$$

where e is the natural base of logarithms. Expression (6.12) was found by inspection.

6.2.2 Advection-dispersion model

The transport equation for a non-reactive solute in a porous stream bed can be written as (*Zheng and Bennett*, 1995)

$$\theta \frac{\partial C}{\partial t} + \frac{\partial}{\partial x_i}\left[u_i C - \theta D_{ij}\frac{\partial C}{\partial x_j}\right] = 0\,, \tag{6.13}$$

where C is the solute concentration, u_i are the components of the seepage (Darcy) velocities, D_{ij} are the components of the hydrodynamic dispersion tensor given by

$$\theta D_{ij} = \alpha_T |\mathbf{u}| \delta_{ij} + (\alpha_L - \alpha_T)\frac{u_i u_j}{|\mathbf{u}|}\,. \tag{6.14}$$

In this study the description of the flow field is limited to two dimensions, hence $i, j = 1, 2$. In equation (6.14) $|\mathbf{u}|$ is the magnitude of the seepage velocity, δ_{ij} is Krnocker's delta, and α_L and α_T are the longitudinal and transverse dispersivities, respectively. In most applications, the longitudinal dispersivity can be assumed to be approximately equal to the mean particle size.

Introducing the normalized quantities

$$C^* = \frac{C}{C_0}, \quad u_i^* = \frac{u_i}{u_m}\,, \tag{6.15}$$

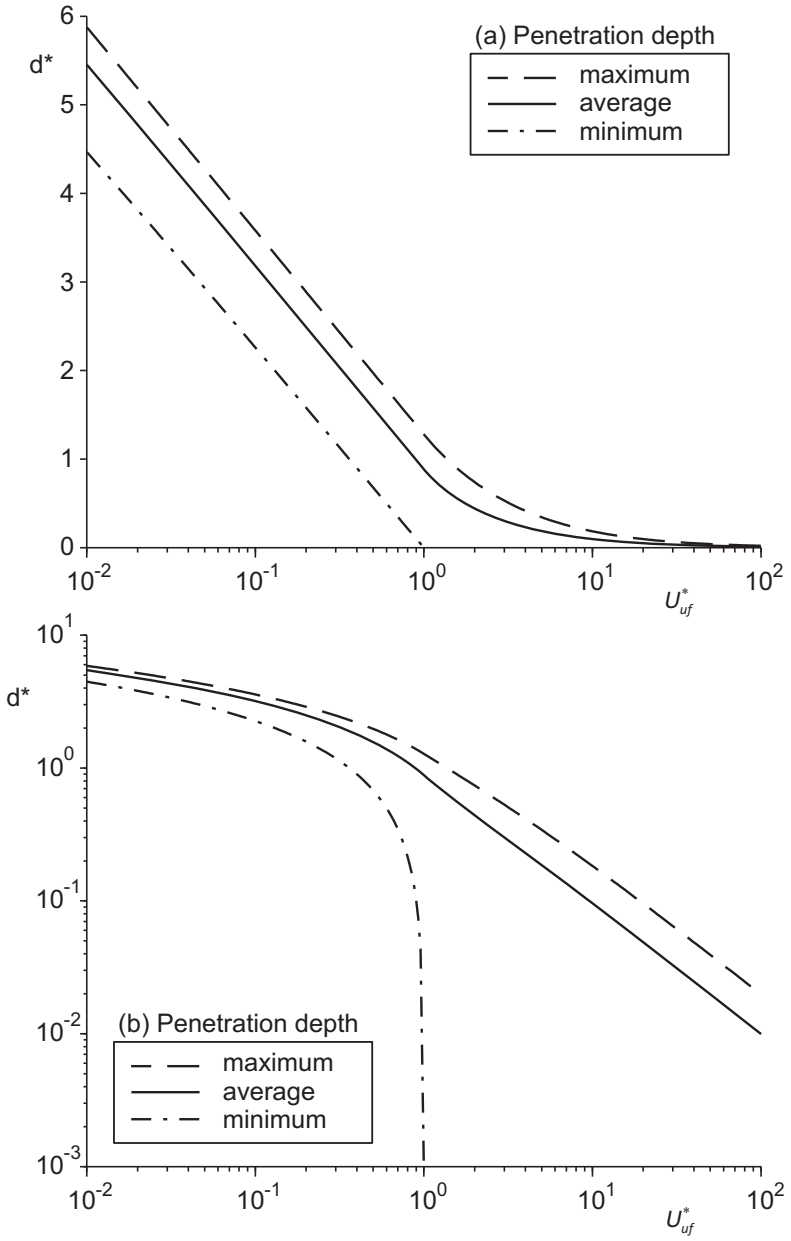

Figure 6.3. Penetration depth of bed form-induced hyporheic exchange. The dashed line represents the maximum penetration depth due to advective pumping, i.e. the distance from the bed surface of the deepest point crossed by streamlines going into and out of the bed. The dashed-dotted line represents the depth of the stagnation point, vanishing for $U^*_{\mathrm{uf}} > 1$. The continuous line represents the average penetration depth, i.e. the average thickness of the hyporheic zone.

where C_0 is a reference concentration, and

$$D^*_{ij} = \frac{\theta D_{ij}}{K h_m} = \frac{k\theta D_{ij}}{u_m} = \alpha^*_T |\mathbf{u}^*| \delta_{ij} + (\alpha^*_L - \alpha^*_T) \frac{u^*_i u^*_j}{|\mathbf{u}^*|}, \tag{6.16}$$

where $\alpha^*_L = k\alpha_L$ and $\alpha^*_L = k\alpha_T$ are the dimensionless dispersivities, equation (6.16) can be written dimensionless form:

$$\frac{\partial C^*}{\partial t^*} + \frac{\partial}{\partial x^*_i} \left[u^*_i C^* - D^*_{ij} \frac{\partial C^*}{\partial x^*_j} \right] = 0. \tag{6.17}$$

When adopting a frame reference moving at the speed of bed from propagation, equation (6.17) remains unaltered and x_i and u_i are respectively the spatial coordinates and the vertical components relative to the moving frame of reference. However, the velocity components defining the dispersion tensor in (6.16) are those relative to the fixed frame of reference.

Equation (6.17) is solved using a modified code from the CLAWPACK software library (*LeVeque*, 1997). The equation is discretized using a finite volume method which is essentially second order accurate for smooth concentration distributions and which can also handle step gradients in C^* (even discontinuities if $D^*_{ij} \equiv 0$). This is accomplished via a fractional step method solving the advection portion of the equation with a high resolution shock-capturing method and the diffusion equation with an implicit finite-volume discretization. The details of the algorithm are described in a work by *Calhoun and LeVeque* (2000). In solving the equation we tested for grid independence and also checked the solutions for independence on the depth of the lower domain boundary where a no-flux condition was applied, so that the solutions can be regarded as relevant to a semi-infinite bed.

6.3 Residence time distributions

In order to incorporate bed form-induced hyporheic exchange in a general RTD transport model such as STIR, an adequate residence time distribution has to be provided. In the STIR model RTDs are used as transfer functions to account for the complex transport dynamics in the storage zones. The effect of the transient storage on the solute concentration in the surface stream can thus be given in terms of the flux entering the retention domains and the statistics of the residence time within them. In this work the term "residence time function", indicated by R, is used to refer to the complementary cumulative residence time distribution, following *Elliott and Brooks* (1997a). For a mass pulse entering the porous medium at time $t_0 = 0$, the function $R(t)$ returns the fraction of solute still in the bed at time t. The corresponding probability density function (PDF) of the residence time is given by $\varphi(t) = -dR/dt$.

6.3.1 Pure advection

Elliott and Brooks (1997a) analyzed the solute exchange induced by pressure variation on the surface considering the effect of pure advection in the porous medium. In this case the residence time distribution can be found using a numerical particle tracking technique applied to the known flow field in the porous medium. Elliott and Brooks provided an analytical solution for the residence time distribution in the idealized case of a bed without stream gradient. The solution was given in implicit form as

$$t^* = \frac{2\cos^{-1} R_0}{R_0}. \tag{6.18}$$

The residence time function R_0 solution of equation (6.18) is a long tail distribution which for $t \to \infty$ follows a power law with $R_0 \propto t^{-1}$. This means that the corresponding probability density function, $\varphi_0(t)$, takes the asymptotic form $\varphi_0 \propto t^{-2}$. A closed form approximation of the solution of equation (6.18) is pro-

posed here as follows

$$R_0(t^*) = 1 - \frac{\pi}{4}\left(\frac{1 - e^{-\beta t^*}}{\beta} - \frac{2}{1 + 2/t^*}\right), \tag{6.19}$$

where

$$\beta = \frac{\pi}{2(\pi - 2)}. \tag{6.20}$$

The function (6.19) was found by direct comparison of different functional forms approximating the numerical solutions of equation (6.18) and represents an alternative of the probability density function given by *Marion and Zaramella* (2005b) (see § 3.2.4). This form is easier to handle because it has a closed form integral and has a simpler Laplace transform (which is often useful for semi-analytical solution of transport models such as STIR or CTRW).

In the case of a gradient induced underflow the RTD no longer follows a power-law indefinitely, because the flowpaths are confined in a zone of finite thickness. When $U^*_{\mathrm{uf}} < 1$, the power-law behavior of the tail is visible only up to a given timescale. The presence of a stagnation point in the flow field (Figure 6.2a-b) implies that there is no finite maximum residence time, but at longer times the R function rapidly decays to zero following an exponential law. In order to give an analytical form to $R(t^*)$ it must be noted that $R(t^*)$ overlaps with $R_0(t^*)$ (equation (6.19)) at initial times and that it follows an exponential decay as $t^* \to \infty$. Inspection of the form of $R(t^*)$ leads to an analytical approximation in which two timescales are specifically introduced as a function of U^*_{uf}. The function R is shown to be approximated extremely well by the following expression

$$\begin{aligned} R(t^*; U^*_{\mathrm{uf}}) &= R\left(t^*; U^*_{\mathrm{uf}}, t^*_c(U^*_{\mathrm{uf}}), t^*_d(U^*_{\mathrm{uf}})\right) = \\ &= \frac{R_0(t^*)\exp\left[-(t^*/t^*_c)^{1+U^*_{\mathrm{uf}}}\right] + R_0(t^*_c)}{1 + R_0(t^*_c)} \cdot \frac{1 + e^{t^*_c/t^*_d}}{e^{t^*/t^*_d} + e^{t^*_c/t^*_d}}, \quad \text{for } U^*_{\mathrm{uf}} < 1, \end{aligned} \tag{6.21}$$

where t^*_c and t^*_d are two timescales linked to the velocity U^*_{uf}. They can be deter-

mined by fitting (6.21) to the residence time functions calculated by numerical particle tracking. The values of t_c^* and t_d^* resulting from the least-square fitting of R for U_{uf}^* in the range between 0.01 and 1 are plotted in Figure 6.4. A comparison between the residence time function numerically derived and the approximating function (6.21) is shown in Figure 6.5 for a few values of the velocity U_{uf}^* logarithmically spaced in the range between 0.01 and 0.95. As shown in Figure 6.4, t_c^* and t_d^* appear to follow a power-law except in a small range of values of U_{uf}^* very close to 1, where the approximation error associated to (6.21) rapidly increases. An approximation for t_c^* and t_d^* is given by

$$t_c^* = 2t_d^* = \frac{4}{U_{\text{uf}}^*}. \tag{6.22}$$

When the function (6.21) is used in combination with (6.22), the mean relative error of $\log(R)$ for R values in the range $10^{-7} < R < 1$ is less than 3% for $U_{\text{uf}}^* < 0.66$ and less than 5% for $U_{\text{uf}}^* < 0.75$.

To understand the meaning of the timescales t_c^* and t_d^*, we observe that at early times, i.e. $t \ll t_d^* \ll t_c^*$, $R(t^*) \to R_0(t^*)$. Another property of equation (6.21) is that, for $t^* > t_c^* > t_d^*$, $R \sim e^{-t^*/t_d^*}$, where the symbol $\sim$ means "asymptotically proportional to". In a semi-log graph the tail of R follows a straight line and the slope is a function of t_d^*. The time t_c^* can be considered as the timescale at which $R(t^*)$ diverges from the idealized behavior given by $R_0(t^*)$ and begins to decrease exponentially with decay rate t_d^{*-1}. Since R_0 exhibits a power-law behavior for about $t^* > 10$, with $R_0 \sim t^{-2}$, t_c^* can be seen as the timescale for transition between the power-law and the exponential decay of R, provided that $t_c^* \gg 10$ (i.e. $U_{\text{uf}}^* \ll 0.4$).

When the relative velocity of the underflow is higher than maximum pumping velocity $U_{\text{uf}}^* > 1$), the flowpaths are confined in a single advective cell, and a stagnation point is no longer present. From a residence time perspective, this

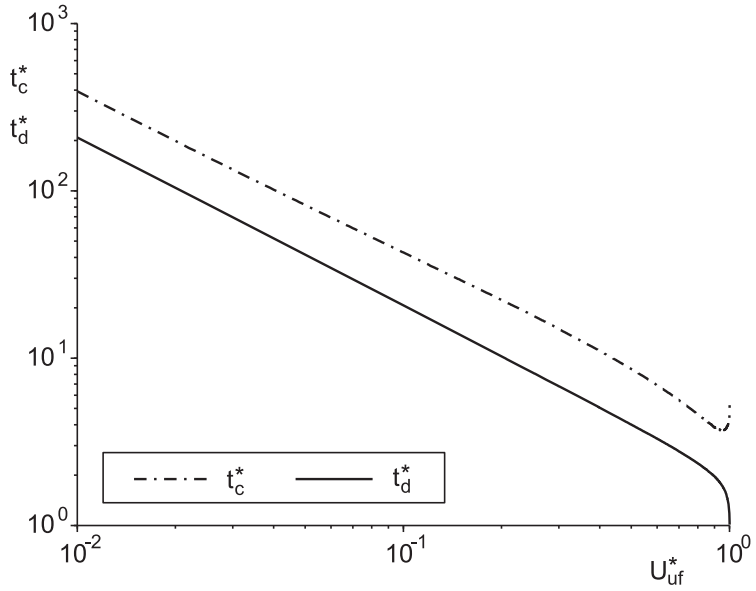

Figure 6.4. Timescales of the residence time distributions for $U^*_{\mathrm{uf}} < 1$ in case of pure advective transport in the porous medium. t^*_c represents the timescale at which the residence time function R departs from the ideal solution for $U^*_{\mathrm{uf}} = 0$, namely R_0, and begins to decrease exponentially with decay rate t^{*-1}_d ($R \sim e^{-(t^*-t^*_c)/t^*_d}$).

implies the existence of a finite maximum residence time, $t^*_{\max}$. For $U^*_{\mathrm{uf}} \gg 1$, $t^*_{\max}$ is linked to U^*_{uf} by the following approximation

$$t^*_{\max} = 2\pi(U^{*-1}_{\mathrm{uf}} + U^{*-4}_{\mathrm{uf}}), \tag{6.23}$$

and the residence time is beta-distributed in the interval $[0, t^*_{\max}]$. However, for $U^*_{\mathrm{uf}} \gg 1$ the advective zone is so thin that the effect of the real shape of the bed forms, both in terms of height and aspect ratio, becomes significant, and the sinusoidal model no longer provides an adequate description of the interfacial exchange dynamics. Nevertheless, the sinusoidal head model can still be used to assess, at least qualitatively, the relative importance of advective pumping and mechanical dispersion.

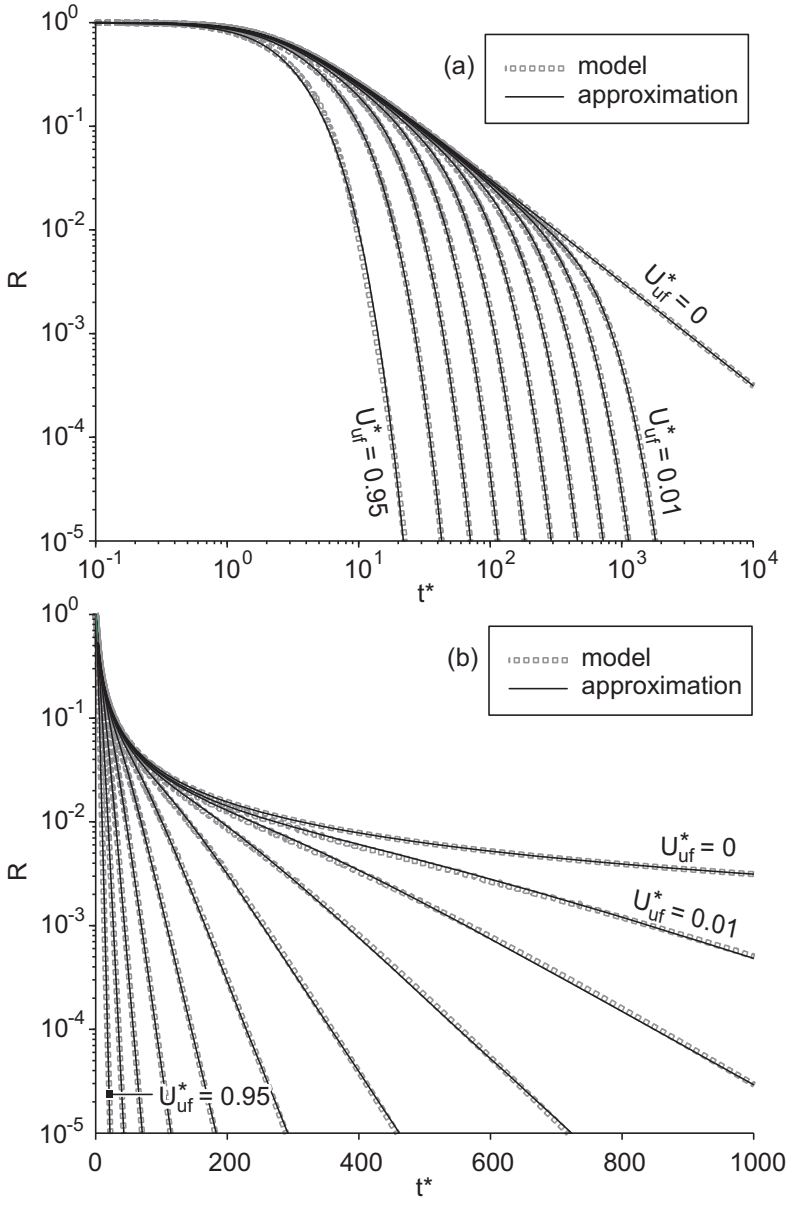

Figure 6.5. Complementary cumulative distributions of the residence time within the bed plotted in (a) log-log scale and (b) log-linear scale. The gray dotted lines represent the distributions obtained by numerical particle tracking and accounts solely for the advective transport in the porous medium. The continuous black lines represents analytical approximations given by equation (6.21). The RTDs display a power-law behavior where $R \sim t^{-1}$ up to a certain timescale after which the probability decays exponentially with time.

6.3.2 Effect of pore-scale dispersion

The residence time distributions in the porous medium are derived by solving the advection-dispersion equation (6.17) for a step injection of a constant concentration $C_0^* = 1$ at the downwelling boundary, $0 \leq x^* \leq \pi$,

$$C^* = 0\,, \qquad t < 0\,, \tag{6.24a}$$

$$C^* = C_0^* = 1\,, \qquad t^* \geq 0\,. \tag{6.24b}$$

The residence time function is then calculated as

$$R(t^*) = 1 - \frac{1}{2\pi q^* C_0^*} \int_{\pi}^{2\pi} v^*(x^*) C^*(x^*, t^*)\, dx^*\,, \tag{6.25}$$

where $2\pi q^* = 2$ is the flow rate per unit width into the bed at the downwelling boundary.

Figure 6.6 presents the simulated residence time functions resulting from the advection-dispersion model compared to the corresponding functions in case of pure advective transport in the porous medium. The curves in Figure 6.6 were obtained for $u_s^* = 0.1$ considering values of U_{uf}^* in the range $0 \div 5$ and three different values of the dispersivities, namely (a) $\alpha_L^* = 0.006$, (b) $\alpha_L^* = 0.06$ and (c) $\alpha_L^* = 0.6$ thus covering a broad range of situations. In the simulations the ration α_T/α_L was assumed to be constant and equal to 1/3 as suggested in other studies (*Benekos*, 2005; *Zheng and Bennett*, 1995; *Qian et al.*, 2008). Note that each distribution must be characterized both in terms of U_{uf}^* and u_s^* because even when adopting a moving frame of reference the dispersion tensor still depends on the actual seepage velocity, and not the relative one. This means the case of dispersive transport is more complex to analyze because the statistics of the residence time is characterized by two more degrees of freedom relative to the pure advective case. In fact the RTD depends on 3 parameters (at least): the relative

underflow velocity U^*_{uf}, the seepage velocity induced by the stream gradient u^*_s and the dispersivity α^*_L, the ratio α_T/α_L being taken as fixed.

Pore-scale dispersion induces longer tails in the residence time distributions (Figure 6.6) by producing a net downward-directed flux at the interface between the advection dominated pumping zone and the underlying porous medium. This flux is associated to permanent mass loss which implies that a fraction of the solute entering the bed has infinite residence time. When the dispersivities are high, the purely advective model can significantly underestimate the mass transfer into the bed at late times. In the dispersion dominated region, where the RTD diverges from the prediction of the advective model, the R function exhibits a pattern similar to a power-law. If the dispersion tensor was constant, $R(t)$ would diverge from the pure advective case following a power-law with exponent $-1/2$ ($R \sim t^{-1/2}$). Since the dispersion tensor is related to the seepage velocity according to (6.16), thus varying along the y-direction and assuming a constant value where the underflow velocity is not affected by pumping, the tail of the R function shows a more complex behavior resulting in $R \sim t^{-1/2}$ only at later timescales (Figure 6.6). At earlier times, pore-scale dispersion induces a pattern that can be approximated by a power-law with exponents lower than $-1/2$. As shown in Figure 6.7, the seepage velocity u^*_s affects the tail of R in the dispersion dominated region inducing longer residence times as u^*_s increases, consistently with the increase of the components of the dispersion tensor (equation (6.16)). Nevertheless, for the range of values determined in laboratory experiments by *Elliott and Brooks* (1997b), namely $u^*_s = 0.04 \div 0.11$, and indicated as typical of field situations where the form drag dominates the total drag, the variations of R for a given U^*_{uf} are rather small.

Depending on the values of the underflow velocity and of the dispersivities, the effect of dispersion is visible at different timescales. The tails of the R function can be divided in different time ranges to which different functional forms

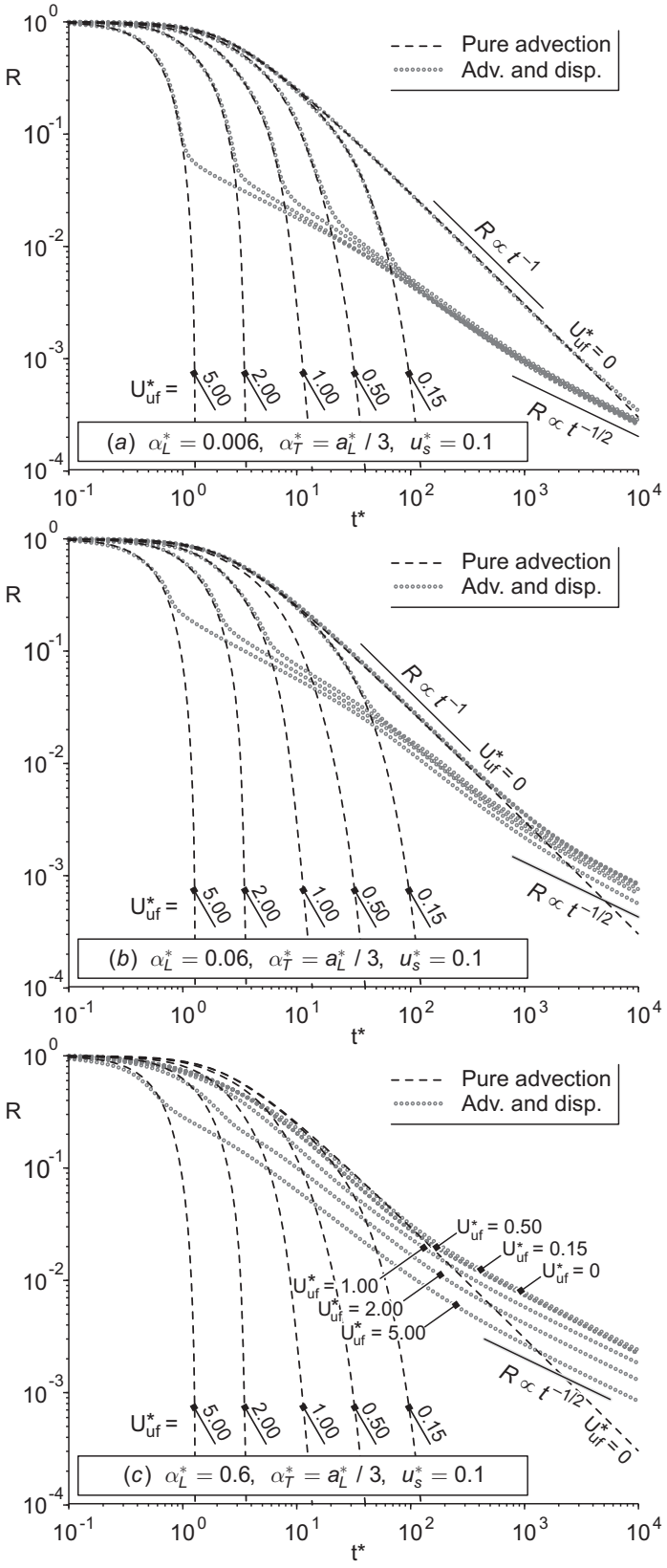

Figure 6.6. Residence time functions of hyporheic exchange in case of advective-dispersive transport in the porous medium for different values of the dispersivity α^*_L and relative underflow velocity U^*_{uf}. In the simulations the ratio α^*_T/α^*_L and the velocity u^*_s are kept constant and equal to 1/3 and 0.1, respectively. Pore-scale dispersion induces longer tails in the R function which teds asymptotically to follow a power-law scaling as $R \propto t^{-1/2}$. At earlier times in the temporal region dominated by dispersion, the slope of the function in a log-log graph is not constant and can assume values lower than $-1/2$ as a consequence of the vertical variability of the dispersion tensor.

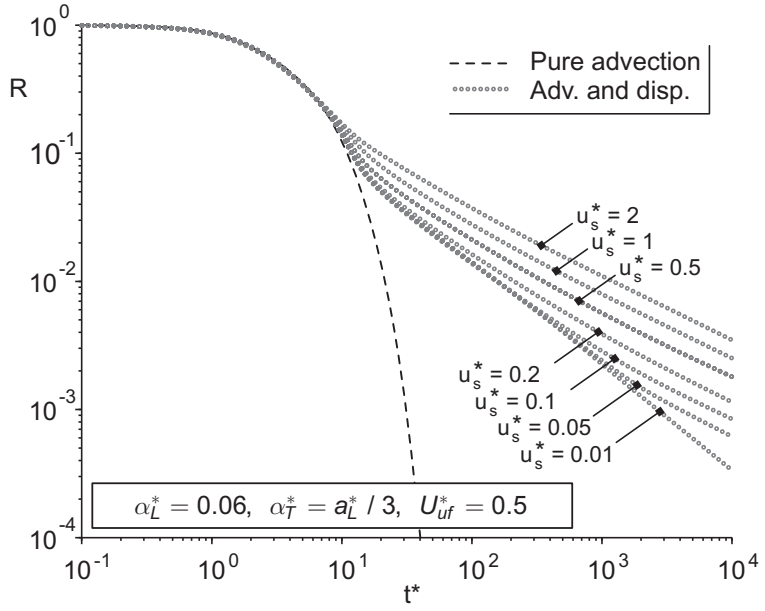

Figure 6.7. Effect of the seepage velocity induced by the stream gradient, u_s^*, on the residence time function, R, for a given relative underflow velocity, $U_{\text{uf}}^* = 0.5$. The curves are generated by keeping U_{uf}^* constant, which implies that an increase of u_s^* is balanced by an increase of the bed form propagation celerity, U_{uf}^*. Higher velocities u_s^* produces higher dispersion coefficients which in turn increase the probability associated to longer residence times.

apply. To illustrate this concept, we consider the case of $u_s^* = 0.1$ presented in Figure 6.6. For $U_{\text{uf}}^* \approx 0$ the late time behavior of the residence time function is characterized by a first power-law region where $R \sim t^{-1}$ and a final region, dominated by dispersion, where $R \sim t^{-1/2}$. This is the limit case characterized by the highest mass transfer. It should be noted that situations where $U_{\text{uf}}^* \approx 0$ can be found when the speed of bed form propagation is approximately equal to the groundwater velocity induced by the stream gradient. For U_{uf}^* sufficiently higher than zero but $U_{\text{uf}}^* < 0.4$ (i.e. $t_c^* < 10$) and relatively small dispersivities ($\alpha_L^* \ll 0.6$), the tail of residence time function shows a power-law pattern with $R \sim t^{-1}$ in the time range where the advective pumping process is dominant, a second range

where the function decays exponentially ($R \sim e^{-t^*/t_d^*}$) due to the limiting effect of the underflow, and then another temporal region, when the exchange process is dominated by mechanical dispersion, where R tends to be asymptotically proportional to $t^{-1/2}$ but with slightly lower exponents at earlier times. For $0.4 < U_{\mathrm{uf}}^* < 1$, the tail is characterized by an exponential region followed by a power law region where $R \sim t^{-1/2}$ at late time. When $U_{\mathrm{uf}}^* \gg 1$ the effect of advective pumping early becomes negligible compared to the effect of dispersion which is the only process responsible for the long term behavior of the residence time function. The result would not sensibly change if the effect of turnover is accounted for. Indeed, pore-scale dispersion can well explain the discrepancy observed by *Elliott and Brooks* (1997b) between the prediction of their turnover model and their experimental results: the turnover model greatly underestimated the exchange for moving bed forms, especially in case of high propagation speeds, and the penetrated mass was found to be increasing with $t^{1/2}$.

As the dispersivity of the porous medium increases, the exchange process is dominated by dispersion at increasingly earlier timescales. When the dispersivity is high, as shown Figure 6.6c for $\alpha_L^* = 0.6$, dispersion is the dominant process affecting the whole tail of R. In this situation the effect of the vertical variability of the dispersion tensor is even more evident: the slope of R in a log-log graph is lower than $-1/2$ in a wide temporal range and $R \sim t^{-1/2}$ only at late times.

6.4 Discussion

In experimental tracer tests, the late time behavior of breakthrough curves is recognized to be the signature of long term retention typically associated to hyporheic exchange. The results presented here show that distinct functional forms of the residence time distributions apply in appropriate time ranges. The temporal extension of these regions depends on the characteristics of the surface flow and the sediment bed. Although these results were derived for a semi-infinite

bed, a qualitative description of how the results would change in case of a permeable bed of limited thickness can be given on conceptual basis.

It is known from solutions of the one-dimensional diffusion equation (e.g. *Polyanin*, 2002) that, when a constant concentration is imposed at one of the edges of a bounded domain and a no-flux condition is applied at the other edge, the ingoing flux decreases exponentially at late times. In the case of bed form-induced exchange, this implies that, when the penetration is limited by an impermeable boundary placed deeper underneath the pumping-dominated advective zone, the final part of the residence time distribution displays an exponential decay. This behavior characterizes the temporal range in which the limiting effect of the impermeable boundary significantly affects the vertical concentration profile, whereas at earlier times the distributions remain unaltered. On the other hand, if the thickness of the permeable layer is small enough to affect the flowpaths induced by the bed form-associated pumping effect, and if the relative underflow velocity is low enough to allow the formation of a stagnation point in the flow field within the bed, then the maximum residence time is infinite (at least from a mathematical perspective), but the associated probability must rapidly decrease to zero at late times, most probably exponentially.

Wörman et al. (2002) suggested that the statistics of the residence time of bed form-induced hyporheic exchange could be represented by a lognormal distribution. For stationary bed forms and typical groundwater velocities induced by the stream gradient, a comparison in linear scale shows that, for properly chosen parameters, a lognormal distribution can be a good approximation of equation (6.21). Nevertheless, when the distributions are compared in a logarithmic scale, their tail behavior appears substantially different, and even more different if the effect of dispersion is accounted for. The importance of comparing model simulations to concentration data in log(concentration) scale at late time has been increasingly recognized in the recent years. Recent studies have shown that tracer

breakthrough curves often exhibit a long tail behavior that may be in the form of power-law patterns. *Haggerty and Wondzell* (2002) reported data from a tracer test in a 2nd-order mountain stream in which the tail of the breakthrough curve followed a power-law scaling as $t^{-1/3}$ over at least 1.5 orders of magnitude in time. *Gooseff et al.* (2003b) performed tracer tests in different reaches of a mountain stream and found that the experimental curves could be well approximated using a truncated power-law RTD to represent transient storage, with exponents ranging from −1.6 to −1.3. More recently *Gooseff et al.* (2007) reported data from tracer tests performed in streams of different channel complexity. Part of them could be represented by a conventional model assuming an exponential RTD, but a few of them displayed power-law patterns with exponents in the range between −1.9 and −1.7. Although the substrate material of the streambed in these tracer studies was primarily gravel, cobbles and bedrock, to which the pumping theory does not apply, it can be noticed that exponents of the power-law reported lie chiefly between −2 and −3/2, the values associated to advective pumping and dispersion, respectively. Intermediate exponents between −2 and −3/2 have been shown to arise as a consequence of the vertical variability of the dispersion tensor, but can also be due to the multi-convolution of the residence time distributions of many bed forms arranged in sequence. Heterogeneity of the porous medium may also play a role in defining the apparent exponent of the power-law (*Sawyer and Cardenas*, 2009). On the other hand, exponents higher than −3/2, indicating a slower release of solutes from the storage zones, cannot be explained within the modeling framework presented here.

The direct application of the multiple region description given in this chapter to real water courses appears at the moment quite difficult given the level of indetermination of the physical quantities of the system, e.g. sediment permeability, hydraulic conductivity and dispersivity. Tracer tests remain the simplest way to extract information about hyporheic exchange in field applications. The

uncertainty arising from the superposition of surface and subsurface retention processes requires that the number of parameters involved in transport models is kept to the minimum necessary to get an acceptable representation of the observed breakthrough curves. The introduction of two distinct exponential distributions, as suggested by some authors (*Harvey et al.*, 2005; *Briggs et al.*, 2009), is the simplest way to move from a single RTD, as for instance in the Transient Storage Model (*Bencala and Walters*, 1983), to multiple RTDs. Recent contributions by *Briggs et al.* (2009) and the analysis presented in Chapter 4 show that models with two exponential RTDs are flexible enough to be successfully calibrated with field tracer data. The results presented in this chapter show that an exponential distribution can well approximate the statistics of the residence time in hyporheic zones of limited thickness. When advective pumping or mechanical dispersion in the porous medium are dominant processes, the use of two exponential RTDs may still provide acceptable results in field tracer applications. This is because the typical timescales of observations are relatively short due to constraints imposed by instrumental detection limits. However, the power-law behavior of the RTD associated to advective pumping and pore-scale dispersion implies that the mean residence time in the hyporheic zones is scale dependent as observed Chapter 4. Power-law patterns requires accurate measures over a wide range of timescales to become clearly recognizable. Over smaller temporal ranges the difference between a power-law and an exponential behavior may not be detectable without uncertainty. However, when the tails of the observed breakthrough curves exhibit seemingly power-law patterns with exponents close to -2 or $-3/2$, this can be regarded as a fingerprint of bed from-induced advective pumping and subsurface dispersion affecting a significant portion of the porous medium. The latter can also be associated to a significant mass loss.

6.5 Conclusions

Simulations have shown that the residence time distributions of bed form-induced hyporheic exchange are characterized by a complex tail behavior due to the combination of advective transport and pore-scale dispersion in the porous medium. At different stage of the exchange process, the RTDs are characterized by different functional forms. When the bed form-induced advective pumping is a dominant process and the flowpaths are not limited by an underlying groundwater flow or by an impermeable boundary, the probability density function of the residence time, $\varphi(t)$, asymptotically tends to a power-law decaying as t^{-2} ($R \sim t^{-1}$). The combination of the seepage velocity induced by the stream gradient, and the celerity of the translating bed forms in case of a moving bed, results in a limitation of the advective transport into deeper portions of the porous medium and causes the PDF to rapidly decay to zero if only advection is accounted for. When the underflow velocity relative to a frame of reference moving at the speed of bed form propagation is lower than the maximum pumping-induced velocity, $\varphi(t)$ decays exponentially, $\varphi \sim e^{-t/t_d}$ ($R \sim e^{-t/t_d}$), and the slope in a semi-log graph depends on a properly defined timescale t_d. When the relative velocity of the underflow is higher than the maximum pumping-induced velocity, the residence time varies in a bounded time interval and is beta-distributed within it. Pore-scale dispersion counteracts the limiting effect of the relative underflow velocity producing longer tails in the RTDs. In the time ranges dominated by dispersion the PDF $\varphi(t)$ follows a power-law tending to $\varphi \sim t^{-3/2}$ at late times ($R \sim t^{-1/2}$), and slightly lower exponents can be found at earlier times as a consequence of the vertical variability of the dispersion tensor.

The results presented highlight that both exponential and power-law patterns in the late time behavior of solute breakthrough curves can be associated to hyporheic exchange. When the first prevail, the thickness of the hyporheic zone

is limited, whereas, when the second prevails, there is deeper exchange with the bed that may be due to advective pumping or mechanical dispersion. The identification of power-law patterns in the breakthrough curves of tracer tests requires measurement over a wide range of timescales, often not available because of instrumental detection limits. This limitation can make calibration models assuming an exponential RTD to represent hyporheic retention sufficient to well reproduce the observed breakthrough curves, even when the mass transfer is not limited to a surficial layer of the bed. However, power-law with exponents in the range from -2 to $-3/2$, when visible, should be regarded as particular signature of hyporheic exchange affecting a significant portion of the streambed.

Chapter 7

Bed form-induced hyporheic exchange in stratified beds[1]

7.1 Introduction

In the previous chapter, bed form-induced hyporheic exchange was analyzed assuming that the porous medium is homogeneous. This assumption is often adopted in hyporheic studies, although stream beds in nature are typically heterogeneous. For a related problem, wind pumping through snowpacks, *Colbeck* (1989) showed that subsurface layering substantially alters patterns and rates of pore fluid flow. *Salehin et al.* (2004) demonstrated that layered sedimentary heterogeneity increases the average interfacial flux but tends to limit vertical penetration because it favor horizontal transport through high-permeability layers. However, that work used an idealized random correlated permeability field because relatively little is known about in situ structure in permeable sediment beds. *Cardenas et al.* (2004, 2003) used structure-imitating interpolation (kriging) to obtain a 3D reconstruction of modern channel bend deposits based on constant

[1] The contents of this chapter have been published in: Marion, A., A. I. Packman, M. Zaramella, and A. Bottacin-Busolin (2008), Hyporheic flows in stratified beds, *Water Resour. Res.*, 44, W09433.

head injection tests and ground-penetrating radar surveys; they used 3D numerical modeling to investigate the influence of heterogeneity on the hyporheic fluxes, showing that residence times can decrease or increase compared to the homogeneous case depending on the relative positions of the heterogeneities and bed forms. More recently, the influence of aquifer heterogeneity on solute exchange with the hyporheic zone was investigated experimentally by in-situ tracer tests and measurements by *Ryan and Boufadel* (2006). In their study higher concentrations were found to be in the upper bed sediments when the hydraulics conductivity was higher than in the lower bed sediments and vice versa. Recently, *Sawyer and Cardenas* (2009) presented numerical simulations on heterogeneous cross-bedded sediments, showing that heterogeneities can alter the residence time distributions in river beds.

A particular type of heterogeneous structure is given by the presence of horizontal sediment layers of different permeability. Horizontal stratifications characterized by a coarse surface layer of sediment and an underlying layer of lower permeability are often found in rivers due to the preferential removal of fines from the bed surface by entrainment or winnowing. This process is described as *armoring*, and the resulting layer of coarse sediments is called *armored layer*. The thickness of the armor layer is normally limited to twice the size of the largest material in the sediment mixture and it is expected to be particularly important for transport processes acting at short time scales and small spatial scales, at which diffusion of momentum plays an important role. When the vertical structure of a porous bed is characterized by an upper coarse layer of sediment thicker than a typical armor layer, the effect of the heterogeneous structure on hyporheic exchange can be visible at longer time scales, at which the interfacial turbulent diffusion is no longer the main transport mechanism in the porous medium. In this chapter, a model is presented to simulate hyporheic exchange for the case of bed form-induced hyporheic exchange in presence of two well defined layers of

different permeability. The predictions of the model are compared to experimental data.

7.2 Hyporheic flow modeling for layered beds

7.2.1 Velocity field in the bed

The advective pore water flow induced within a layered sediment bed is modeled here starting from the assumption that Darcy's law applies for the pore water flow within the sediments. Following *Elliott and Brooks* (1997a) analysis of pore water flows under dune-shaped bed forms, the upper boundary condition is taken as a sinusoidal variation in dynamic pressure with wavelength λ coinciding with the bed form wavelength. The bed is idealized as being composed of an upper layer of thickness d_1 and hydraulic conductivity K_1 sitting on top of a lower layer of thickness d_2 and conductivity K_2. The bed is considered impermeable at the bottom of the lower layer and periodic in the downstream direction. The pressure head at the bed surface can be written as

$$h(x, y = 0) = h_m \sin(kx), \tag{7.1}$$

where h_m is the half amplitude of the pressure at the surface, $k = 2\pi/\lambda$ is the wave number and x and y are the horizontal and vertical Cartesian coordinates, respectively (y positive upward).

In the subsurface, the hydraulic head follows Laplace's equation in two dimensions $\nabla^2 h = 0$, valid for homogeneous porous media. The solution for the induced subsurface head distribution can be found by solving the Laplace equation in both layers, while matching the solution at the interface. Symmetry requires that the hydraulic head remains sinusoidal over any horizontal plane with the same wavelength of the surface forcing. Thus the pressure at the interface

between the two layers is:

$$h(x, y = -d_1) = h_{12} \sin(kx), \tag{7.2}$$

where h_{12} is the unknown half-amplitude of the dynamic head at the interface. For these boundary conditions, the head distribution can be shown to be:

$$h(x,y) = h_m \sin(kx) \frac{\sinh[k(d_1+y)] - h_{12}/h_m \sinh(ky)}{\sinh(kd_1)}, \quad \text{for } -d_1 < y < 0, \tag{7.3a}$$

$$h(x,y) = h_m \sin(kx) \frac{\cosh[k(d_1+d_2+y)]}{\cosh(kd_2)}, \quad \text{for } -(d_1+d_2) < y < -d_1. \tag{7.3b}$$

This solution agrees with prior solutions for homogeneous, isotropic beds: the magnitude of the subsurface head decays exponentially with depth for a semi-infinite homogeneous bed (*Elliott and Brooks*, 1997a), and hyperbolically for beds with finite depth (*Packman et al.*, 2000b). Application of Darcy's law in the two layers, $(u,v) = -K\nabla h$, leads to the following velocity field:

$$\begin{cases} u(x,y) = -kK_1 h_m \cos(kx) \dfrac{\sinh[k(d_1+y)] - h_{12}/h_m \sinh(ky)}{\sinh(kd_1)} \\ v(x,y) = -kK_1 h_m \sin(kx) \dfrac{\cosh[k(d_1+y)] - h_{12}/h_m \cosh(ky)}{\sinh(kd_1)} \end{cases}, \quad \text{for } -d_1 < y < 0, \tag{7.4a}$$

$$\begin{cases} u(x,y) = -kK_2 h_{12} \cos(kx) \dfrac{\cosh[k(d_1+d_2+y)]}{\cosh(kd_2)} \\ v(x,y) = -kK_2 h_{12} \sin(kx) \dfrac{\sinh[k(d_1+d_2+y)]}{\cosh(kd_2)} \end{cases}, \quad \text{for } -(d_1+d_2) < y < -d_1. \tag{7.4b}$$

The half-amplitude of the head at the interface, h_{12}, can be obtained by matching the vertical velocity at the interface:

$$h_{12} = h_m \frac{\operatorname{csch}(kd_1)}{\coth(kd_1) + K_2/K_1 \tanh(kd_2)}. \tag{7.5}$$

Defining the non-dimensional ratios $h_{12}^* = h_{12}/h_m$ and $K^* = K_1/K_2$, a dimensionless solution for the subsurface velocity field can be obtained by dividing the velocity components in equation (7.4) by the velocity scale of pumping defined as $u_m = kK_1h_m$:

$$\begin{cases} u^* = \dfrac{u}{kK_1h_m} = -\cos(x^*)\dfrac{\sinh(d_1^*+y^*)-h_{12}^*\sinh(y^*)}{\sinh(y^*)} \\ v^* = \dfrac{v}{kK_1h_m} = -\sin(x^*)\dfrac{\cosh(d_1^*+y^*)-h_{12}^*\cosh(y^*)}{\sinh(d_1^*)} \end{cases}, \quad \text{for } -d_1^* < y^* < 0, \tag{7.6a}$$

$$\begin{cases} u^* = \dfrac{u}{kK_1h_m} = -\dfrac{h_{12}}{K^*}\cos(x^*)\dfrac{\cosh(d_1^*+d_2^*+y^*)}{\cosh(d_2^*)} \\ v^* = \dfrac{v}{kK_1h_m} = -\sin(x^*)\dfrac{\sinh(d_1^*+d_2^*+y^*)}{\cosh(kd_2)} \end{cases}, \quad \text{for } -(d_1^*+d_2^*) < y^* < -d_1^*. \tag{7.6b}$$

where $x^* = kx$, $y^* = ky$, $d_1^* = kd_1$ and $d_2^* = kd_2$. The effect of the stream gradient S and, in case of a moving bed, of velocity of the translating bed forms U_b, can easily be accounted for by adopting a frame of reference moving at the speed of bed form propagation and adding to the horizontal streamwise component u^* in equation (7.6) the velocity $u_s^* - U_b^*$, where $u_s^* = S/(kh_m)$ and $U_b^* = \theta U_b/u_m$ as explained in Chapter 6.

The average influx across the stream-subsurface interface is given by the integral of the vertical velocity,

$$q = \frac{1}{\lambda}\int_0^{\lambda/2} |v(x, y=0)|\,dx = -\frac{1}{\lambda}\int_0^{\lambda/2} v(x, y=0)\,dx. \tag{7.7}$$

The velocity is integrated between 0 and $\lambda/2$ because it is only over this part of the bed surface that the flux occurs into the bed. The dimensionless average flux is:

$$q^* = \frac{q}{kK_1h_m} = \frac{1}{\pi}\left[\frac{\cosh(d_1^*)-h_{12}^*}{\sinh(d_1^*)}\right]. \tag{7.8}$$

Figure 7.1 shows the streamlines and resulting front positions for a sample

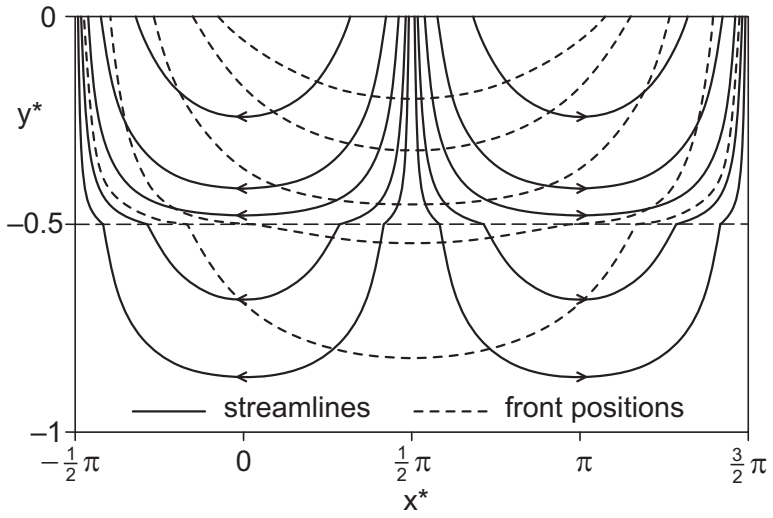

Figure 7.1. Streamlines and front positions within a homogeneous layered bed. Results are plotted for a sample case where the ratio between the two hydraulic conductivities is $K^* = 10$ and the dimensionless thickness of the two layers are $d_1^* = 0.5$ and $d_2^* = 0.5$. The longitudinal dimensionless distance scales with the bed form wavelength, $x^* = kx$. Front positions are drawn for non-dimensional timescales $t^* = 0.5$, 1, 2, 4 and 16.

case where the ratio between the two hydraulic conductivities is $K^* = 10$ and the dimensionless thickness of the two layers are $d_1^* = 0.5$ and $d_2^* = 0.5$. Front positions are drawn for non-dimensional timescales $t^* = 0.5$, 1, 2, 4 and 16. Time is normalized using the conductivity K_1 and porosity θ_1 of the upper layer, $t^* = tk^2K_1h_m/\theta_1$. In the lower layer, the streamlines are less dense compared to the upper layer because of the decrease in pore water velocity and hence in water flux induced by the lower permeability of the second layer. Streamlines in the upper layer of the bed are also constrained by the presence of the underlying less permeable sediments, and have different patterns than would be found in a homogeneous bed having a depth of either d_1 or $d_1 + d_2$.

7.2.2 Residence time distributions and mass exchange

The effect of surface-subsurface exchange on downstream solute transport must be evaluated in terms of total solute mass transfer storage within the bed (*Bencala and Walters*, 1983; *Elliott and Brooks*, 1997a). The cumulative mass exchange can be determined by solving a convolution integral involving the surface water concentration history, the interfacial flux, and the distribution of solute residence time within the bed. The complementary cumulative distribution function of residence times, $R(t^*)$, is defined as the fraction of solute entering the bed at $t^* = 0$ still trapped in the bed at time t^* (*Elliott and Brooks*, 1997a). The R function was evaluated with a numerical particle tracking technique based on the known velocity field (equation (7.6)) for five different cases having infinite lower layer ($d_2^* \to \infty$), and $d_1^* = 1, 2, 3, 4$ and 5. These five cases were also analyzed with two different ratios between the upper and the lower hydraulic conductivity, $K^* = 10$ and $K^* = 100$. The residence time function R is plotted in Figure 7.2a and Figure 7.2b for $K^* = 10$ and $K^* = 100$, respectively. A distinctive behavior is visible in all cases. The slope of R, which is negative by definition, is very close to zero at times corresponding to transport across the interface between the higher- and lower-permeability layers, forming a well-defined deflection point. The time at which the deflection occurs increases as the depth of the upper layer increases, as expected. It is interesting to note that the curves describing R for any two layer thicknesses always cross (Figure 7.2). A thicker layer always produces higher values of R at short time scales and smaller values of R at long time scales. With a higher conductivity ratio between the upper and lower layers the variation of R becomes more significant, as can be seen by comparing the results for $K^* = 10$ and $K^* = 100$ in Figure 7.2a and Figure 7.2b.

The dimensionless form of the cumulative mass exchange between the overlying flow and the bed is commonly expressed as $m^* = 2\pi km/\theta_1$, where m is

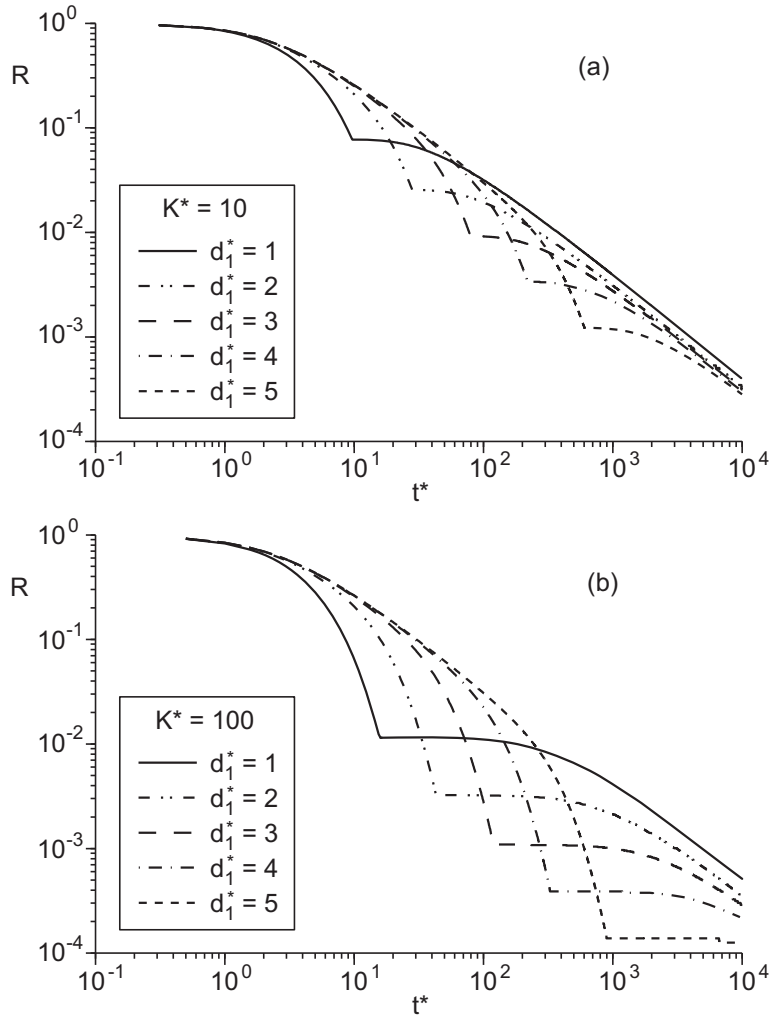

Figure 7.2. Complementary cumulative distribution function of the residence time within the bed, $R(t^*)$, plotted for (a) $K^* = 10$ and for (b) $K^* = 100$ in log-log scale. The curves are obtained from particle tracking applied to the flow field described by equation (7.6).

the accumulated mass per unit plan area of stream divided by a reference concentration C_0 [L], and can be computed in all systems for a constant in-stream concentration C_W with the integral (*Elliott and Brooks*, 1997a)

$$m^* = 2\pi q^* \int_0^{t^*} C_W^*(t^* - \tau^*) R(\tau^*)\, d\tau^*. \tag{7.9}$$

Mass exchanges have bee evaluated for the five cases analyzed in the previous section for the case of mass transfer to an initially clean sediment bed. The initial conditions at $t = 0$ are: the in-stream concentration $C_W(0) = C_0$ and the subsurface concentration $C_S(0) = 0$ for $y < 0$. The results presented in Figure 7.3a and Figure 7.3b show that the rate of mass transfer is controlled by the hydraulic conductivity of the upper layer at very short times, while at sufficiently long times it is controlled by the conductivity of the lower layer, i.e., it becomes completely independent of the thickness of the upper layer. At intermediate times the mass exchange is highly dependent on both the thickness and conductivity ratio of the upper layer.

7.3 Experiments

The predictions of the model presented in the previous section can be compared to data from flume experiments with layered beds conducted in 2003 at the Northwestern University (USA) in a joint project with the University of Padova. In the following two sections, the experimental setup and the main experimental results are presented.

7.3.1 Experimental setup

The experiments were conducted in a 7.5 m long, 20 cm deep tilting and recirculating flume located in the Environmental and Biological Transport Processes laboratory at Northwestern University. A bed composed of non-uniform sedi-

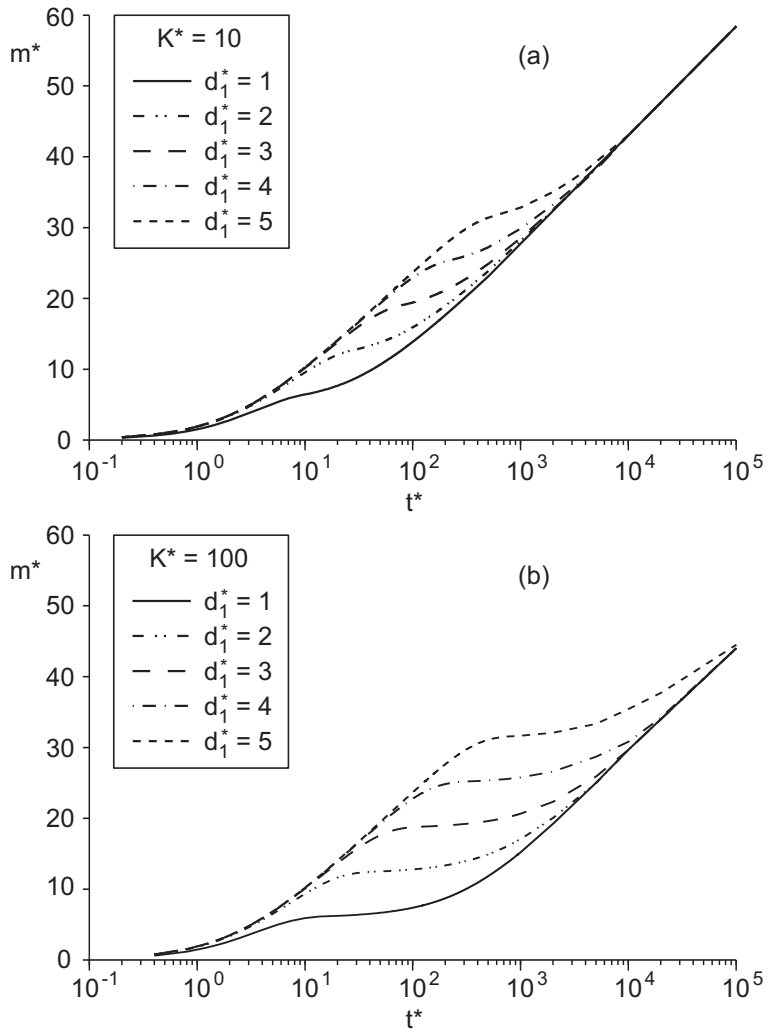

Figure 7.3. Dimensionless penetrated mass $m^*(t^*)$ in the bed plotted for (a) $K^* = 10$ and for (b) $K^* = 100$. The curves are calculated from the residence time distribution presented in Figure 7.2 using equation (7.9).

ment was placed in the channel and a constant volume of water was continuously recirculated over the bed.

Sodium chloride (NaCl) was used as a conservative tracer to evaluate mass transfer from the overlying flow to the pore water. A concentrated NaCl solution was prepared using reagent-grade salt and then added to the downstream end of the flume over one recirculation period in order to establish a uniform salt concentration in the stream. The surface-subsurface exchange flux was determined from the rate of change of the in-stream concentration by considering the mass balance between the recirculation stream and the pore water in the sediment bed.

Seven tests were performed to observe exchange with different sediment structures under different flow conditions. Four experiments (Exp. 1–3, 5) were performed with flat beds having different subsurface structure and will not be considered here. The reader is invited to read the paper by *Marion et al.* (2008a) for a complete description of the tests and the relevant results.

Three tests (Exp. 4, 6 and 7) were performed with stationary bed forms, and had both layered and homogeneous sediment structure. The bed forms were formed manually to approximate a natural dune shape and had a wavelength $\lambda = 50\,\mathrm{cm}$ and a height of $H = 5\,\mathrm{cm}$. In Experiments 4 and 6, the sediment structure was layered, with a 3 cm-thick layer of gravel overlying a 12 cm-thick layer of a sand-gravel mixture with bed forms formed in the gravel layer. The sand-gravel mixture was composed of 50% pea gravel and 50% coarse sand. The pea gravel had a relatively narrow distribution with diameters $D_{10} = 2\,\mathrm{mm}$, $D_{50} = 6\,\mathrm{mm}$, $D_{90} = 9\,\mathrm{mm}$. The mean bulk porosity of the clean gravel was $\theta = 0.38$. The sand had $D_{10} = 0.2\,\mathrm{mm}$, $D_{50} = 0.8\,\mathrm{mm}$ and $D_{90} = 2\,\mathrm{mm}$ and also had a porosity of approximately 0.38. The composition of the gravel and the sand-gravel mixture is shown in Figure 7.4.

Exp. 4 had a mean overlying velocity $U = 0.36\,\mathrm{m\,s^{-1}}$ while Exp. 6 had a mean overlying velocity $U = 0.21\,\mathrm{m\,s^{-1}}$. Exp. 7 was conducted with the sand-gravel

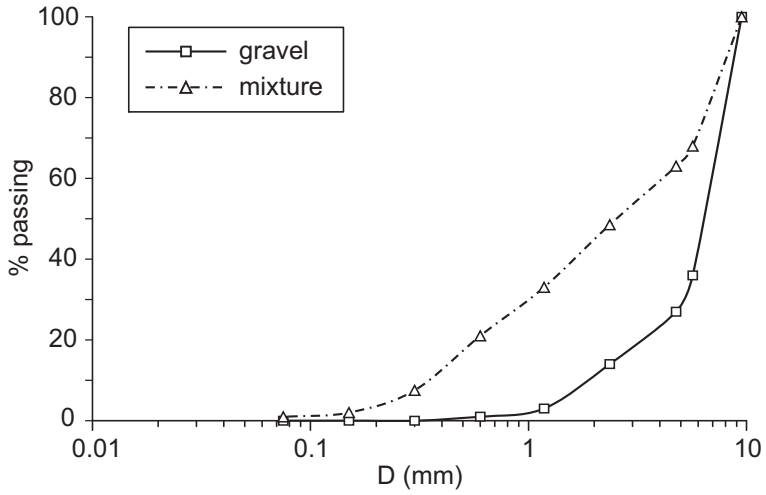

Figure 7.4. Grain size distributions of sand-gravel mixture and gravel.

Exp.	U ($\mathrm{m\,s^{-1}}$)	d_W (m)	Q ($\mathrm{m^3\,s^{-1}}$)	S ($\times 10^{-4}$ m/m)	Bed structure
4	0.36	0.15	0.009	9	Layered
6	0.21	0.12	0.006	9	Layered
7	0.21	0.12	0.006	9	Homogeneous

Table 7.1. Summary of experimental conditions.

mixture and with bed forms at a velocity of $U = 0.21\,\mathrm{m\,s^{-1}}$. With no stratification, Exp. 7 is used for comparison with the two tests having layered bed structure. A summary of the flow conditions and the characteristics of the sediment bed in the three Experiments 4, 6 and 7 is given in Table 7.1.

7.3.2 Results

The experimental data are presented in Figure 7.5 for Experiments 4, 6 and 7. Data are reported in terms of the change in the dimensionless in-stream concentration over time, $C^*_W(t) = C_W(t)/C_0$, where C_0 is the initial in-stream concentration, i.e., $C_W(0)$.

Comparison of the results of Experiments 6 and 7, characterized by the same

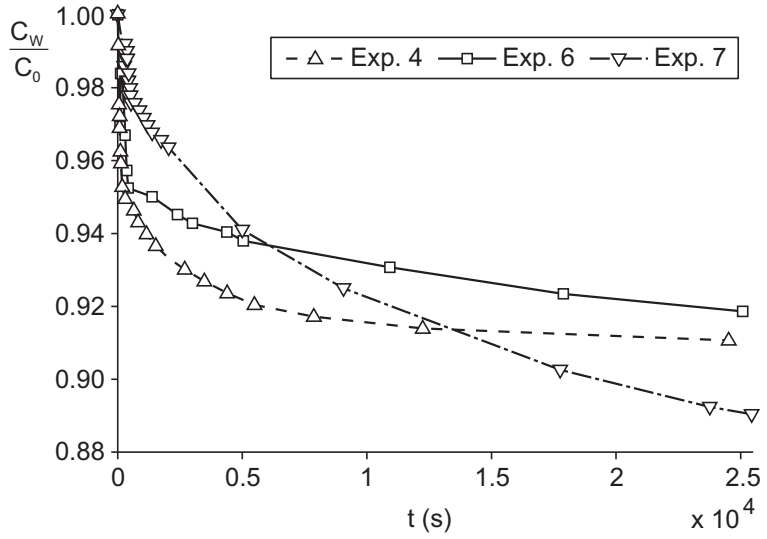

Figure 7.5. Dimensionless in-stream concentration $C_W(t)/C_0$ versus time t for Experiments 4, 6 and 7. Exp. 4: $U = 0.36\,\mathrm{m\,s^{-1}}$, $d_W = 15\,\mathrm{cm}$, layered bed; Exp. 6: $U = 0.21\,\mathrm{m\,s^{-1}}$, $d_W = 12\,\mathrm{cm}$, layered bed; Exp. 7: $U = 0.21\,\mathrm{m\,s^{-1}}$, $d_W = 12\,\mathrm{cm}$, homogeneous bed. In all the experiments the bed surface was characterized by bed forms with wavelength $\lambda = 50\,\mathrm{cm}$ and height $H = 5\,\mathrm{cm}$.

flow conditions, reveals that heterogeneity can have significant effects on interfacial solute transport. The initial rate of mass transfer is much greater in the layered systems than in the homogeneous bed. This reflects the fact that the hydraulic conductivity of the gravel is around two orders of magnitude greater than that of the mixture. However, the rate of mass transfer decreases much faster with the layered bed than with the homogeneous bed because of the limiting effect of the horizontal interface between the two sediment layers. Note that the composition of the lower portion of the bed is identical in experiments 4, 6 and 7, and only the uppermost 3 cm layer differs. The potential to exchange mass across the lower interface is greatly reduced by the damping of head in the upper sediment. This damping still affects exchange with a homogeneous bed because ongoing mass transfer requires mixing into progressively deeper portions of the bed, but

the rate of decrease is greater with a layered bed due to the deflection of the flow paths at the interface induced by the lower conductivity of the underlying layer. This is the source of the effective anisotropy that has previously been observed to limit vertical penetration in heterogeneous beds (*Salehin et al.*, 2004). The overall result is that the rate of mass exchange with the homogeneous bed becomes greater than with layered beds at long times, as can be seen from the crossing of the curves in Figure 7.5. Comparison of Exp. 4, where $U = 0.36\,\mathrm{m\,s^{-1}}$, with Exp. 6, where $U = 0.21\,\mathrm{m\,s^{-1}}$, shows that the increase of velocity induces an increase of mass transfer and the upper layer becomes saturated more rapidly. This is an expected result since the exchange rates normally increase as the square of the overlying velocity, as shown by *Packman et al.* (2004).

7.4 Comparison between model and experimental results

The exchange mass can be evaluated from the in-stream concentration history using the following relationship for the mass balance of solute in the system:

$$m^* = d_W^*(1 - C_W). \tag{7.10}$$

The parameter d_W^* is the dimensionless effective water depth, equal to $2\pi k d_W'/\theta_1$, where d_W' is the ratio between the total recirculating volume of water and the bed surface area.

The hydraulic conductivity used to model hyporheic exchange was evaluated with the following empirical relation (*McCarthy*, 2006):

$$K = 0.35 D_{15}^2. \tag{7.11}$$

where hydraulic conductivity, K, has units of $\mathrm{cm\,s^{-1}}$ and D_{15} is in cm. The hydraulic conductivity was evaluated to be $K = 3 \times 10^{-4}\,\mathrm{m\,s^{-1}}$ for the sand-gravel mixture and $K = 0.002\,\mathrm{m\,s^{-1}}$ for gravel only.

The half-amplitude h_m of the sinusoidal dynamic head over bed forms was evaluated with *Felhman* (1985) equation:

$$h_m = 0.28\frac{U^2}{2g} \times \begin{cases} \left(\frac{H/d}{0.34}\right)^{3/8}, & H/d_W \leq 0.34, \\ \left(\frac{H/d}{0.34}\right)^{3/2}, & H/d_W > 0.34, \end{cases} \tag{7.12}$$

where H is the bed form height (through-to-crest). In Experiments 6 and 7 the half-amplitude of the dynamic head predicted by equation (7.12) is $h_m = 0.85\,\text{mm}$, while in Exp. 4 it is $h_m = 2.51\,\text{mm}$.

The observed and predicted mass transfer for Experiments 4 and 6 are compared in Figure 7.6. A linear time scale is used in Figure 7.6a, while a semi-log scale is used in Figure 7.6b for direct comparison with Figure 7.3. The scatter of data at short times is to be attributed to the difficulty of the advective model to represent in detail the complex interactions affecting early transfer at flow/bed interface. These tests both had bed forms and layered sediment structure, with $K^* = 67$, d_1^* and $d_2^* = 1.51$, but different overlying velocities. The collapse of data from the two tests onto a single unique curve shows that the scalings used to non-dimensionalize mass transfer and time are correct. Thus, the scaling of the exchange rate with U^2 still holds even with the heterogeneous bed. The first phase of the exchange is fast and governed by the 3 cm-deep upper layer. The inflection point of the curve corresponds to the time at which the upper permeable layer becomes saturated with solute. After this time the exchange process is governed by mass transfer into the lower and less permeable layer. Therefore it can be seen that the initial phase of mass transfer is regulated by the characteristics of the surficial sediment layer, while tracer exchange rate over longer timescales depends on the characteristics of the underlying less permeable material.

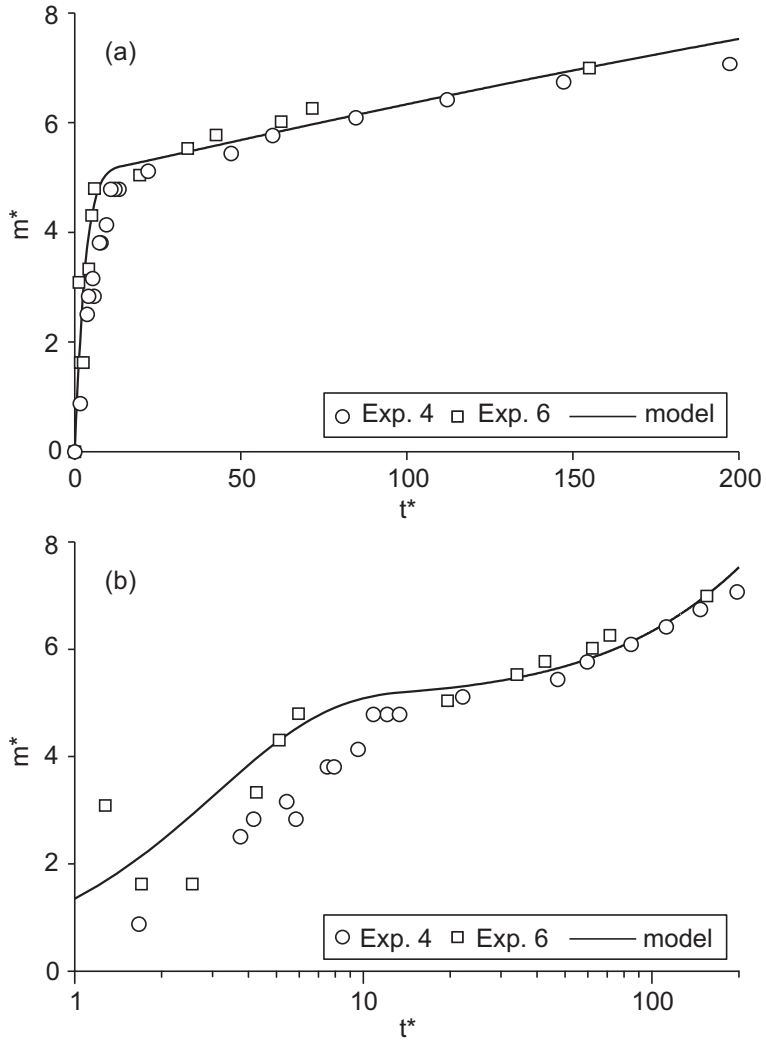

Figure 7.6. Observed and predicted dimensionless penetrated mass $m^*(t^*)$ for Exp. 4 and Exp. 6 plotted in (a) linear scale and (b) semi-log sclae. In both experiments the bed was made of two horizontal layers with artificial bed forms at the flow/bed interface. The difference between the two tests was the mean flow velocity and the water depth, as reported in Table 7.1.

7.5 Conclusions

A mathematical model was developed for the pore water flow induced in a layered sediment bed by the dynamic pressure variation over dune-shaped bed forms. For the case of a coarser surface layer over a finer and less permeable layer, the flow paths in the upper layer are compressed by the presence of the underlying low permeability layer thus suppressing mass transfer into the lower layer. A comparison of exchange with homogeneous and layered beds shows that the presence of a coarse near-surface layer increases the interfacial flux and initial rate of mass transfer, but decreases vertical solute penetration into the underlying finer sediments and the corresponding net mass transfer at longer time scales.

These results emphasize the importance of sediment structure on surface-subsurface flow coupling and solute exchange. The presence of deeper layers of differing permeability, which are often found in rivers because of episodic sediment transport events (*Leopold et al.*, 1964), causes rates of mass transfer into the bed to vary over time as solute penetrates to the different layers of sediments. When such systems are analyzed using a model that assumes homogeneous subsurface structure, the instantaneous exchange rate will be overestimated and underestimated at different stages of the overall exchange process. The results and theoretical analysis presented here support the recommendation previously made by other authors (*Harvey and Wagner*, 2000; *Zaramella et al.*, 2003) that it is important to combine observations of tracer concentration in surface waters with characterization of the subsurface structure and direct observations of tracer penetration to particular depths of interest.

Notation

The symbols and notation appearing in this thesis are listed below. Within the main body of the text, symbols are usually defined at their first usage within a chapter, or at other times when needed for clarity. In some cases equations have been presented using the same notation used in the original papers; in other cases, original notation has been altered to better fit with the surrounding material.

Acronyms

ADE	Advection-Dispersion Equation;
APM	Advective Pumping Model;
BTC	Breakthrough Curve;
CTRW	Continuous Time Random Walk;
FADE	Fractional Advection Dispersion Equation;
GME	Generalized Master Equation;
MRMT	Multi-Rate Mass Transfer;
PDF	Probability Density Function;
RMSE	Root Mean Square Error;
RTD	Residence Time Distribution;
RWT	Rodhamine-WT;
STIR	Solute Transport In Rivers;

TSM Transient Storage Model.

Roman symbols

Upper case

A average stream cross-sectional area [L^2];

A_S average cross-sectional area of storage zones [L^2];

C concentration [ML^{-3}];

C^* dimensionless concentration, $C^* = C/C_0$ [-];

C_0 reference concentration [ML^{-3}];

$C_{AD\delta}$ solution of conventional advection-dispersion equation for an input mass pulse [ML^{-3}];

C_L concentration of solute in lateral inflow [ML^{-3}];

C_{obs} observed concentration [ML^{-3}];

C_S concentration of solute in the sediments [ML^{-3}];

C_{sim} simulated concentration [ML^{-3}];

C_W concentration in the main channel [ML^{-3}];

$C_{W\delta}$ impulsive solution for the concentration in the main channel [ML^{-3}]

D_{10} grain size for which 10% by weight of the sediment is finer [L];

D_{50} grain size for which 50% by weight of the sediment is finer [L];

D_{90} grain size for which 90% by weight of the sediment is finer [L];

D_ϵ dispersion coefficient of fractional advection-dispersion equation [L^2T^{-1}];

D_m molecular diffusion coefficient [L^2T^{-1}];

D_L longitudinal dispersion coefficient [L^2T^{-1}];

D_S diffusion coefficient in the porous medium of the diffusive transport model [L^2T^{-1}];

D_{ij} components of the dispersion tensor of the porous medium [L^2T^{-1}];

D_{ij}^T components of the turbulent dispersion tensor [L^2T^{-1}];

F F-value of F-test of the overall linear fit [-];

H bed form height [L];

I set of observed concentration values, $I = I_U \cup I_L$;

I_L set of observed concentration values lower than a given threshold concentration;

I_U set of observed concentration values higher than a given threshold concentration;

K hydraulic conductivity of the porous bed [$\mathrm{L\,T^{-1}}$];

K^* ratio of conductivities of upper and lower sediment layer, $K^* = K_1/K_2$ [-];

K_1 hydraulic conductivity of the upper sediment layer [$\mathrm{L\,T^{-1}}$];

K_2 hydraulic conductivity of the lower sediment layer [$\mathrm{L\,T^{-1}}$];

L length of study reach [L];

L_{mix} distance from injection at which a solute can be considered well-mixed over the cross-section [L];

M_0 injected mass [M];

M_{S} retained mass [M];

P wetted perimeter [L];

P_0 probability of rejecting, when true, the null hypothesis that the angular coefficient of linear regression is zero [-];

Q flow discharge [$\mathrm{L^3\,T^{-1}}$];

R complementary cumulative residence time distribution [-];

R_0 complementary cumulative distribution of the residence time within the bed induced by advective pumping in the ideal case of stream gradient and bed form propagation celerity equal to zero [-];

R_{ad} retardation factor due to reversible adsorption onto sediments [-];

R^2_{det} coefficient of determination [-];

S stream gradient [-];

T residence timescale [T];

T_B residence timescale in the hyporheic zone [T];

T_D residence timescale in the surface dead zones [T];

U average flow velocity [$\mathrm{L\,T^{-1}}$]

U_b celerity of moving bed forms [$\mathrm{L\,T^{-1}}$];

U_b^* dimensionless celerity of moving bed forms, $U_b^* = \theta U_b/u_m$ [-];

U_{uf}^* dimensionless magnitude of relative underflow velocity [-].

Lower case

b channel width [L];

c local instantaneous concentration [$\mathrm{M\,L^{-3}}$];

$\overline{c}$ time average of the local instantaneous concentration [$\mathrm{M\,L^{-3}}$];

d_W water depth [L];

d average depth of the hyporheic zone [L];

d^* average dimensionless depth of the hyporheic zone, $d^* = kd$ [-];

d_1 thickness of the upper sediment layer [L]

d_2 thickness of the lower sediment layer [L]

e_{MS} residuals from a linear model explaining $\delta M_{\mathrm{S,max}}$ as a function chlorophyll-a [M];

f_M memory function [$\mathrm{T^{-1}}$];

h dynamic head [L];

h^* dimensionless dynamic head, $h^* = h/h_m$ [-];

h_{12}^* dimensionless semi-amplitude of the dynamic head at the interface between the upper and lower layer [-];

h_m semi-amplitude of the dynamic head on the bed surface [L];

m accumulated mass in the bed per unit plan area of stream divided by a reference concentration C_0 [L];

m^* dimensionless penetrated mass, $m^* = 2\pi km/\theta$ [-];

p_α probability density function of first-order coefficients [T];

p_i conditional probability distribution of the random variable $\mathcal{N}_i$ [-];

q average volumetric flux across the stream-subsurface interface [$\mathrm{L\,T^{-1}}$];

q^* dimensionless volumetric average flux across the stream-subsurface interface [$\mathrm{L\,T^{-1}}$];

q_B average volumetric flux in the hyporheic zones [$\mathrm{L\,T^{-1}}$];

q_L volumetric flux due to lateral inflow [$\mathrm{L\,T^{-1}}$];

r_W probability density function (PDF) of the residence time the surface water, $\mathcal{T}_W$ [$\mathrm{T^{-1}}$];

r_S probability density function (PDF) of the overall residence time in the storage zones, $\mathcal{T}_S$ [$\mathrm{T^{-1}}$];

r_{S_i} probability density function (PDF) of the overall residence time in the i-th storage domain, $\mathcal{T}_{Si}$ [$\mathrm{T^{-1}}$];

$r_{S_i|n}$ conditional residence time probability density function (PDF) in the i-th storage domain given that a particle has entered the storage domain n times [$\mathrm{T^{-1}}$];

s Laplace variable [$\mathrm{T^{-1}}$];

t time [T];

$\overline{t}$ averaging timescale [T];

t^* dimensionless time [-];

t_{ad} average advection time, $t_{\mathrm{ad}} = L/U$ [T];

t_B biofilm age [T];

t_c cutoff time scale of advective pumping-induced power-law behavior [T];

t_c^* dimensionless cutoff time scale of advective pumping-induced power-law behavior [-];

t_d time scale of exponential decay [T];

t_d^* dimensionless time scale of exponential decay [-];

$\mathbf{u}$ velocity vector, $\mathbf{u} = (u, v, w)$ [$\mathrm{L\,T^{-1}}$];

$\overline{\mathbf{u}}$ time average of velocity field, $\overline{\mathbf{u}} = (\overline{u}, \overline{v}, \overline{w})$ [$\mathrm{L\,T^{-1}}$];

$\mathbf{u}^*$ dimensionless velocity field, $\mathbf{u}^* = (u^*, v^*, w^*)$ [-];

u_* shear velocity [$\mathrm{L\,T^{-1}}$];

u_m maximum pumping-induced velocity, $u_m = kKh_m$ [$\mathrm{L\,T^{-1}}$];

u_s seepage velocity induced by the stream gradient [$\mathrm{L\,T^{-1}}$];

u_s^* dimensionless seepage velocity induced by the stream gradient [-];

$\mathbf{x}$ position vector, $\mathbf{x} = (x, y, z)$ [L];

$\mathbf{x}^*$ dimensionless position vector, $\mathbf{x}^* = k\mathbf{x} = (x^*, y^*, z^*)$ [-];

z_{chla} z-standardized value of chlorophyll-a [-].

Calligraphic symbols

$\mathcal{N}_i$ number of times a particle enters the i-th storage domain (random variable) [-];

$\mathcal{T}$ total residence time in the study reach (random variable) [T];

$\mathcal{T}_S$ overall residence time in the storage zones (random variable) [T];

$\mathcal{T}_{Si}$ overall residence time in the i-th storage domain (random variable) [T];

$\mathcal{T}_W$ residence time in the surface water (random variable) [T].

Greek symbols

Upper case

Γ_S source/sink term of advection-dispersion-mass-transfer equation [$\mathrm{M\,L^{-3}\,T^{-1}}$];

Δt_{inj} time length of injection period [T];

Φ mass flux [$\mathrm{M\,L^{-2}\,T^{-1}}$];

Φ_L mass flux accounting for mass gains due to lateral inflow [$\mathrm{M\,L^{-2}\,T^{-1}}$];

Φ_S mass flux into the storage zones [$\mathrm{M\,L^{-2}\,T^{-1}}$];

Ψ joint probability density function of length and duration of particle jumps [$\mathrm{L^{-1}\,T^{-1}}$].

Lower case

α transfer rate [T^{-1}];

α_L longitudinal dispersivity [L];

α_L^* dimensionless longitudinal dispersivity, $\alpha_L^* = k\alpha_L$ [-];

α_T transverse dispersivity [L];

α_T^* dimensionless transverse dispersivity, $\alpha_T^* = k\alpha_T$ [-];

β_{tot} capacity coefficient [-];

$\delta\alpha$ transfer rate associated to biofilm-induced retention [T^{-1}];

δM_S increment of retained mass [M];

$\delta\varphi$ residence time PDF associated to biofilm-induced retention [T^{-1}];

$\delta M_{S,\max}$ peak of increment of retained mass [M];

ϵ order of fractional derivative [-];

θ porosity of the porous medium [-];

θ_1 porosity of the upper sediment layer [-];

κ exponent of power-law RTD [-];

λ bed form wavelength [L];

λ_c horizontal distance between the crest and the upstream trough of a bed form [L];

$\nu(s)$ composite Laplace variable [T^{-1}];

ς skewness coefficient of fractional advection-dispersion equation [-];

φ probability density function (PDF) of the residence time in the storage zones for a single entry event [T^{-1}];

φ_0 PDF of the residence time within the bed for advective pumping in the ideal case of stream gradient and bed form propagation celerity equal to zero [T^{-1}];

φ_i probability density function (PDF) of the residence time in the i-th storage domain for a single entry [T^{-1}];

φ_B probability density function (PDF) of the residence time in the hyporheic zone for a single entry [T^{-1}];

φ_D probability density function (PDF) of the residence time in the surface dead zones fora single entry [T^{-1}];

ψ_L probability density function (PDF) of the length of particle jumps [L^{-1}];

ψ_T probability density function (PDF) of the duration of particle jumps [T^{-1}];

ψ_{T0} probability density function (PDF) of the duration of particle jumps in the absence of retention processes [T^{-1}].

Bibliography

Battin, T. J., L. A. Kaplan, J. D. Newbold, and C. M. E. Hansen (2003), Contributions of microbial biofilms to ecosystem processes in stream mesocosms, *Nature*, *426*(6965), 439–442.

Battin, T. J., L. A. Kaplan, S. Findlay, C. S. Hopkinson, E. Marti, A. I. Packman, J. D. Newbold, and F. Sabater (2008), Biophysical controls on organic carbon fluxes in fluvial networks, *Nature Geosci.*, *1*(2), 95–100.

Bencala, K. E. (1984), Interactions of solutes and streambed sediment. II. A dynamic analysis of coupled hydrologic and chemical processes that determine solute transport, *Water Resour. Res.*, *20*(12), 1804–1814.

Bencala, K. E., and R. A. Walters (1983), Simulation of solute transport in a mountain pool-and-riffle stream: A transient storage model, *Water Resour. Res.*, *19*(3), 718–724.

Benekos, D. I. (2005), On the determination of transverse dispersivity: Experiments and simulations in a helix and a cochlea, Ph.D. diss., Dept. of Civil and Environ. Eng., Standford Univ., Standford (CA).

Berkowitz, B., and H. Scher (1995), On characterization of anomalous dispersion in porous and fractured media, *Water Resour. Res.*, *31*(6), 1461–1466.

Besemer, K., G. Singer, R. Limberger, A. Chlup, G. Hochedlinger, I. Hodl, C. Baranyi, and T. J. Battin (2007), Biophysical controls on community succession in stream biofilms, *Appl. Environ. Microbiol.*, *73*(15), 4966–4974.

Blank, L. (1996), Numerical treatment of differential equations of frac-tional order, *Tech. Rep. 287*, Manchester Centre for Computational Mathematics Numerical Analysis.

Boano, F., C. Camporeale, R. Revelli, and L. Ridolfi (2006a), Sinuosity-driven hyporheic exchange in meandering rivers, *Geophys. Res. Lett.*, *33*, L18,406.

Boano, F., R. Revelli, and L. Ridolfi (2006b), Bedform-induced hyporheic exchange with unsteady flow, *Geophys. Res. Lett.*, *30*(1), 148–156.

Boano, F., A. I. Packman, A. Cortis, R. Revelli, and L. Ridolfi (2007), A continuous time random walk approach to the stream transport of solutes, *Water Resour. Res.*, *43*, W10,425.

Boano, F., R. Revelli, and L. Ridolfi (2008), Reduction of the hyporheic zone volume due to the stream-aquifer interaction, *Geophys. Res. Lett.*, *35*, L09,401.

Briggs, M. A., M. N. Gooseff, C. D. Arp, and M. A. Baker (2009), A method for estimating surface transient storage parameters for streams with concurrent hyporheic storage, *Water Resour. Res.*, *45*, W00D27.

Brinkman, H. C. (1949), A calculation of the viscous force exerted by a flowing fluid on a dense swarm of particles, *App. Sci. Res.*, *1*(1), 27–34.

Calhoun, D., and R. J. LeVeque (2000), A cartesian grid Finite-Volume method for the Advection-Diffusion equation in irregular geometries, *J. Comput. Phys.*, *157*(1), 143–180.

Cardenas, M. B. (2003), Three-dimensional model of modern channel bend deposits, *Water Resour. Res.*, *19*(6), 1141.

Cardenas, M. B., and J. L. Wilson (2006), The influence of ambient groundwater discharge on exchange zones induced by current-bedform interactions, *J. Hydrol.*, *331*(1-2), 103–109.

Cardenas, M. B., and J. L. Wilson (2007), Dunes, turbulent eddies, and interfacial exchange with permeable sediments, *Water Resour. Res.*, *43*, W08,412.

Cardenas, M. B., J. L. Wilson, and V. A. Zlotnik (2004), Impact of heterogeneity, bed forms, and stream curvature on subchannel hyporheic exchange, *Water Resour. Res.*, *40*, W08,307.

Carrera, J., X. SÃąnchez-Vila, I. Benet, A. Medina, G. Galarza, and J. GuimerÃă (1998), On matrix diffusion: formulations, solution methods and qualitative effects, *Hydrogeol. J.*, *6*(1), 178–190.

Castro, N. M., and G. M. Hornberger (1991), Surface-subsurface interactions in an alluviated mountain stream channel, *Water Resour. Res.*, *27*(7), 1613–1621.

Chaves, A. S. (1998), A fractional diffusion equation to describe Lévy flights, *Phys. Lett. A*, *239*(1-2), 13–16.

Choi, J., S. M. Hulseapple, M. H. Conklin, and J. W. Harvey (1999), Modeling CO2 degassing and pH in a stream-aquifer system, *J. Hydrol.*, *209*(1-4), 297–310.

Choi, J., J. W. Harvey, and M. H. Conklin (2000), Characterizing multiple timescales of stream and storage zone interaction that affect solute fate and transport in streams, *Water Resour. Res.*, *36*(6), 1511–1518.

Colbeck, S. C. (1989), Air movement in snow due to wind-pumping, *J. Glaciol.*, *35*(120), 209âĂŞ213.

Cortis, A., T. Harter, L. L. Hou, E. R. Atwill, A. I. Packman, and P. G. Green (2006), Transport of cryptosporidium parvum in porous media: Long-term evolution

experiments and continuous time random walk filtration modeling, *Water Resour. Res.*, *42*(12), W12S13.

Czernuszenko, W., and P. M. Rowinski (1997), Properties of the dead zone model of longitudinal dispersion in rivers, *J. Hydraul. Res.*, *35*(4), 491–504.

Day, T. J. (1975), Longitudinal dispersion in natural channels, *Water Resour. Res.*

De Smedt, F. (2006), Analytical solutions for transport of decaying solutes in rivers with transient storage, *J. Hydrol.*, *330*(3-4), 672–680.

De Smedt, F., and P. J. Wierenga (2005), Analytical solution for solute transport resulting from instantaneous injection in streams with transient storage, *J. Hydrol.*, *315*(1-4), 25–39.

DeAngelis, D. L., M. Loreau, D. Neergaard, P. J. Mulholland, and E. R. Marzolf (1995), Modelling nutrient-periphyton dynamics in streams: the importance of transient storage zones, *Ecol. Model.*, *80*(2-3), 149–160.

Deng, Z.-Q., V. P. Singh, and L. Bengtsson (2004), Numerical solution of fractional advection-dispersion equation, *J. Hydraul. Eng.*, *130*(5), 422–431.

Deng, Z.-Q., L. Bengtsson, and V. P. Singh (2006), Parameter estimation for fractional dispersion model for rivers, *Environ. Fluid. Mech.*, *6*(5), 451–475.

Dent, C. L., and J. C. Henry (1999), Modelling nutrient-periphyton dynamics in streams with surface-subsurface exchange, *Ecol. Model.*, *122*(1-2), 97–116.

Dierberg, F. E., and T. A. DeBusk (2005), An evaluation of two tracers in suface-flow wetlands: Rhodamine-WT and lithium, *Wetlands*, *25*(1), 8–25.

Elder, J. W. (1959), The dispersion of marked fluid in turbulent shear flow, *J. Fluid. Mech.*, *5*(04), 544–560.

Elliott, A. H., and N. H. Brooks (1997a), Transfer of nonsorbing solutes to a streambed with bed forms: Theory, *Water Resour. Res.*, *33*(1), 123–136.

Elliott, A. H., and N. H. Brooks (1997b), Transfer of nonsorbing solutes to a streambed with bed forms: Laboratory experiments, *Water Resour. Res.*, *33*(1), 137–151.

Felhman, H. S. (1985), Resistance components and velocity distributions of open channel flows over bedforms, Master's thesis, Colorado State University, Fort Collins, Colorado.

Fernald, A. G., P. J. Wigington, and D. H. Landers (2001), Transient storage and hyporheic flow along the Willamette River, Oregon: Field measurements and model estimates, *Water Resour. Res.*, *37*(6), 1681–1694.

Fick, A. (1855), *Annln. Phys.*, *170*, 59.

Fischer, H. B. (1968), Dispersion prediction in natural streams, *J. Sanit. Eng. Div., ASCE*, *94*(5), 927–943.

Fischer, H. B. (1975), Discussion of "Simple method for predicting dispersion in streams", *J. Env. Eng. Div., ASCE*, *101*(3), 435–455.

Fischer, H. B., J. E. List, C. R. Koh, J. Imberger, and N. H. Brooks (1979), *Mixing in Inland and Coastal Waters*, Academic Press.

Gooseff, M. N., D. M. McKnight, R. L. Runkel, and B. H. Vaughn (2003a), Determining long time-scale hyporheic zone flow paths in Antarctic streams, *Hydrol. Process.*, *17*(9), 1691–1710.

Gooseff, M. N., S. M. Wondzell, R. Haggerty, and J. Anderson (2003b), Comparing transient storage modeling and residence time distribution (RTD) analysis in geomorphically varied reaches in the lookout creek basin, oregon, USA, *Adv. Water. Resour.*, *26*(9), 925–937.

Gooseff, M. N., D. M. McKnight, R. L. Runkel, and J. H. Duff (2004), Denitrification and hydrologic transient storage in a glacial meltwater stream, McMurdo dry valleys, antarctica, *Limnol. Oceanogr.*, *49*(5), 1884–1895.

Gooseff, M. N., J. LaNier, R. Haggerty, and K. Kokkeler (2005), Determining in-channel (dead zone) transient storage by comparing solute transport in a bedrock channel-alluvial channel sequence, Oregon, USA, *Water Resour. Res.*, *41*, W06014.

Gooseff, M. N., R. O. H. Jr., and J. L. Tank (2007), Relating transient storage to channel complexity in streams of varying land use in jackson hole, wyoming, *Water Resour. Res.*, *43*, W01,417.

Haggerty, R., and S. M. Gorelick (1995), Multiple-Rate mass transfer for modeling diffusion and surface reactions in media with Pore-Scale heterogeneity, *Water Resour. Res.*, *31*(10), 2383–2400.

Haggerty, R., and S. M. Wondzell (2002), Power-law residence time distribution in the hyporheic zone of a 2nd-order mountain stream, *Geophys. Res. Lett.*, *29*(13), 1640.

Haggerty, R., S. A. McKenna, and L. C. Meigs (2000), On the late-time behavior of tracer test breakthrough curves, *Water Resour. Res.*, *36*(12), 3467–3479.

Hall Jr., R. O., E. S. Bernhardt, and G. E. Likens (2002), Relating nutrient uptake with transient storage in forested mountain streams, *Limnol. Oceanogr.*, *47*(1), 255–265.

Hart, D. R. (1995), Parameter estimation and stochastic interpretation of the transient storage model for solute transport in streams, *Water Resour. Res.*, *31*(2), 323–328.

Harvey, J. W., and K. E. Bencala (1993), The effect of streambed topography on Surface-Subsurface water exchange in mountain catchments, *Water Resour. Res.*, *29*(1), 89–98.

Harvey, J. W., and C. C. Fuller (1998), Effect of enhanced manganese oxidation in the hyporheic zone on basin-scale geochemical mass balance, *Water Resour. Res.*, *34*(4), 623–636.

Harvey, J. W., and B. J. Wagner (2000), Quantifying hydrologic interactions between streams and their subsurface hyporheic zones, in *Streams and Groundwater*, edited by J. B. Jones and P. J. Mulholland, pp. 3–44, Academic, Sand Diego (CA).

Harvey, J. W., B. J. Wagner, and K. E. Bencala (1996), Evaluating the reliability of the stream tracer approach to characterize stream-subsurface water exchange, *Water Resour. Res.*, *32*(8), 2441–2451.

Harvey, J. W., J. E. Saiers, and J. T. Newlin (2005), Solute transport and storage mechanisms in wetlands of the everglades, south florida, *Water Resour. Res.*, *41*, W05,009.

Hays, J. R., P. A. Krenkel, and K. B. J. Schnelle (1966), Mass transport mechanism in open channel flow, *Tech. Rep. 8*, Vanderbilt University, Nashville, Tennessee.

Jackman, A., R. Walters, and V. Kennedy (1984), Transport and concentration controls for chloride, strontium, potassium and lead in uvas creek, a small cobble-bed stream in santa clara county, california, U.S.A.: 2. Mathematical modeling, *J. Hydrol.*, *75*(1-4), 111–141.

Johansson, H., K. Jonsson, K. J. Forsman, and A. Wörman (2001), Retention of conservative and sorptive solutes in streams – Simultaneous tracer experiment, *Sci. Total. Environ.*, *266*(1-3), 229–238.

Jonsson, K., H. Johansson, and A. Wörman (2003), Hyporheic exchange of reactive and conservative solutes in streams – Tracer methodology and model interpretation, *J. Hydrol.*, *278*(1-4), 151–169.

Jonsson, K., H. Johansson, and A. Wörman (2004), Sorption behaviour and long-term retention of reactive solutes in the hyporheic zone of streams, *J. Eniviron. Eng.*, *130*(5), 573–584.

Kim, B. K., A. I. Packman, and F. J. Triska (1990), Modeling transient storage and nitrate uptake kinetics in a flume containing a natural periphyton community, *Water Resour. Res.*, *26*(3), 505–515.

Kim, B. K. A., A. P. Jackman, and F. J. Triska (1992), Modeling biotic uptake by periphyton and transient hyporrheic storage of nitrate in a natural stream, *Water Resour. Res.*, *28*(10), 2743–2752.

Kim, S., and M. L. Kavvas (2006), Generalized Fick's law and fractional ADE for pollution transport in a river: Detailed derivation, *J. Hydraul. Eng.*, *11*(1), 80–83.

Krenkel, P. A., and G. T. Orlob (1962), Turbulent diffusion and the reaereation coefficient, *J. Sanit. Eng. Div.*, *ASCE*, *88*(SA2), 3079.

Lees, M. J., L. A. Camacho, and S. C. Chapra (2000), On the relationship of transient storage and aggregated dead zone models of longitudinal solute transport in streams., *Water Resour. Res.*, *36*(1), 213–224.

Leopold, L. B., M. G. Wolman, and J. P. Miller (1964), *Fluvial processes in geomorphology*, Freeman and Co., San Francisco (CA).

LeVeque, R. J. (1997), Wave propagation algorithms for multidimensional hyperbolic systems, *J. Comput. Phys.*, *131*(2), 327–353.

Margolin, G., and B. Berkowitz (2000), Application of continuous time random walks to transport in porous media, *J. Phys. Chem.*, *104*(16), 3942–3947, erratum: 104(36), 8762, 2000.

Margolin, G., M. Dentz, and B. Berkowitz (2003), Continuous time random walk and multirate mass transfer modeling of sorption, *Chem. Phys.*, *295*(1), 71–80.

Marion, A., and M. Zaramella (2005a), Diffusive behavior of bedform-induced hyporheic exchange in rivers, *J. Eniviron. Eng.*, *131*(9), 1260–1266.

Marion, A., and M. Zaramella (2005b), A residence time model for stream-subsurface exchange of contaminants, *Acta Geophysica Polonica*, *53*(4), 527.

Marion, A., and M. Zaramella (2006), Effects of velocity gradients and secondary flow on the dispersion of solutes in a meandering channel, *J. Hydraul. Eng.*, *132*(12), 1295–1302.

Marion, A., M. Bellinello, I. Guymer, and A. I. Packman (2002), Effect of bed form geometry on the penetration of nonreactive solutes into a streambed, *Water Resour. Res.*, *38*(10), 1209.

Marion, A., M. Zaramella, and A. I. Packman (2003), Parameter estimation of the transient storage model for stream-subsurface exchange, *Water Resour. Res.*, *129*(5), 456–463.

Marion, A., A. I. Packman, M. Zaramella, and A. Bottacin-Busolin (2008a), Hyporheic flows in stratified beds, *Water Resour. Res.*, *44*, W09,433.

Marion, A., M. Zaramella, and A. Bottacin-Busolin (2008b), Solute transport in rivers with multiple storage zones: The STIR model, *Water Resour. Res.*, *44*, W10,406.

McCarthy, D. F. (2006), *Essentials of Soil Mechanics and Foundations: Basic Geotechnics*, 7 ed., Prentice Hall.

Metzler, R., and J. Klafter (2000), Subdiffusive transport close to thermal equilibrium: from the Langevin equation to fractional diffusion, *Phys. Rev. E*, *61*(6), 6308–6311.

Montroll, E. W., and G. H. Weiss (1965), Random walks on lattices, *J. Math. Phys.*, *6*, 167–181.

Mulholland, P. J., A. D. Steinman, E. R. Marzolf, D. R. Hart, and D. L. DeAngelis (1994), Effect of periphyton biomass on hydraulic characteristics and nutrient cycling in streams, *Oecologia*, *98*(1), 40–47.

Mulholland, P. J., E. R. Marzolf, J. R. Webster, D. R. Hart, and S. P. Hendricks (1997a), Evidence that hyporheic zones increase hetrotrophic metabolism and phosphorus uptake in forest streams, *Limnol. Oceanogr.*, *42*, 443–451.

Mulholland, P. J., E. R. Marzolf, J. R. Webster, D. R. Hart, and S. P. Hendricks (1997b), Evidence that hyporheic zones increase heterotrophic metabolism and phosphorus uptake in forest streams, *Limnology and Oceanography*, *42*(3), 443–451.

Mulholland, P. J., A. M. Helton, G. C. Poole, R. O. Hall, S. K. Hamilton, B. J. Peterson, J. L. Tank, L. R. Ashkenas, L. W. Cooper, C. N. Dahm, W. K. Dodds, S. E. G. Findlay, S. V. Gregory, N. B. Grimm, S. L. Johnson, W. H. McDowell, J. L. Meyer, H. M. Valett, J. R. Webster, C. P. Arango, J. J. Beaulieu, M. J. Bernot, A. J. Burgin, C. L. Crenshaw, L. T. Johnson, B. R. Niederlehner, J. M. O/'Brien, J. D. Potter, R. W. Sheibley, D. J. Sobota, and S. M. Thomas (2008), Stream denitrification across biomes and its response to anthropogenic nitrate loading, *Nature*, *452*(7184), 202–205.

Nagaoka, H., and A. J. Ohgaki (1990), Mass transfer mechanism in a porous riverbed, *Water Resour.*, *24*(4), 417–425.

Nordin, C. F., and G. V. Sabol (1974), Empirical data on longitudinal dispersion in rivers, *U.S. Geological Survey*, pp. 20–74.

Nordin, C. F., and B. M. Troutman (1980), Longitudinal dispersion in rivers: The persistence of skewness in observed data, *Water Resour. Res.*

Orr, C. H., J. J. Clark, P. R. Wilcock, J. C. Finlay, and M. W. Doyle (2009), Comparison of morphological and biological control of exchange with storage zones in a field-scale flume, *J. Geophys. Res.*, *114*, G02,019.

Packman, A. I., and N. H. Brooks (2001), Hyporheic exchange of solutes and colloids with moving bed forms, *Water Resour. Res.*, *37*(10), 2591–2605.

Packman, A. I., N. H. Brooks, and J. J. Morgan (2000a), Kaolinite exchange between a stream and streambed: Laboratory experiments and validation of a colloid transport model, *Water Resour. Res.*, *36*(8), 2363–2372.

Packman, A. I., N. H. Brooks, and J. J. Morgan (2000b), A physicochemical model for colloid exchange between a stream and a sand streambed with bed forms, *Water Resour. Res.*, *36*(8), 2351–2361.

Packman, A. I., S. Mashfiqus, and M. Zaramella (2004), Hyporheic exchange with gravel beds: Basic hydrodynamic interactions and bedform-induced advective flows, *J. Hydraul. Eng.*, *130*(7), 647–656.

Polyanin, A. D. (2002), *Handbook of linear partial differential equations for engineers and scientists*, Chapman & Hall/CRC Press.

Price, K. V., R. M. Storn, and J. A. Lampinen (2005), *Differential evolution*, Natural Computing Series, Springer.

Qian, Q., V. R. Voller, and H. G. Stefan (2008), A vertical dispersion model for solute exchange induced by underflow and periodic hyporheic flow in a stream gravel bed, *Water Resour. Res.*, *44*, W07,422.

Runkel, R. L. (1998), One-dimensional Transport with Inflow ans Storage (OTIS): A solute transport model of streams and rivers, *US Geol. Surv. Water Resour. Invest. Rep.*, pp. 98–4018.

Runkel, R. L., and S. C. Chapra (1993), An efficient numerical solution of the transient storage equations for solute transport in small streams, *Water Resour. Res.*, *29*(1), 211–215.

Runkel, R. L., D. M. McKnight, K. E. Bencala, and S. C. Chapra (1996), Reactive solute transport in streams 2. simulation of a pH modification experiment, *Water Resour. Res.*, *32*(2), 419–430.

Runkel, R. L., D. M. McKnight, and E. D. Andrews (1998), Analysis of transient storage subject to unsteady flow: Diel flow variation in an antarctic stream, *J. N. Am. Benthol. Soc.*, *17*(2), 143–154.

Rutherford, J. C. (1994), *River Mixing*, 1 ed., John Wiley & Sons.

Ryan, R. J., and M. C. Boufadel (2006), Influence of streambed hydraulic conductivity on solute exchange with the hyporheic zone, *Environmental Geology*, *51*(2), 203–210.

Salehin, M., A. I. Packman, and M. Paradis (2004), Hyporheic exchange with heterogeneous streambeds: Laboratory experiments and modeling, *Water Resour. Res.*, *40*, W11,504.

Samko, S. G., A. A. Kilbas, and O. I. Marichev (1993), *Fractional Integrals and Derivatives: Theory and Applications*, 1 ed., CRC.

Savant, S. A., D. D. Reible, and L. J. Thibodeaux (1987), Convective transport within stable river sediments, *Water Resour. Res.*, *23*(9), 1763–1768.

Sawyer, A. H., and M. B. Cardenas (2009), Hyporheic flow and residence time distributions in heterogeneous cross-bedded sediment, *Water Resour. Res.*, *45*, W08,406.

Scher, H., and M. Lax (1973), Stochastic transport in a disored solid. I. Theory, *Phys. Rev.*, *137*, 4491–4502.

Scher, H., G. Margolin, and B. Berkowitz (2002), Towards a unified framework for anomalous transport in heterogeneous media, *Chem. Phys.*, *284*(1-2), 349–359.

Schumer, R., D. A. Benson, M. M. Meerschaert, and S. W. Wheatcraft (2001), Eulerian derivation of the fractional advection-dispersion equation, *J. Contaminant. Hydrol.*, *48*(1), 69–88.

Shimizu, Y., T. Tsujimoto, and H. Nakagawa (1990), Experiment and microscopic modeling of flow in highly permeable porous medium under free-surface flow, *J. Hydrosci. Hydraul. Eng.*, *8*(1), 69–78.

Sigee, D. C., and D. C. Sigee (2005), *Freshwater Microbiology*, Wiley.

Smart, P. L., and I. M. S. Laidlaw (1977), An evaluation of some fluorescent dyes for water tracing, *WRR*, *13*, 15–33.

Storn, R., and K. Price (1997), Differential evolution – a simple and efficient heuristic for global optimization over continuous spaces, *J. Global Optim.*, *11*, 341–359.

Taylor, G. (1954), The dispersion of matter in turbulent flow through a pipe, *Proceedings of the Royal Society of London. Series A. Mathematical and Physical Sciences*, *223*(1155), 446–468.

Thackston, E. L., and K. B. J. Schnelle (1970), Predicting effects of dead zones on stream mixing, *J. Sanit. Eng. Div., ASCE*, *92*(2), 319–331.

Thomas, S. A., M. V. H., W. J.R., and M. P.J. (2003), A regression approach to estimating reactive solute uptake in advective and transient storage zones of stream ecosystems, *Adv. Water. Resour.*, *26*, 965–976.

Tonina, D., and J. M. Buffington (2007), Hyporheic exchange in gravel bed rivers with pool-riffle morphology: Laboratory experiments and three-dimensional modeling, *Water Resour. Res.*, *43*, W01,421.

Valentine, E. M., and I. R. Wood (1977), Longitudinal dispersion within dead zones, *J. Hydraul. Div. Am. Soc. Civ. Eng.*, *103*, 975âĂŞ1006.

Vallet, H. M., J. A. Morice, C. N. Dahm, and M. E. Campana (1996), Parent lithology, surface-groundwater exchange, and nitrate retention in headwater streams, *Limnol. Oceanogr.*, *41*(2), 333–345.

van Genuchten, M. T., and P. J. Wierenga (1976), Mass Transfer Studies in Sorbing Porous Media I. Analytical Solutions, *Soil. Sci. Soc. Am. J.*, *40*(4), 473–480.

Wimpenny, J. W., and R. Colasanti (1997), A unifying hypothesis for the structure of microbial biofilms based on cellular automaton models, *FEMS Microbiology Ecology*, *22*(1), 1–16.

Wörman, A., A. I. Packman, H. Johansson, and K. Jonsson (2002), Effect of flow-induced exchange in hyporheic zones on longitudinal transport of solutes in streams and rivers, *Water Resour. Res.*, *38*(1), 1001.

Wörman, A., A. I. Packman, L. Marklund, J. W. Harvey, and S. H. Stone (2006), Exact three-dimensional spectral solution to surface-groundwater interactions with arbitrary surface topography, *Geophys. Res. Lett.*, *33*, L07,402.

Wörman, A., A. I. Packman, L. Marklund, J. W. Harvey, and S. H. Stone (2007), Fractal topography and subsurface water flows from fluvial bedforms to the continental shield, *Geophys. Res. Lett.*, *34*, L07,402.

Zaramella, M., A. I. Packman, and A. Marion (2003), Application of the transient storage model to analyze advective hyporheic exchange with deep and shallow sediment beds, *Water Resour. Res.*, *39*(7), 1198.

Zaramella, M., A. Marion, and A. I. Packman (2006), Applicability of the Transient Storage Model to the hyporheic exchange of metals, *J. Contaminant. Hydrol.*, *84*(1-2), 21–35.

Zheng, C., and G. D. Bennett (1995), *Applied Contaminant Transport Modeling*, John Wiley & Sons, Incorporated, New York.

Zhou, D., and C. Mendoza (1993), Flow through porous bed of turbulent stream, *J. Eng. Mech.*, *119*(2), 365–383.